NASA TECHNICAL NOTE

NASA TN D-5949

NOMOLOGY OF EARTH-MOON ORBITS, C = 4.00 AND C = C(L_1)

by R. F. Hoelker

Electronics Research Center
Cambridge, Mass. 02139

NATIONAL AERONAUTICS AND SPACE ADMINISTRATION • WASHINGTON, D. C. • DECEMBER 1970

1. Report No. NASA TN D-5949	2. Government Accession No.	3. Recipient's Catalog No.
4. Title and Subtitle Nomology of Earth-Moon Orbits, C = 4.00 and C = C(L_1)		5. Report Date December 1970 6. Performing Organization Code
7. Author(s) R.F. Hoelker		8. Performing Organization Report No. C-130
9. Performing Organization Name and Address Electronics Research Center Cambridge, Mass.		10. Work Unit No. 129-04-22-07 11. Contract or Grant No.
12. Sponsoring Agency Name and Address National Aeronautics and Space Administration		13. Type of Report and Period Covered Technical Note 14. Sponsoring Agency Code
15. Supplementary Notes		

16. Abstract

This volume is intended to begin to generate a classifying survey of the orbits of the Earth-Moon field. The mathematical representation of the problem is done by the restricted problem of three bodies with a mass ratio μ of 1/80.

Orbits are generated by computational means and represented in their geometry in pictorial form.

The series is arranged according to descending values of the Jacobi integration constant "C" which procedure is in agreement with the first-line ordering applied to the body of E-M orbits.

Further breakdowns of the orbit classes are made according to geometrical regions and the directions of motion.

This volume covers the orbits on the C-levels of C = 4.00 and C = 3.20388, the latter of which closely corresponds to that of the cis-lunar equilibrium point L_1.

17. Key Words ·Orbital Stability ·Earth-Moon Orbits ·Fly by Effect ·Restricted Three Body Problem ·Zero-Velocity Curves ·Capture ·Jacobi Integration Constant ·Equilibrium Points ·Lunar Orbits ·Orbital Stability ·Escape	18. Distribution Statement Unclassified - Unlimited		
19. Security Classif. (of this report) Unclassified	20. Security Classif. (of this page) Unclassified	21. No. of Pages 79	22. Price * $3.00

NOMOLOGY OF EARTH-MOON ORBITS, C = 4.00 AND C = C(L_1)

By R. F. Hoelker
Electronics Research Center

SUMMARY

The mathematical representation of earth-moon orbits is done by the restricted problem of three bodies with a mass ratio μ of 1/80.

Orbits are generated by computational means and represented in their geometry in pictorial form.

The series is arranged according to descending values of the Jacobi integration constant "C" which procedure is in agreement with the first-line ordering applied to the body of E-M orbits.

Further breakdowns of the orbit classes are made according to geometrical regions and the directions of motion.

This volume covers the orbits on the C-levels of C = 4.00 and C = 3.20388, the latter of which closely corresponds to that of the cis-lunar equilibrium point L_1.

INTRODUCTION

Past investigations about the existence of orbits in the restricted problem of three bodies are either aiming at representations of one-parametric families of orbits or exploring more-parametric orbit spaces within a small region of state space.

The rich scope of literature concerned herewith, however, is still not sufficient to enable a researcher to form for himself a mental picture of all orbits existing, in the sense as he has this of all Kepler orbits.

This lack of conceptualization is felt strongly by the engineer in all cases of practical applications as well as by the student in the course of studying this problem.

The present report represents the first part of an attempt to establish a rather complete survey of orbits of the restricted problem. This is to be understood in the following sense:

(1) Since the study is made by numerical methods, the density of the survey is contingent upon the step size of the numerical variational process. In general the aim will be to have the coverage dense enough to facilitate interpolation with respect to structural form of orbits.

(2) The extension of coverage will range to such limits as to allow extrapolation to regions further out.

(3) Orbits will be represented pictorially with emphasis on shape rather than tabulation of time histories.

PROBLEM DESCRIPTION AND METHOD OF COMPUTATION

The restricted problem of three bodies is concerned with the motion of a massless (third) body in the gravity field of two masses. The masses exert inverse-square gravitational forces on each other and on the third body, whereas the third body does not on the two masses.

The motion of the two masses is here assumed to be circular, the center of the circle being at the center of mass. Their motion is planar.

The ratio of the masses is 1:79 and in accordance with the proximity of this ratio to that of Moon to Earth, reference to the masses as well as to the problem will be made in terms of these. However, the masses here are assumed to be point-masses.

The motion of the third body will, for the length of this report, be restricted to the motion plane of the two masses. Its orbits will be studied and depicted within the frame of a rotating Cartesian coordinate system (X_R Y_R), lying in the motion plane, with the X_R-axis through the masses and the Y_R- axis orthogonal to it through the mass center (Figure 1).

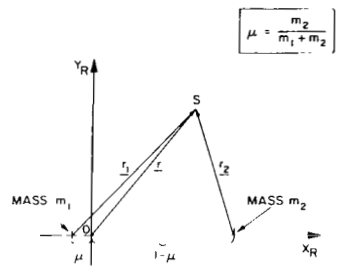

THE ROTATING COORDINATE SYSTEM (X_R, Y_R) USED FOR THE RESTRICTED PROBLEM OF THREE BODIES

Figure 1

The equations of motion for the third body (ref. 1) are as follows:

$$\ddot{\underline{r}} + 2\underline{\omega} \times \dot{\underline{r}} - \omega^2 \underline{r} = -\frac{Gm_1}{r_1^3}\underline{r_1} - \frac{Gm_2}{r_2^3}\underline{r_2} \qquad (1)$$

with m_1, m_2 being the masses, representing Earth E and Moon M, respectively; $\underline{r_1}$, $\underline{r_2}$ being the vectors from the masses to the third body; $\underline{r}$ being the vector from the mass center (origin) to the body; ω being the rate of rotation of the

system; and G being the gravitational constant. For ω the relationship holds

$$\omega^2 = \frac{G(m_1 + m_2)}{D^3} \tag{2}$$

with D being the distance between the two masses (Kepler's Third Law).

All representation in this report is done in normalized units. This means that the distance between the masses is unit length, the sum of the masses is unit mass, and the measure of the gravitational constant is unity. From this follows that the system rotation is at unit rate, which then determines also the time unit.

If the symbols are redefined to represent the normalized variables, the equations of motion read

$$\ddot{\underline{r}} + 2\underline{\omega} \times \dot{\underline{r}} - \omega^2 \underline{r} = -\frac{1-\mu}{r_1^3}\underline{r_1} - \frac{\mu}{r_2^3}\underline{r_2} \tag{3}$$

with the "mass ratio" μ being defined as

$$\mu = \frac{m_2}{m_1 + m_2} \tag{4}$$

The Jacobi Integral of this system can be written in the following form

$$V_R^2 = (1-\mu)\left(\frac{2}{r_1} + r_1^2\right) + \mu\left(\frac{2}{r_2} + r_2^2\right) - C \tag{5}$$

where C is the integration constant, which in this report will be referred to as the "Jacobi Constant".

All orbits depicted in this report are derived by numerical computation, using either the IBM 7094 or 360. Plotting is done on the Stromberg-Carlson 4020 using taped output of the computer.

The method of computation is based on the series-type special perturbation method as developed by R. Arenstorf (ref. 2) and for this application implemented by Berl Winston (ref. 3).

The computation of the zero-velocity curves is based on methods developed by J. McGann and P. Masucci (refs. 4 and 5).

FIRST LINE DIVISION OF E-M-ORBITS ACCORDING TO VALUES OF THE JACOBI CONSTANT C

Though the problem of this report is only two-dimensional, the dimension of possible variation of initial conditions, which is four, would imply a number of orbit-runs unmanageable to oversee and organize, if this variation is done for all initial conditions independently. This method also would result in many unnecessary duplications of orbits.

A more indigenous way of subdividing and organizing the problem solutions is found by making use of knowledge one possesses of the problem in analytical form. This is formulated in the Jacobi Integral (Eq. 5).

An exploitation of this integral can be made in various ways:

(a) The Jacobi-Integral yields a relationship between position and velocity magnitude for any point of an orbit.

(b) In relation to the task of structuring and classifying the solutions of the restricted problem, the integral provides the most natural means of a first degree ordering of orbits. It simply suggests the definition of classes of orbits according to the value of the Jacobi constant C.

(c) For values of the Jacobi constant C larger than 3.00, the Jacobi integral defines Zero-Velocity curves, which separate the areas of existence of orbits from the "empty" areas. This property of the Jacobi Integral will be of great utility, in two respects: (1st) The procedure of surveying the orbits within a C-level will be based upon it. (2nd) A classification within a C-level will be derived from the "Keplerian" behavior of the E-M-orbits in levels of large C-values.

THE ZERO-VELOCITY CURVES AND THE EMPTY AREAS OF THE RESTRICTED PROBLEM OF THREE BODIES

For the benefit of those readers who are not familiar with the geometrical implications of the Jacobi Integral, these may briefly be discussed and illustrated.

If the integration constant C of the Jacobi Integral

$$(1-\mu)\left(\frac{2}{r_1} + r_1^2\right) + \mu\left(\frac{2}{r_2} + r_2^2\right) - C = V_R^2 \qquad (6)$$

is larger than 3, the velocity V_R assumes the value zero on curves of the (X_R, Y_R) plane. These curves represent boundary lines between areas of existence and areas where orbits do not exist with that particular C-value. The overall appearance of these "zero-velocity-curves" is depicted in Figure 2, for the C-values of 3.30; 3.20388; 3.18720; 3.10; 3.02484; 3.010 and 3.0010.

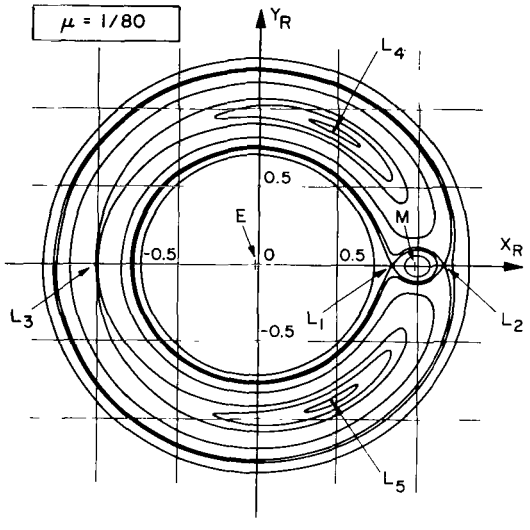

RESTRICTED PROBLEM OF THREE BODIES:
CURVES OF ZERO ORBITAL VELOCITY
FOR VARIOUS INTEGRATION CONSTANTS C
OF THE JACOBI INTEGRAL

Figure 2

For better visualization as well as future reference, the areas delineated by various Zero-Velocity curves are illustrated separately on the following six figures, Figures 3 to 8. The shaded areas are areas of non-existence of orbits for that particular value of the integration constant C.

The first of these six figures, Figure 3, shows that for C = 3.30 orbits exist in three separate regions, a "terrestrial", a "lunar" and an "outer" region.

With decrease of the Jacobian constant to C = 3.20388 the terrestrial and lunar regions increase such that they touch each other (see Figure 4). The point of tangency is marked as L_1, which is also one of the collinear equilibrium points.

The succeeding example (Figure 5) shows the instant where contact occurs between the outer region and the inner region (which latter consists of the terrestrial and lunar region).

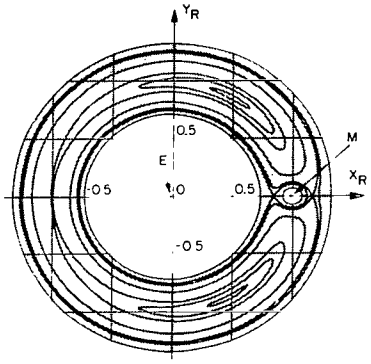

SHADED AREA IS EMPTY OF ORBITS OF JACOBI CONSTANT C=3.30

Figure 3

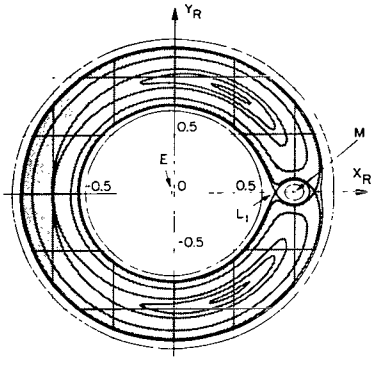

SHADED AREA IS EMPTY OF ORBITS OF JACOBI CONSTANT C=3.20388

Figure 4

The point of first contact is again a dynamically important point, i.e., the translunar collinear equilibrium point L_2.

Figure 6 shows the development progressed so far that the gate between inner and outer region of existence has opened considerably. This situation corresponds to the integration constant C = 3.100.

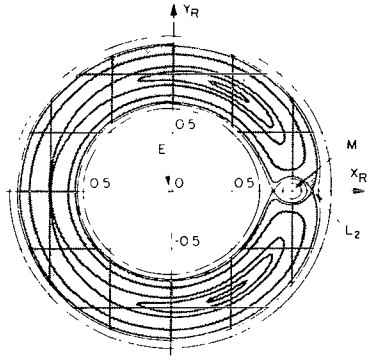

SHADED AREA IS EMPTY OF ORBITS OF JACOBI CONSTANT C=3.1872

Figure 5

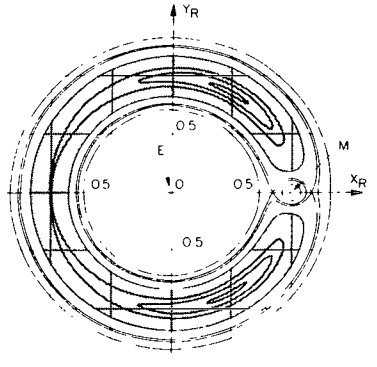

SHADED AREA IS EMPTY OF ORBITS OF JACOBI CONSTANT C=3.10

Figure 6

Figure 7 then illustrates the point of C-curve development at which the third gate at L_3 starts to open. The corresponding C-value is C = 3.02484. From this point on, the empty area is split into two separate areas that are reflective to each other with respect to the X_R-axis.

The last figure of this group (Figure 8) shows an advanced stage of separation of the two empty areas. Its C-value is 3.010.

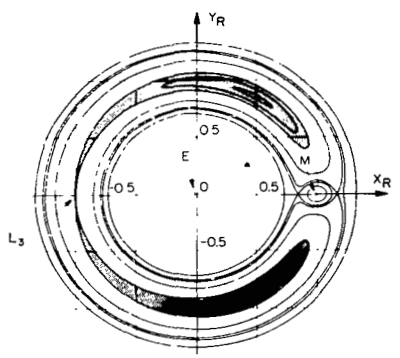

SHADED AREA IS EMPTY OF ORBITS OF JACOBI CONSTANT C=3.02484

Figure 7

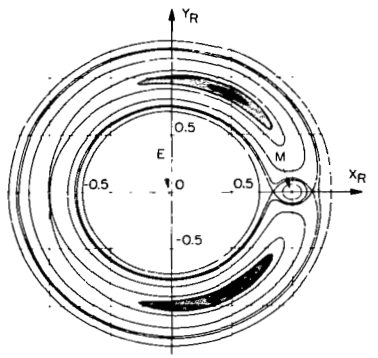

SHADED AREA IS EMPTY OF ORBITS OF JACOBI CONSTANT C=3.010

Figure 8

For a value of C = 3.00 these two parts degenerate to a single point each (L_4 and L_5), which are equilateral to the masses. These two points represent the only stable ones of the five equilibrium points.

As mentioned before, the boundary curves of the orbit areas for a given C-value are curves on which all orbits of that particular value of Jacobi constant assume zero velocity. If C_1 is larger than $C_0 \geq 3$, the boundaries of the orbit areas of C_1 lie in the interior of the C_0-areas and constitute for C_0-orbits curves of constant velocity, with the magnitude calculated from the formula

$$V_R^2 = C_1 - C_0. \tag{7}$$

Since the use of the term "zero-velocity curve" is appropriate only for particular curves, once the C-value is chosen, this report will refer to the curves of equal velocity within an orbital area as to "isotachs". The term "C-curves" will also be used for isotachs.

The possible use of the isotachs as one set of new orthogonal coordinates may, at this place, only be mentioned.

SUBCLASSIFICATION OF ORBITS WITHIN A CONSTANT-C-LEVEL DEMONSTRATED ON KEPLER ORBITS OF C = 4.00

The principle of classifying the orbits within a constant-C-level is now derived from phenomena observable for Kepler orbits that are represented in a rotating coordinate system.

The formulation of the Kepler problem in rotating coordinates can immediately be deduced from the equations listed before by reducing the smaller of the two masses to zero. This is expressed in $\mu = 0$. Their motion and integral are described by the following equations:

Kepler Motion in rotating coordinates:

$$\ddot{\underline{r}} + 2\underline{\omega} \times \dot{\underline{r}} - \omega^2 \underline{r} = -\frac{1}{r^3}\underline{r} \tag{8}$$

Jacobi Integral for Kepler Motion:

$$V_R^2 = \frac{2}{r} + r^2 - C \tag{9}$$

with r being the distance from the mass, which is located at the origin.

For the Kepler problem the zero velocity curves are concentric circles, and the regions of motions for $C > 3$ are an inner and outer region of the plane, separated by a circular ring-shaped area which is empty of orbits for the C-value chosen. The empty ring-shaped area degenerates into the circle of unity radius for $C = 3$. Figure 9 displays the boundary lines of the two areas of existence of orbits for the four values of $C = 3.30$; 3.10; 3.01; and 3.00.

To introduce the classification principle, a value for C will be chosen that is still larger than those shown on the graph, namely $C = 4.0$. For this value the inner region is bounded by the circle of radius .539 and the outer region comprises all points of the plane with radius larger or equal to 1.675.

It is evident that Kepler orbits of the inner region assume their apocenters and those of the outer region assume their pericenters. Also, their shapes are independent of their alignments or "orientations" with respect to the axes (X_R, Y_R).

Therefore, for the two regions a complete survey of Kepler orbits is obtained, if the orbits of the inner region are ordered

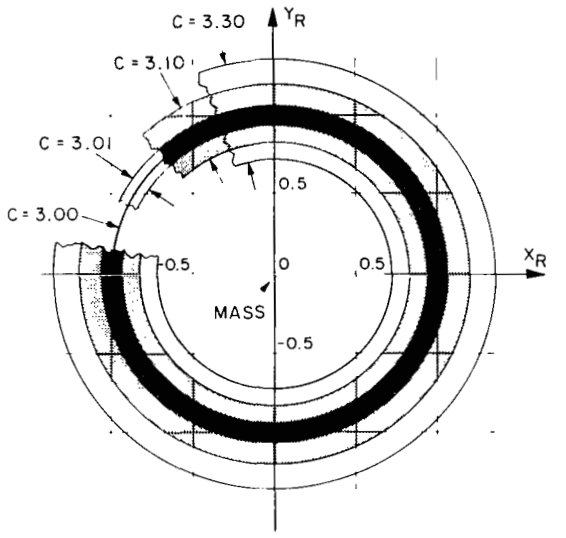

KEPLER PROBLEM IN ROTATING COORDINATES
CURVES OF ZERO ORBITAL VELOCITY
FOR VARIOUS INTEGRATION CONSTANTS C
OF THE JACOBI INTEGRAL

Figure 9

with their apocenters along the positive X_R-axis and those of the outer region are ordered with their pericenters along this axis branch. This procedure allows the identification ("tagging") of any orbit by the X_R-axis position of its apo- or pericenter, i.e., by values of a one-dimensional parameter. There is a duality of orbits with each value of this parameter, however, since the direction of the velocity vector at an apsidal point can be chosen twofold.

In the following this method of ordering will be carried through. In the course of it the subclassification of the orbits will become evident.

Selecting first the inner region and apocenters whose velocity vectors are directed in positive Y_R-direction, a class of orbits can be defined in the following way. The very first orbit is that whose apocenter lies at the border and therefore shows zero-velocity there. Orbits then are chosen by varying the initial position toward the mass center with velocities increasing in magnitude in accordance with the Jacobi integral for C = 4.0. The behavior of this class and its termination is best discussed in Figure 10. The first orbit on Figure 10 is that marked "A", forming a cusp at the border and then moving about the center in a "direct" sense of revolution. Its time history is shown to a length that just covers its pericenter. The same orbit is shown for a longer time history in Figure 11.

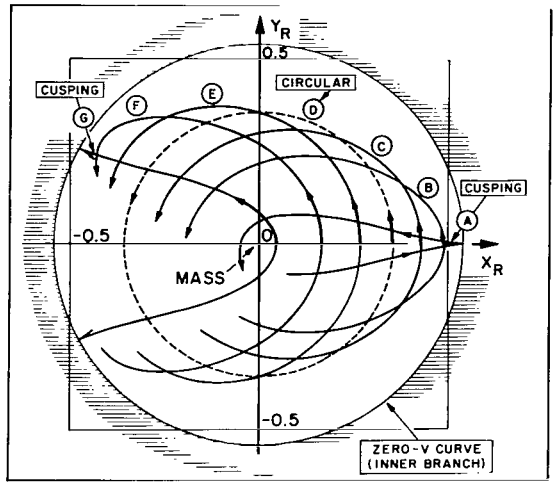

KEPLER ORBITS OF JACOBI CONSTANT C = 4.0
CLASS I : INNER REGION ORBITS
WITH PROGRADE MOTION AT APSES

Figure 10

Orbits "B" and "C" on Figure 10 are orbits with apocenters moved further in. With respect to their pericenters one observes that these move further out. Orbit "B" is individually shown on Figure 12.

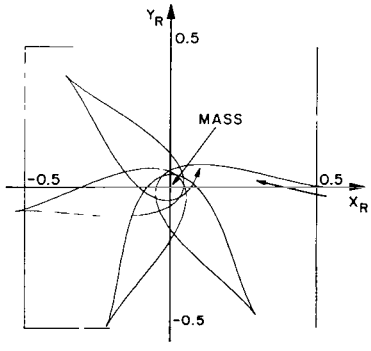

KEPLER ORBIT; C = 4.0; CLASS I & II
X_R = 0.53919; Y_R = 0.0; V_R = 0.0
TIME SHOWN : 4.505; CUSPING

Figure 11

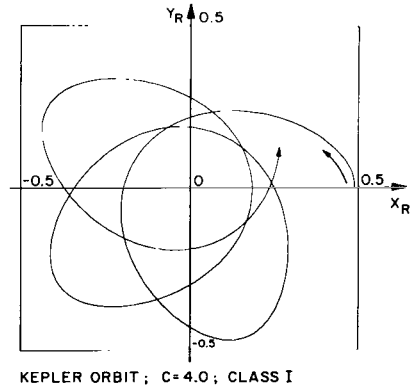

KEPLER ORBIT; C = 4.0; CLASS I
X_R = 0.490; Y_R = 0.0
$\dot{X}_R$ = 0.000; $\dot{Y}_R$ = 0.56721
TIME SHOWN : 4.5

Figure 12

Apocenter and pericenter have identical radii for the orbit "D", which, in fact, is a circular orbit.

Orbits whose initial points are moved still further inside, will have points outside the circular orbit "D", as is demonstrated

on orbits "E", "F", and "G". This means that these orbit types have been encountered before, except for their orientation which is ignored here.

All orbit shapes between and including orbit "A" and the circular "D" (or if one prefers, between "A" and "G") are now said to form a subclass to the Kepler orbits of C = 4. These orbits have at all times the direct sense of motion, on account of which one could call the class: the direct class. It is felt, however, that the term "direct" is somewhat weak as class-description, whence the term "prograde" will be used instead in this report. Also this word seems to be an appropriate parallel to the term "retrograde".

It may be noted that the apsidal positions (apocenters and pericenters) of the prograde class do not fully occupy the total positive segment of the X_R = axis within the inner region.

There is a finite interval left free between the pericenter of orbit "G" and the origin. This will be occupied by the orbits of the next class.

To develop the second class, again the cusping orbit "A" is taken as initial orbit, and apocenters are chosen starting at the boundary circle and moving toward the interior. However, now the velocity direction at the apocenters is to be retrograde.

The development and the extent of this class can be seen on Figure 13. Characteristic of this class is the change of sense of motion found within every orbit of the class i.e., retrograde motion at apocenter and prograde motion at pericenter. The class is bordered on one side by the cusping orbit and on the other side by the orbit that impacts the mass (Orbit "K" of Figure 13). Two orbits of this class are shown for extended time histories on Figures 14 and 15.

The changing sense of motion of the orbits gives rise to defining this class as the class of ambigrade orbits of the inner region of the Kepler orbits of C = 4.0.

The third class, depicted on Figure 16, is then characterized by containing all orbits whose sense of revolution is retrograde at all points on their orbits. It therefore is called the class of retrograde orbits. This class starts with orbit "K", itself being the limit between this and the former class, and continues to the circular orbit "N". Orbits starting inside "N" with retrograde direction belong still to the class, but duplicate shapes that are encountered before. One example of a retrograde orbit for an extended time period is exhibited on Figure 17.

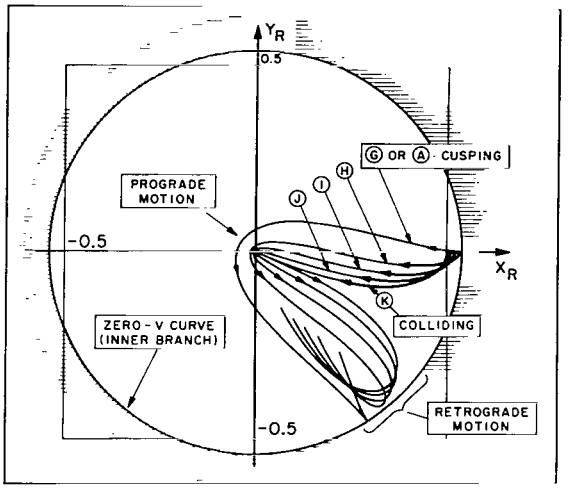

Figure 13

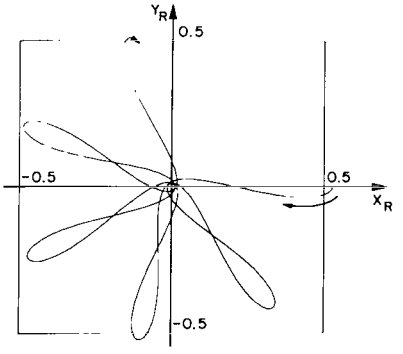

KEPLER ORBIT: C = 4.0; CLASS II
X_R = 0.530; Y_R = 0.000
$\dot{X}_R$ = 0.000; $\dot{Y}_R$ = -0.23342
TIME SHOWN: 4.518

Figure 14

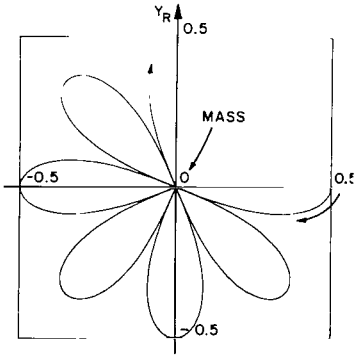

KEPLER ORBIT; C = 4.0; CLASS II & III
X_R = 0.500; Y_R = 0.000; COLLIDING
$\dot{X}_R$ = 0.000; $\dot{Y}_R$ = -0.500
TIME SHOWN · 4.514

Figure 15

The three defined classes take up all radial magnitudes of apocenters that are possible in the inner region (or also all possible pericenter magnitudes), ignoring the orbit orientation.

Of the three classes, the prograde and retrograde classes possess circular orbits. Also they may be considered "closed" in the sense that apocenter radii and pericenter radii form a continuum. Both characteristics cannot be ascribed to the class of ambigrade orbits of the inner region of Kepler orbits of C = 4.0.

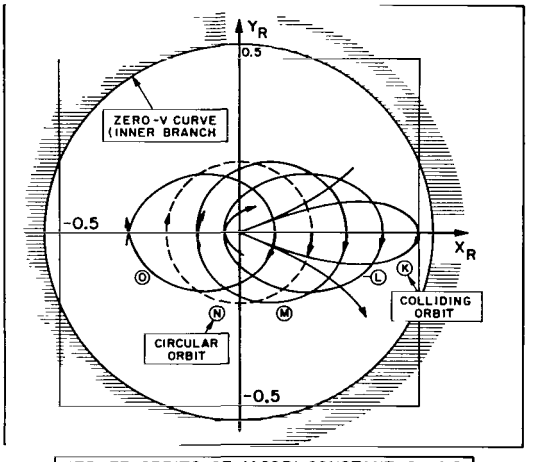

KEPLER ORBITS OF JACOBI CONSTANT C = 4.0
CLASS III: INNER REGION ORBITS
WITH RETROGRADE MOTION AT APSES

Figure 16

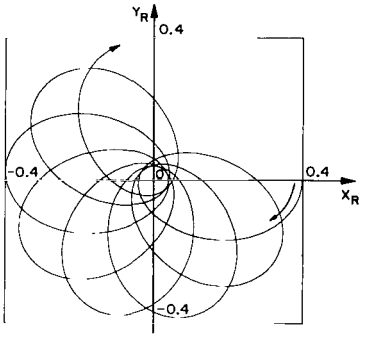

KEPLER ORBIT: C = 4.0; CLASS III
X_R = 0.400, Y_R = 0.000
$\dot{X}_R$ = 0.000; $\dot{Y}_R$ = -1.07703
TIME SHOWN: 4.515

Figure 17

For surveying the Kepler orbits of the outer region of C = 4.0, a procedure is applied that is quite similar to that used for the inner region: Restricting the pericenters to lie on the positive X_R-axis facilitates an "ordering" of the orbits by identifying the orbits with their pericenter locations on the positive X_R-axis. This procedure again leads to a useful classification of the orbits.

First all orbits with initially positive velocity direction ($\dot{Y}_R \geq 0$) may be chosen. The pericenter location is varied from the smallest possible value toward infinity. Figure 18 displays three

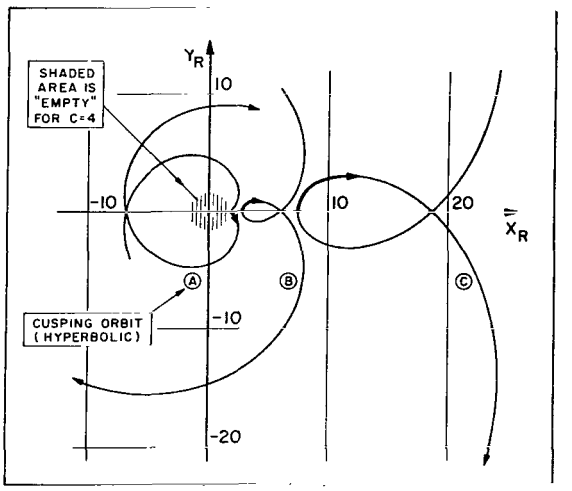

KEPLER ORBITS OF JACOBI CONSTANT C = 4.0
CLASS IV: OUTER REGION ORBITS WITH PROGRADE MOTION AT APSES

Figure 18

orbit examples. Orbit "A" is the orbit that has a cusp on the outer zero-velocity curve, i.e., on the inner border of the outer region. All orbits, started on points further out, (see orbits "B" and "C"), move first prograde and later retrograde, maintaining the latter direction for all time after. Hence, the class is ambigrade. All orbits of this class are hyperbolic orbits, if studied in reference to an inertial system.

Figure 19 displays a longer time-history of the orbit "B" of this class.

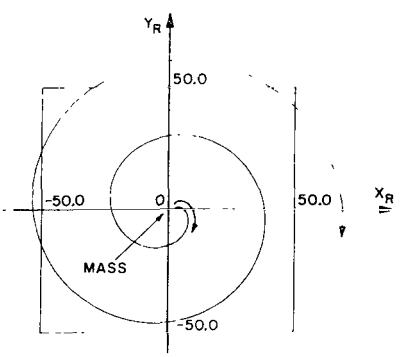

KEPLER ORBIT · C = 4.0, CLASS IV
X_R = 2.800, Y_R = 0.000
$\dot{X}_R$ = 0.000; $\dot{Y}_R$ = 2.13408
TIME SHOWN · 14.27

Figure 19

The orbits of the outer region that start in retrograde direction can be subdivided into two classes. Those with pericenter nearest to the border (r = 1.675) are still hyperbolic. For pericenters located at radii larger than 2.00, the orbits are finite, i.e., elliptical with respect to an inertial system. The hyperbolic and the elliptic retrograde classes are represented in selected orbits on Figures 20 and 21. It is important to observe that the elliptic retrograde class produces a circular orbit and that this class may also be considered "closed" in the sense mentioned before.

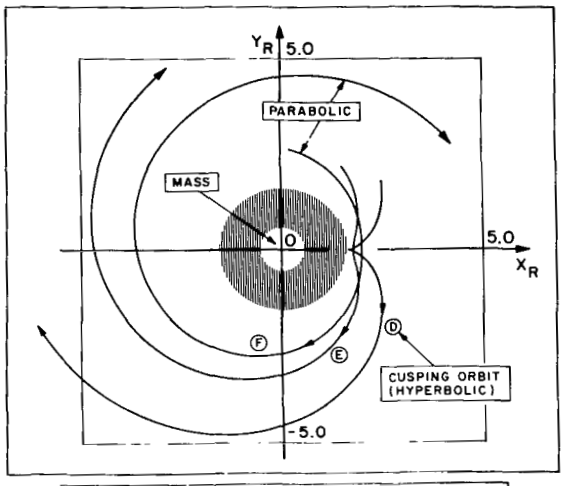

KEPLER ORBITS OF JACOBI CONSTANT C = 4.0
CLASS V: OUTER REGION ORBITS: RETROGRADE - HYPERBOLIC

Figure 20

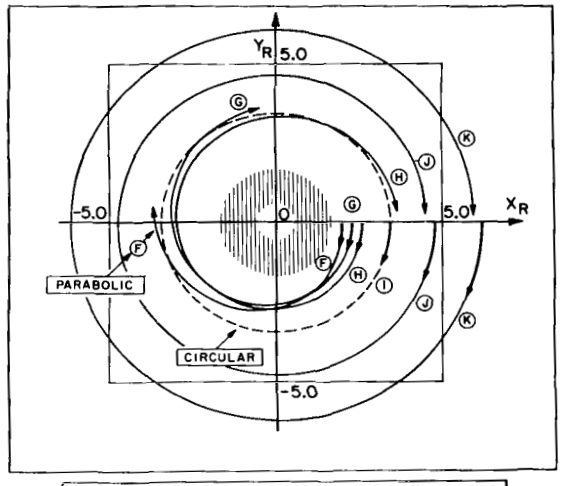

KEPLER ORBITS OF JACOBI CONSTANT C = 4.0
CLASS VI: OUTER REGION ORBITS RETROGRADE-ELLIPTIC

Figure 21

Two examples of the last class are illustrated individually on Figures 22 and 23.

The orbit patterns that have been discussed in this chapter for the Kepler problem and the classifications introduced will now be the basis for pattern classifications of orbits of the Earth-Moon (E-M) problem.

Though the orbital patterns of the E-M problem will increasingly deviate from the "Keplerian" patterns as the study moves toward smaller values of the Jacobi constant C, the reference to the patterns of Kepler orbits will prove to be a very convenient handle for getting descriptively hold of the patterns of E-M flight.

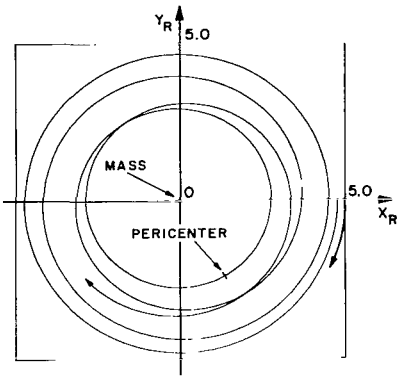

KEPLER ORBIT: C = 4.0; CLASS VI
X_R = 4.800, Y_R = 0.000
$\dot{X}_R$ = 0.000; $\dot{Y}_R$ = -4.41097
TIME SHOWN: 32.56

Figure 22

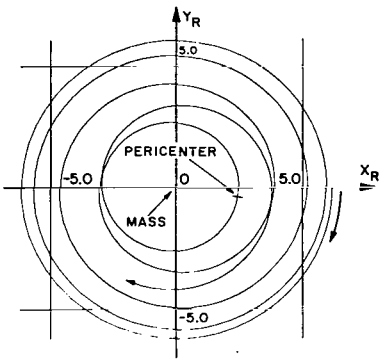

KEPLER ORBIT: C = 4.0; CLASS VI
X_R = 6.200; Y_R = 0.000
$\dot{X}_R$ = 0.000; $\dot{Y}_R$ = -5.89598
TIME SHOWN: 38.57

Figure 23

E-M-ORBITS OF JACOBI CONSTANT C = 4.00

With the value of the Jacobi constant C as high as 4.00, there is still a close similarity of orbits of the E-M problem to those of the Kepler orbits in regions where they can be compared. There is, of course, a third region, i.e., the lunar region, for the E-M problem.

Orbits of the terrestrial region are first shown for short-time histories on Figures 24 to 26 for the three classes of prograde, ambigrade, and retrograde orbits. Aside from the slight shift that is caused by the change in position of the mass, a deviation from the corresponding Kepler figures is hardly recognizable.

The similarity between the two problems for this region is confirmed by the examples of long-time histories that are shown on the next five graphs. The first four of them, Figures 27 to 30, concern the prograde class. The sequence is arranged so as to bring out the contraction that occurs in the width of the ring-shaped area in which each orbit moves. The process of contraction ends with the formation of a single-loop orbit, called "central" for obvious reasons. Its deviation from a circular shape is hardly detectable by visual inspection. (Note that the meaning of the term "central" is not coinciding with that used in Danby's book FUNDAMENTALS OF CELESTIAL MECHANICS.)

The class of retrograde orbits of the terrestrial region is represented by three long-history orbits (Figure 31). This time recourse was taken to superimposing all three orbits on each other to bring out the phenomenon of class development by contraction, starting from the collision orbit and ending with achieving the "central" orbit of retrograde sense of motion.

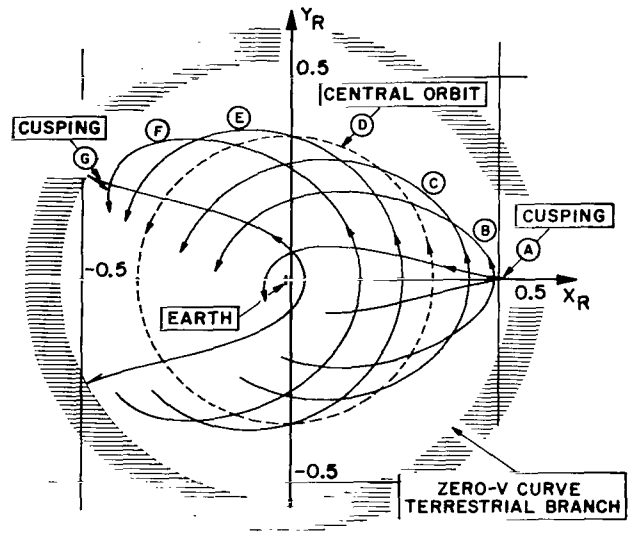

E-M ORBITS OF JACOBI CONSTANT C= 4.0
CLASS I: ORBITS OF TERRESTRIAL REGION WITH PROGRADE MOTION AT APSES

Figure 24

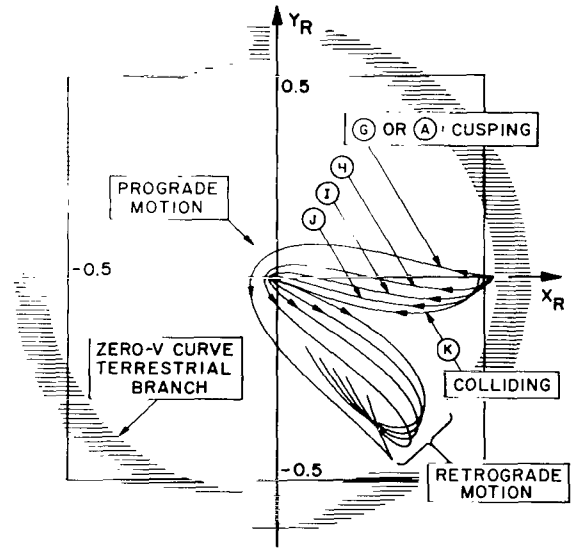

E-M ORBITS OF JACOBI CONSTANT C = 4.0
CLASS II: ORBITS OF TERRESTRIAL REGION WITH AMBIGRADE MOTION AT APSES

Figure 25

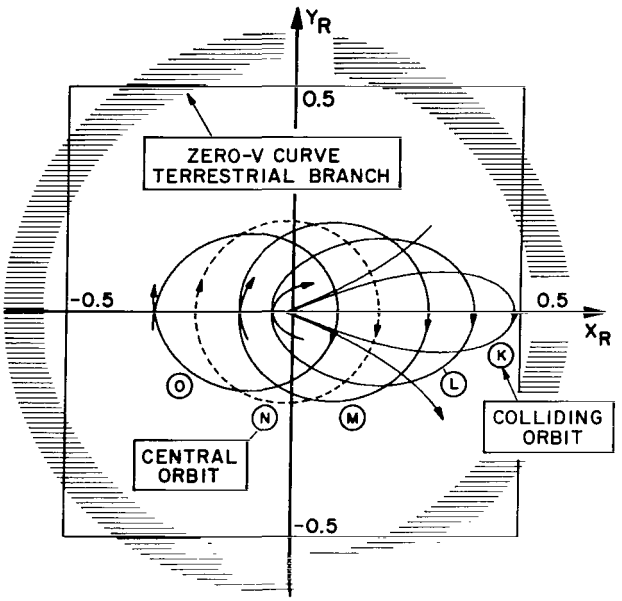

E-M ORBITS OF JACOBI CONSTANT C = 4.0
CLASS III: ORBITS OF TERRESTRIAL REGION WITH RETROGRADE MOTION AT APSES

Figure 26

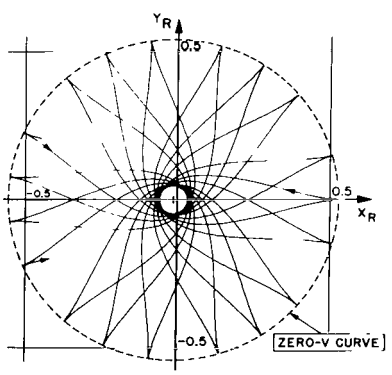

E-M ORBIT OF JACOBI CONSTANT C = 4.0
CUSPING ORBIT Ⓐ OF ORBIT CLASS I

Figure 27

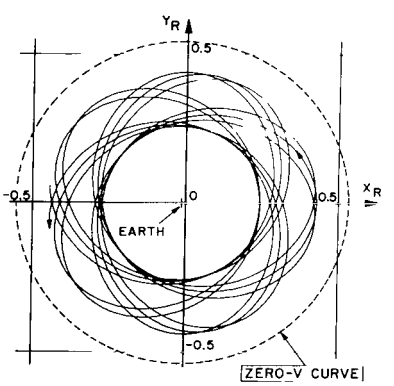

E-M ORBIT OF JACOBI CONSTANT C = 4.0
ORBIT Ⓒ OF CLASS I

Figure 28

For the ambigrade class, which also is quite similar to its Kepler-model, the showing of long-time history orbits was dispensed with.

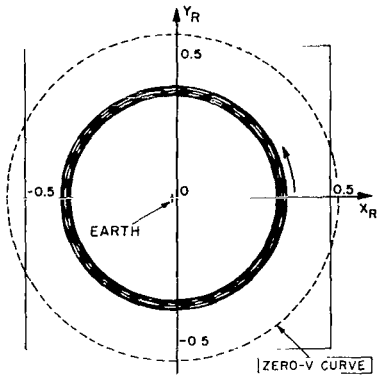

E-M ORBIT OF JACOBI CONSTANT C=4.0
ORBIT OF CLASS I

Figure 29

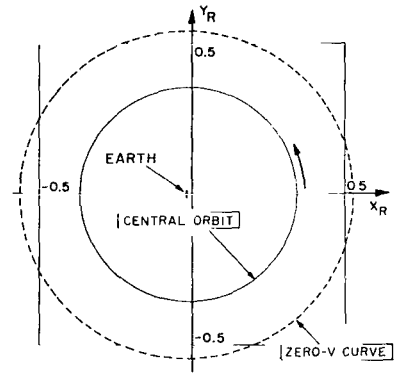

E-M ORBIT OF JACOBI CONSTANT C=4.0:
CENTRAL ORBIT ⓪ OF CLASS I

Figure 30

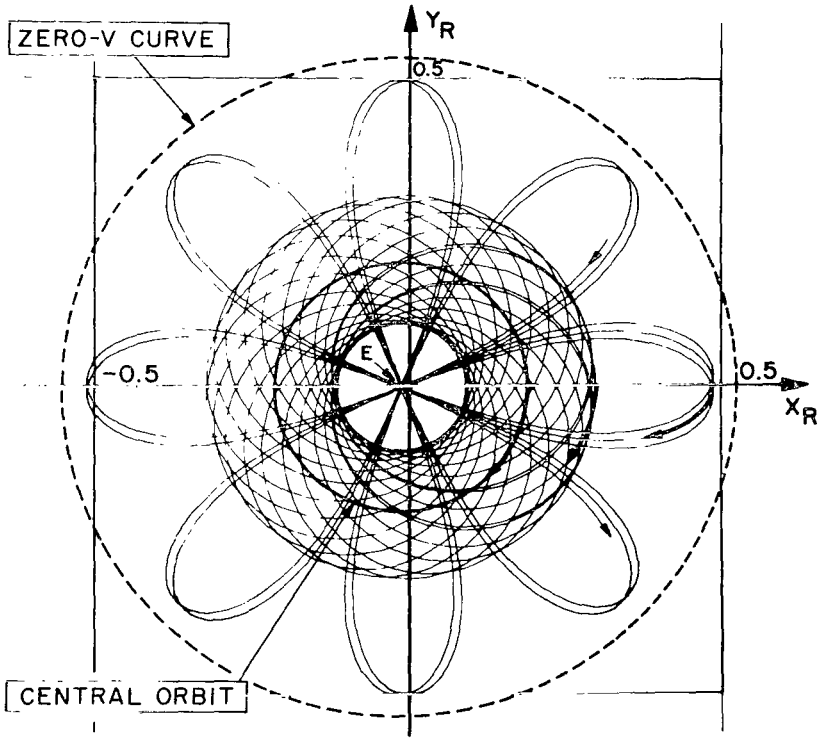

E-M ORBITS OF JACOBI CONSTANT C=4.0:
ORBITS Ⓚ, Ⓜ, Ⓝ OF ORBIT CLASS III

Figure 31

The behavior of the E-M orbits of the outer region of motion for C = 4.00 is represented on Figures 32 to 34. These figures closely resemble the corresponding figures of Kepler Motion.

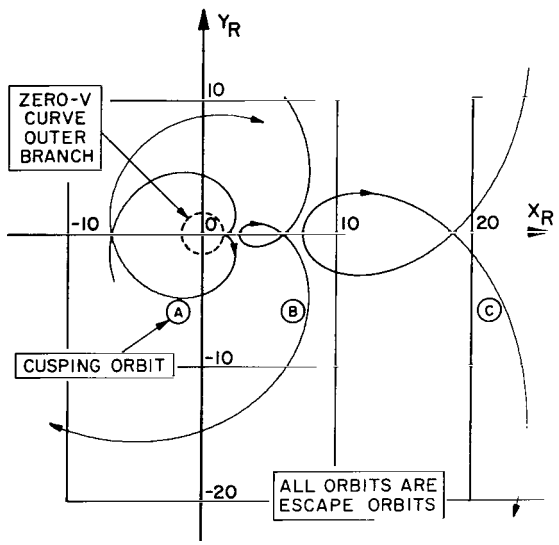

E-M ORBITS OF JACOBI CONSTANT C = 4.0
CLASS IV : OUTER REGION ORBITS WITH PROGRADE MOTION AT APSES

Figure 32

It may be mentioned that the terminology of conic sections cannot truly be applied to E-M orbits, for which reason the information is given in terms of "bounded" and "escaping". The isolation of orbits that represent the border between bounded and escaping orbits is not straightforward. This will become clearer when outer orbits will be discussed on the next lower C-level.

For the class of bounded orbits, one observes the existence of a central orbit.

The succeeding three figures, Figures 35 to 37, are concerned with motion in the lunar region. To appreciate the behavior of the orbits, one has to be aware that the diameter of the lunar region is not larger than 0.05 units, and that the consequent closeness of the motion to the lunar mass causes very short periods of revolution. The comparatively slow revolution of the moon about the origin then effects a slow "backward walking" of the loops.

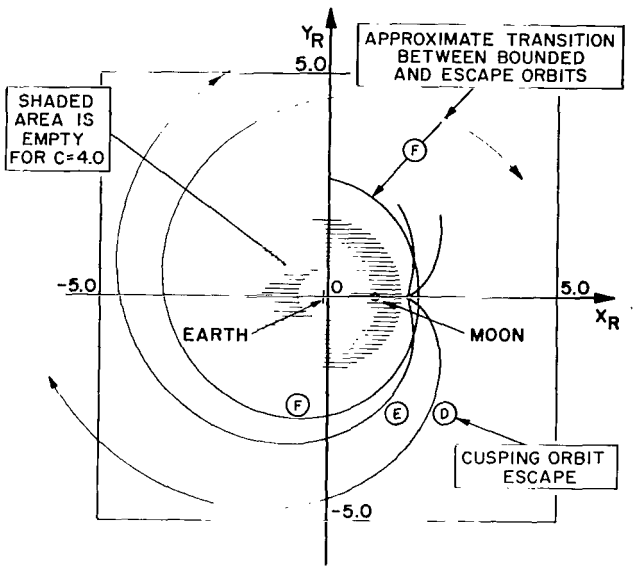

E-M ORBITS OF JACOBI CONSTANT C = 4.0

CLASS V : OUTER REGION ORBITS : RETROGRADE ESCAPE ORBITS

Figure 33

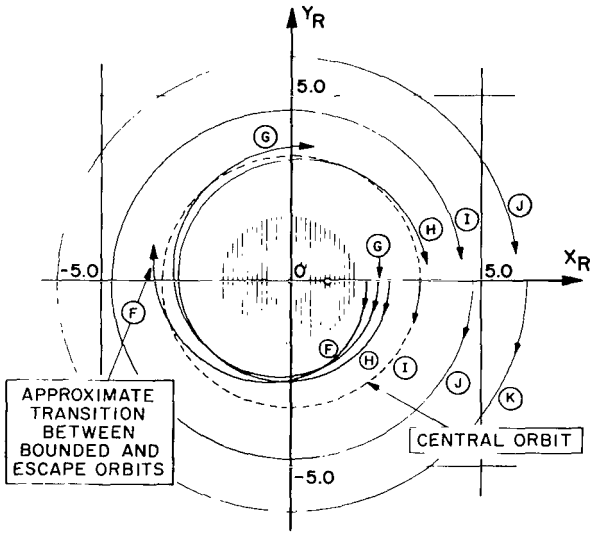

E-M ORBITS OF JACOBI CONSTANT C = 4.0

CLASS VI : OUTER REGION ORBITS RETROGRADE BOUNDED ORBITS

Figure 34

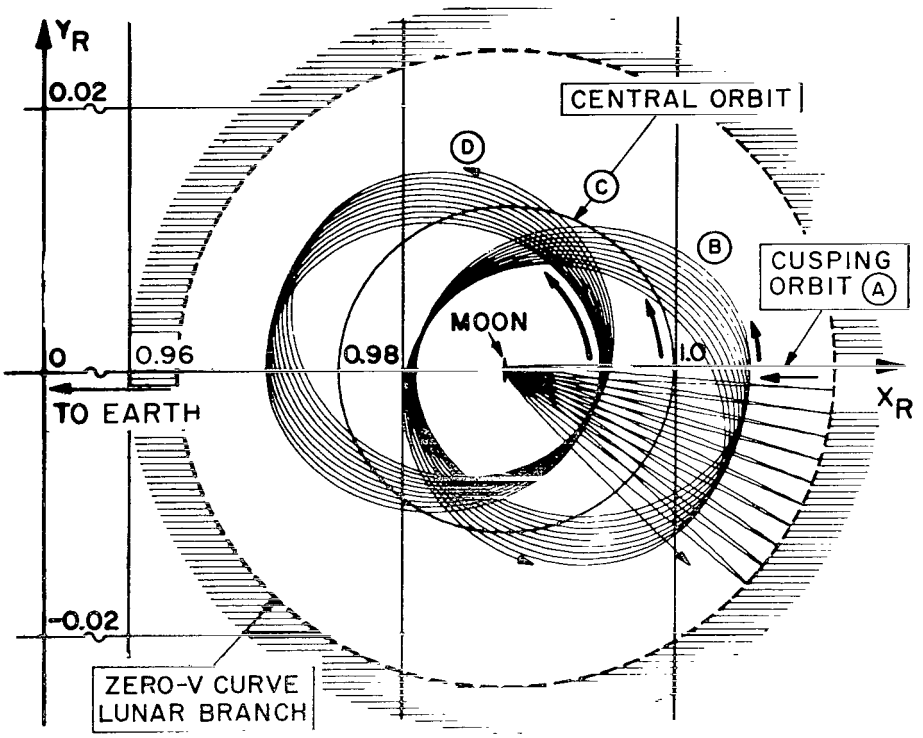

E-M ORBITS OF JACOBI CONSTANT C=4.0

CLASS VII: LUNAR REGION ORBITS WITH PROGRADE MOTION

Figure 35

The same fact is also responsible for the scanty-only appearance of ambigrade orbits in the lunar region of C = 4.00. They will not be discussed for this C-level. (This is consistent with maintaining a certain grid size in the survey.)

Representations of the lunar prograde and retrograde classes are given on Figures 35 and 37. Geometrically the orbits "B", "C" and "D" of Figure 35 resemble orbits "F", "G", and "H" of Figure 37, but the motion on the second group is opposite to that on the first group.

Figure 36 displays again orbits A, B, C of Figure 35, but to much larger periods. This is done to demonstrate that the principle of contraction toward a central orbit holds also here quite well.

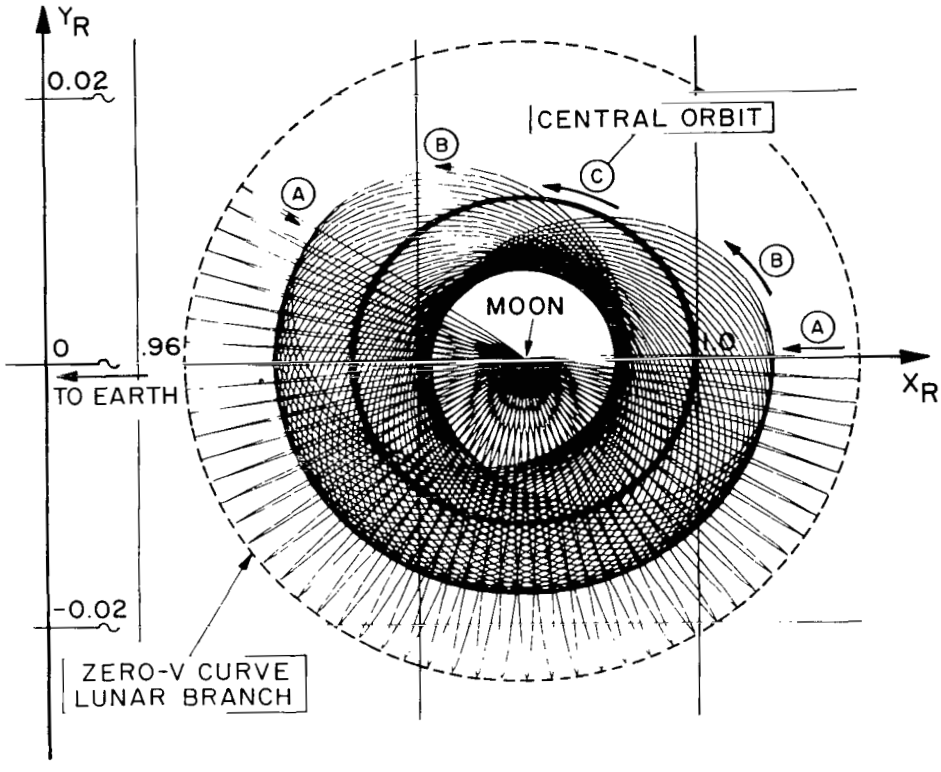

E-M ORBITS OF JACOBI CONSTANT C = 4.0

ORBITS OF CLASS VII SHOWN FOR EXTENDED TIME PERIODS

Figure 36

This last graph is significant for another reason. It gives the first demonstrable sign of a behavior different from Keplerian. This is observed on orbit "A" and i.e., on the patterns of the aposelenum points. At 0° and at 180°, as measured from the Moon positive upward from the positive X_R-axis, the points are cusps; with approaching minus 90° these apses become more rounded.

As one progresses to levels of smaller Jacobi constants, the deviations from a symmetrical pattern distribution become more pronounced.

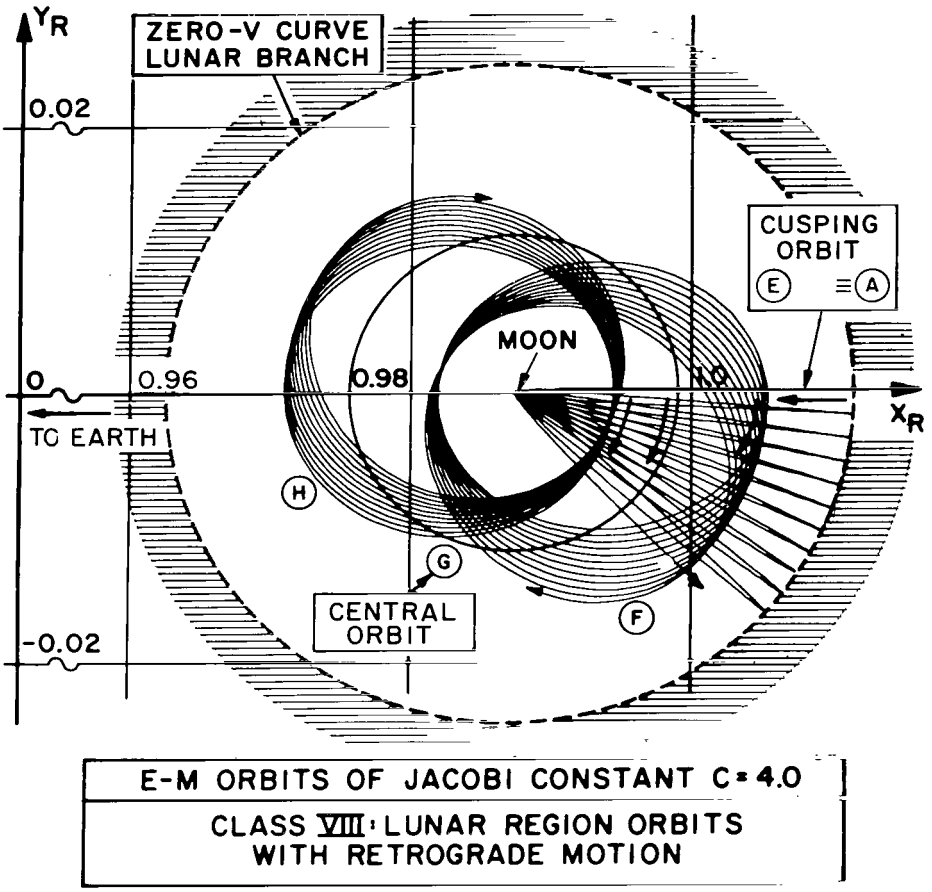

Figure 37

E-M-ORBITS OF JACOBI CONSTANT C = 3.20388 ≈ $C(L_1)$

The reason for selecting the value of C = 3.20388 as next in line of the levels to be studied is the occurrence of first contact between the terrestrial and the lunar region. The geometry of the boundary lines for this level is shown on Figure 38.

The procedure of investigation is, in general, that of the former chapter though the order in which the classes or orbits are discussed, will be different.

ORBITS OF THE TERRESTRIAL REGION

The retrograde class of the terrestrial region will be studied first. It is represented on Figure 39 in the fashion of the formerly used overviews, giving a series of short-period time

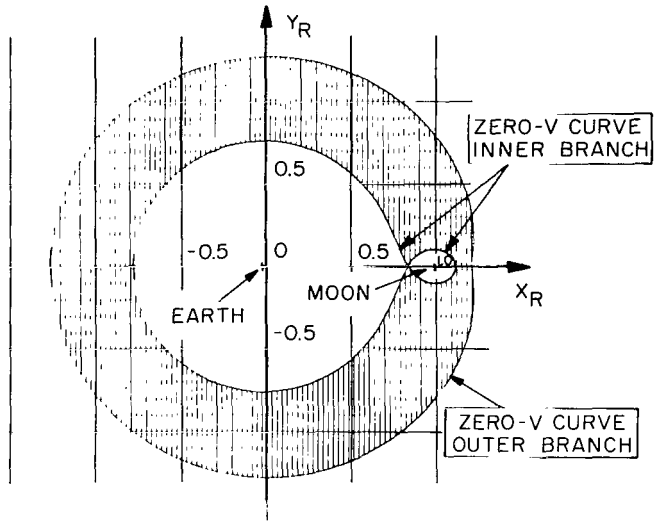

SHADED AREA IS EMPTY
OF ORBITS OF JACOBI CONSTANT C=3.20388

Figure 38

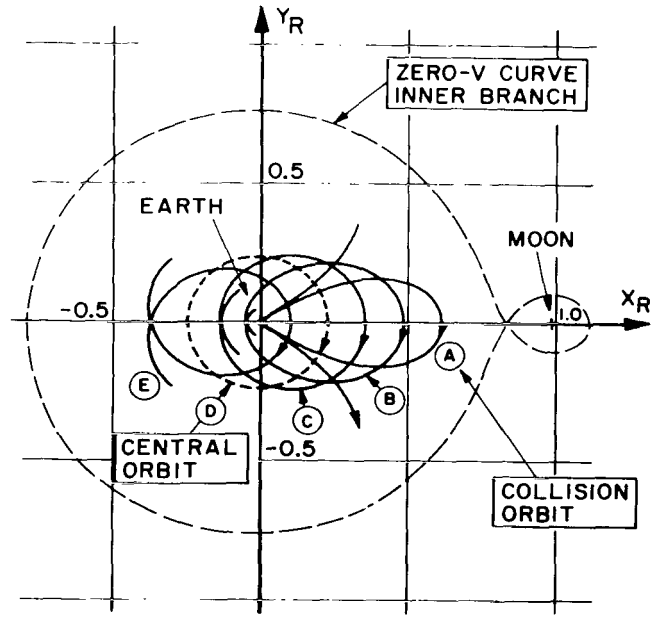

E.M. ORBITS OF JACOBI CONSTANT C=3.20388
CLASS OF ORBITS IN TERRESTRIAL REGION
WITH RETROGRADE MOTION AT APSES

Figure 39

histories. This graph serves also to bring the sizes of the orbits into perspective with that of the border-curve of the terrestrial region. Longer-time histories of selected orbits of this class are then presented in the following sequence of six graphs (Figures 40 to 45). Again this class is clearly defined by the collision orbit on one end of the development and the retrograde central orbit on the other end.

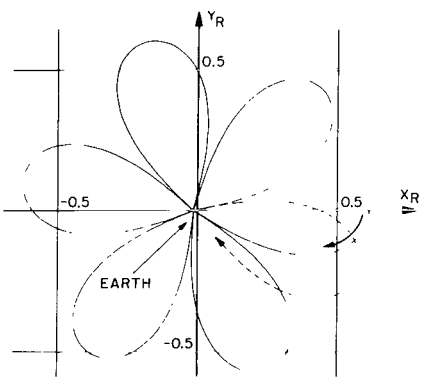

E.M. ORBIT OF JACOBI CONSTANT C=3.20388
COLLISION ORBIT (A) OF RETROGRADE CLASS
TIME SHOWN: 7.2

Figure 40

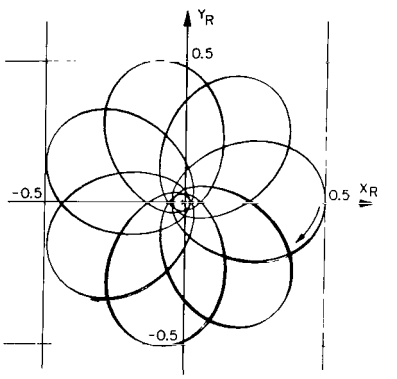

E.M ORBIT OF JACOBI CONSTANT C=3.20388
RETROGRADE ORBIT THROUGH (X_R=0.5; Y_R=0)
TIME SHOWN 15.0

Figure 41

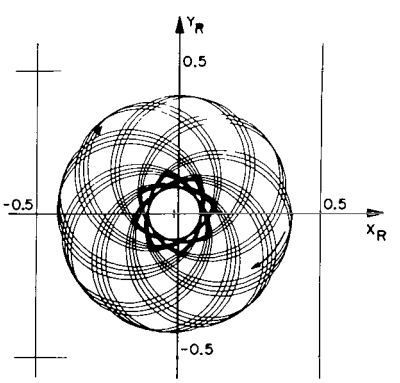

E.M. ORBIT OF JACOBI CONSTANT C=3.20388
RETROGRADE ORBIT THROUGH (X_R=0.4; Y_R=0)
TIME SHOWN: 23.0

Figure 42

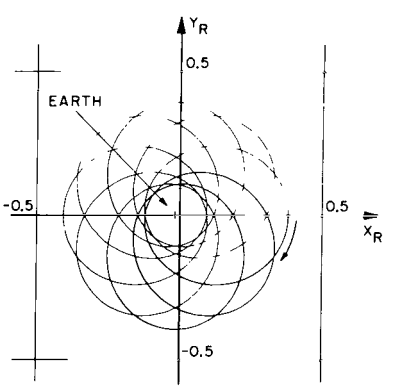

E.M. ORBIT OF JACOBI CONSTANT C=3.20388
RETROGRADE ORBIT THROUGH (X_R=0.38; Y_R=0)
PERIODIC WITH P=6.27

Figure 43

Attention is drawn to the orbits on Figures 42 and 43. The second of these is periodic, and the first of them can be looked upon as a perturbation to the periodic one. The behavior of the

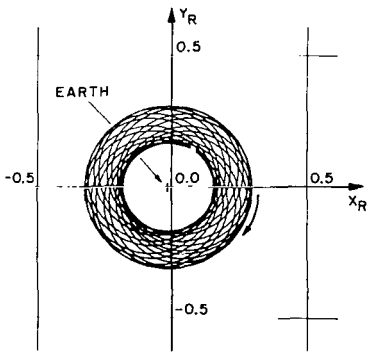

E.M. ORBIT OF JACOBI CONSTANT C=3.20388
RETROGRADE ORBIT THROUGH (X_R=0.30; Y_R=0)
TIME SHOWN: 13.0

Figure 44

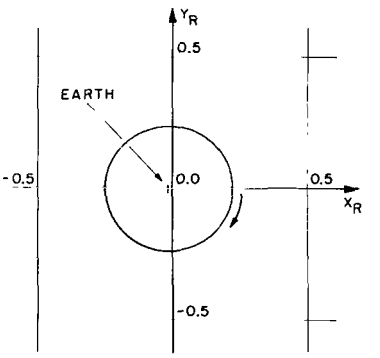

E.M. ORBIT OF JACOBI CONSTANT C=3.20388
CENTRAL ORBIT OF RETROGRADE CLASS
X_R=0.2261; Y_R=0; PERIOD P=0.660

Figure 45

perturbed orbit will be called "Keplerian", since the cycles, of which nearly three are shown, follow each other in regular and one-directional sequence. This is mentioned here, since soon perturbations will be encountered that exhibit different patterns.

The retrograde class is again represented on Figure 46, this time in superposition of three orbits. The dashed curve here represents the central orbit.

The prograde class of the terrestrial region is taken up next. Its short-period synopsis is exhibited on Figure 47. It is noticed that the prograde central orbit has considerably larger dimensions than its retrograde counterpart. To set this contrast out still stronger, the two central orbits are shown together on Figure 48. (For a comprehensive treatise on those orbits that are here listed as central, the reader is referred to Ref. 6.)

What follows now is the stepwise development of the prograde class, beginning with the central orbit on Figure 48. While the initial position of an orbit is pushed successively further out along the positive X_R-axis, the belt-shaped area of its orbital motion widens out consistently. The terminal orbit of this sequence (Figures 49 to 55) starts quite close to the point where the terrestrial and the lunar region meet. This orbit is pursued for a time period of 120 units, which corresponds to a time of about 17 months. On this same picture, the central orbit is superimposed for comparison.

In this group the reader will take notice of two features in which the orbits deviate from Keplerian orbits; i.e., first, in the overall shapes of the orbits which accommodate to the shape

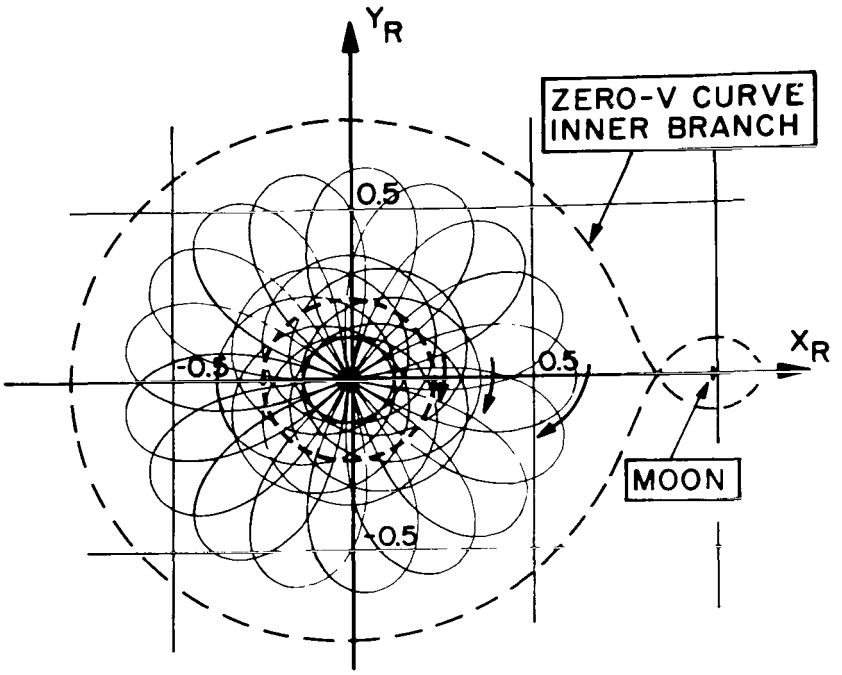

E.M. ORBIT OF JACOBI CONSTANT C=3.20388
THREE RETROGRADE ORBITS OF TERRESTRIAL REGION

Figure 46

of the zero-velocity curve; and secondly, in the seeming disorder that appears in the placement as well as shapes of the apogees of an orbit. The first of these features points to the proximity (in the C-level development) of orbits that commute between the terrestrial and lunar regions. The second feature is closely connected with the "fly-by" phenomenon. This phenomenon will be seen to influence the shape of orbits in other classes of this C-level and i.e., to a stronger measure than seen here.

For the ambigrade class of the terrestrial region of C = 4.0, the short-time overview is presented on Figure 56. Here seven orbits are shown that start in retrograde direction from the positive X_R-axis at points that increase in distance from the origin.

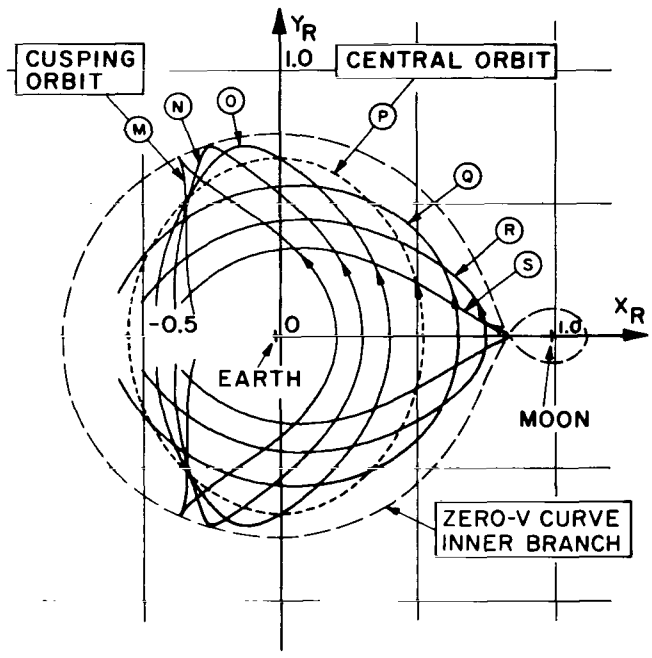

E.M. ORBITS OF JACOBI CONSTANT C= 3.20388
CLASS OF ORBITS IN TERRESTRIAL REGION WITH PROGRADE MOTION AT APSES

Figure 47

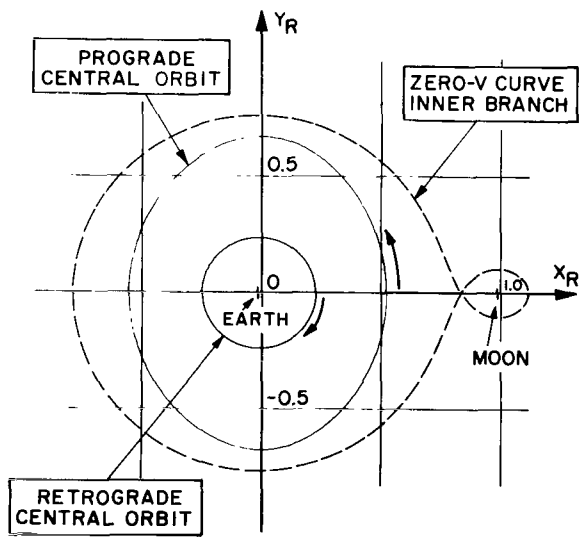

E.M. ORBITS OF JACOBI CONSTANT C = 3.20388
CENTRAL ORBITS OF TERRESTRIAL REGION
X_R=0.5227 WITH P=5.693 AND X_R=0.2261 WITH P=0.6600

Figure 48

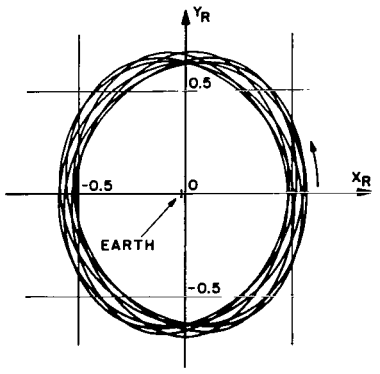

E.M. ORBIT OF JACOBI CONSTANT C = 3.20388
PROGRADE ORBIT THROUGH (X_R = 0.570; Y_R = 0)
TIME SHOWN · 39.58

Figure 49

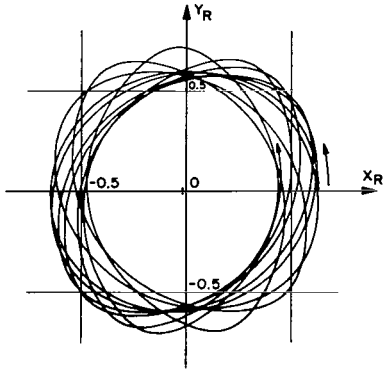

E.M. ORBIT OF JACOBI CONSTANT C = 3.20388
PROGRADE ORBIT THROUGH (X_R = 0.630; Y_R = 0)
TIME SHOWN · 50.0

Figure 50

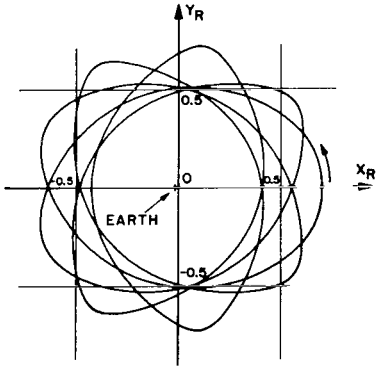

E.M. ORBIT OF JACOBI CONSTANT C = 3.20388
PROGRADE ORBIT THROUGH (X_R = 0.700; Y_R = 0)
TIME SHOWN · 26.20

Figure 51

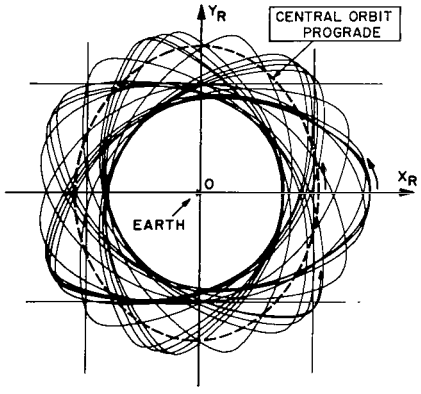

E.M. ORBITS OF JACOBI CONSTANT C = 3.20388
SUPERPOSITION OF CENTRAL PROGRADE ORBIT
AND PROGRADE ORBIT THROUGH (X_R = 0.750; Y_R = 0)
TIME SHOWN · 100 2

Figure 52

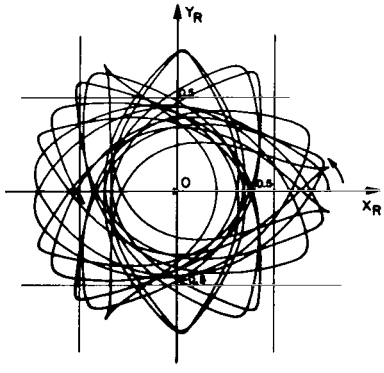

E.M. ORBIT OF JACOBI CONSTANT C = 3.20388
PROGRADE ORBIT THROUGH (X_R = 0.780; Y_R = 0)
TIME SHOWN · 69.84

Figure 53

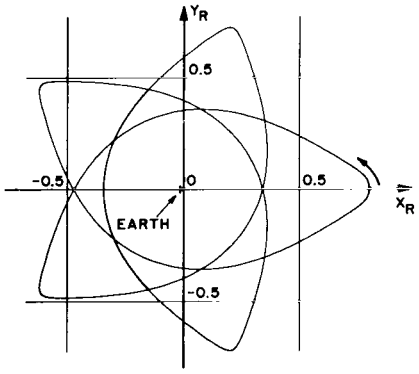

E.M. ORBIT OF JACOBI CONSTANT C = 3.20388
PROGRADE ORBIT THROUGH (X_R = 0.803; Y_R = 0)
PERIOD · 14.0

Figure 54

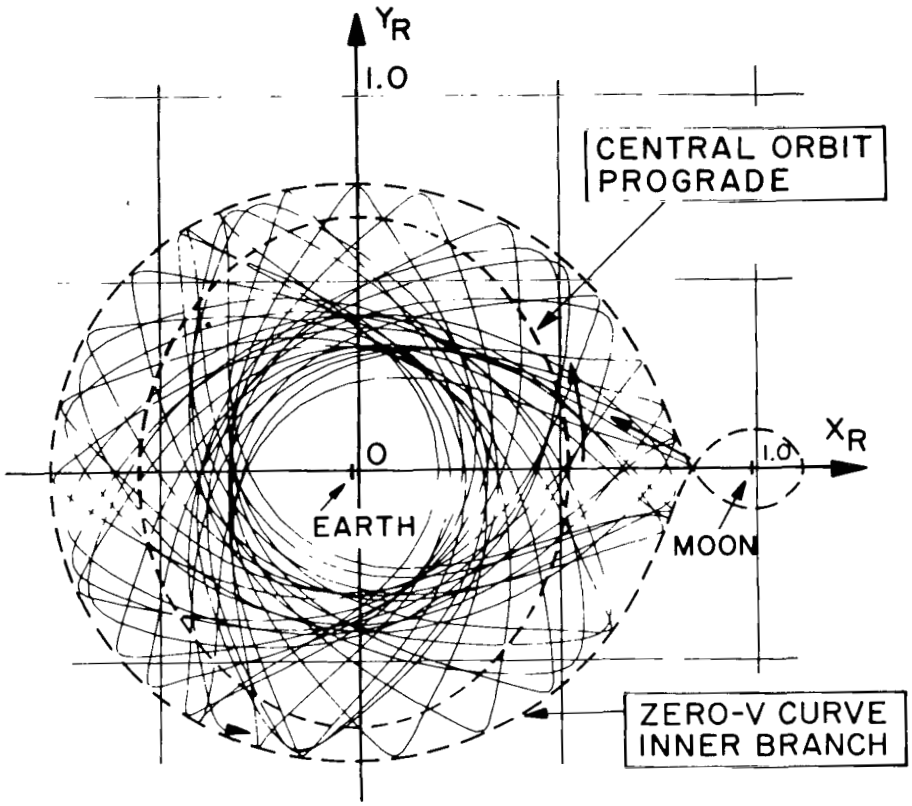

E.M. ORBITS OF JACOBI CONSTANT C = 3.20388

SUPERPOSITION OF CENTRAL PROGRADE ORBIT AND PROGRADE ORBIT WITH (X_R = 0.83; Y_R = 0)
TIME SHOWN: 120.0

Figure 55

Attention of the reader is here directed to the fact that the orbits which originate furthest out, do not regain their retrograde sense of motion, when they encounter their second apogee. As the figure demonstrates, orbit "K" is cusping and orbit "L" is prograding at the second apogee occurrence. This orbital behavior will soon be discussed in more detail.

The following three figures, Figures 57 to 59, represent the first examples concerned with probing directional effects, insofar as all orbits depicted originate at the same isotach, but at varied positions along the isotach. The problem can be formulated

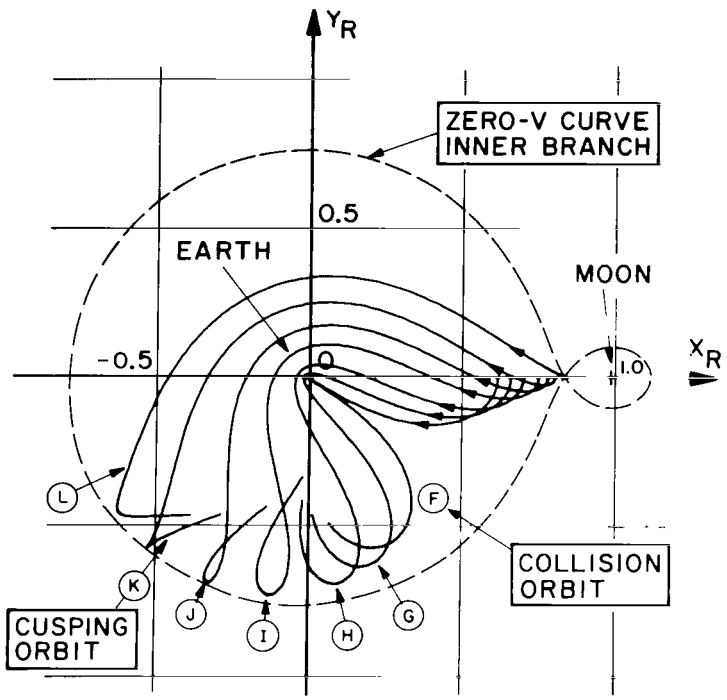

E.M. ORBITS OF JACOBI CONSTANT C = 3.20388

CLASS OF ORBITS IN TERRESTRIAL REGION
WITH AMBIGRADE MOTION AT APSES

Figure 56

as follows: If the orbit departure is at the zero-velocity curve (and therefore is in form of a cusp), will the succeeding apogee be a cusp? If not, toward which direction will the succeeding apogee change? For the present C-level, the three figures provide the answers:

(1) If both (first and second) apogees of an orbit are far away from the moon (say half an E-M distance), cusps indeed map into cusps. This is demonstrated on Figure 57.

(2) Orbits that have their arrival-apogee shortly ahead, and at, the positive X_R-axis, experience a change of apogee characteristics from cusps toward apogees of more retrograde motion. This is visible on orbits "3", "4", and "5" of Figure 58.

(3) With orbits that depart from points that trail, or are at, the positive X_R-axis, the departing cusps are mapped into apogees of more prograde motion. This is recognizable on orbits "5" and "6" of Figure 59.

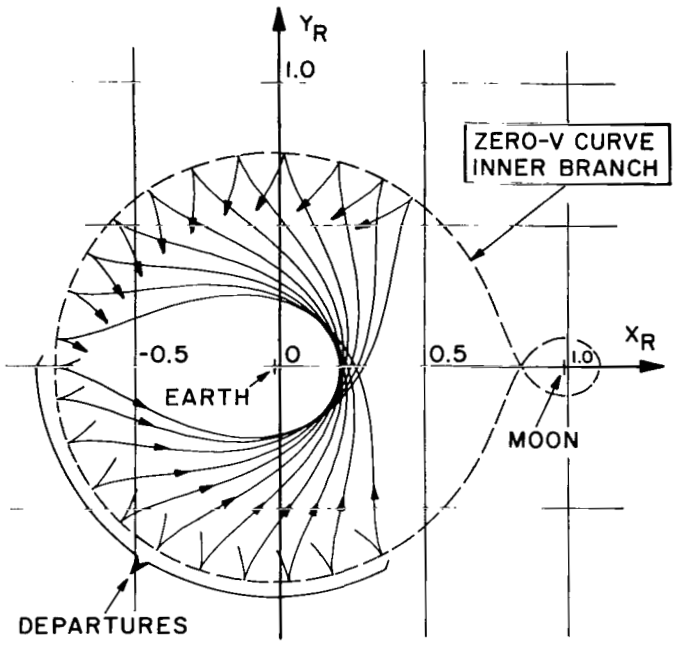

E.M. ORBITS OF JACOBI CONSTANT C = 3.20388
ORBITS THROUGH POINTS OF THE ZERO-V CURVE

Figure 57

The mapping characteristics of (2) and (3) correspond to the principle of reflection on the X_R-axis, valid for the present problem.

The effect that comes to light in these three pictures is, of course, attributable to the presence of the Moon, and can – popularly speaking – be considered as one form of "fly-by effect". Shortly an orbit will be depicted in which this effect is utilized in two directions.

For orbits that originate on isotachs other than the zero-velocity curve, these fly-by effects diminish, and i.e., the more, the further the isotach is removed from the border-curve.

There are several other interesting features that are peculiar to the class of ambigrade orbits. Since the phenomena, that are observable on this C-level, are symptomatic for the lower C-levels, they will here be introduced and discussed to some detail in the course of discussing individual orbits of this class.

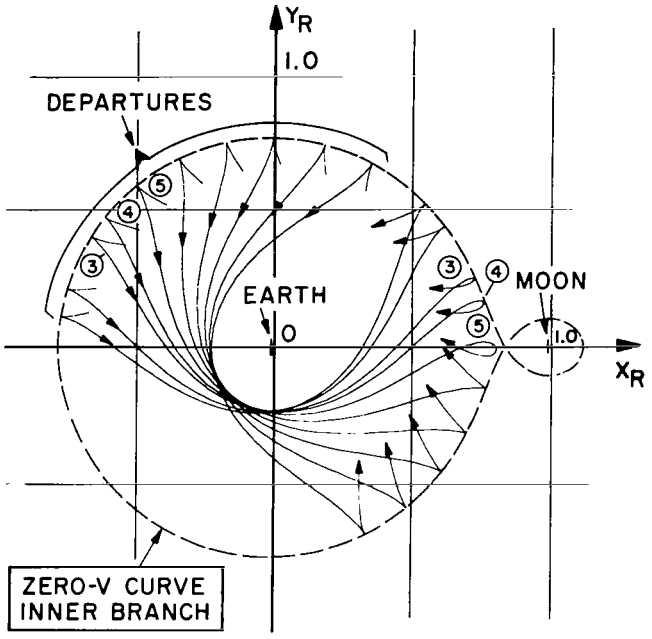

E.M. ORBITS OF JACOBI CONSTANT C = 3.20388
ORBITS THROUGH POINTS OF THE ZERO-V CURVE

Figure 58

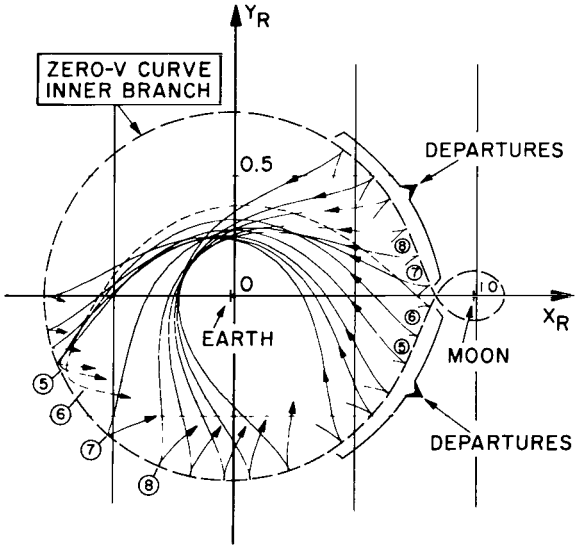

E.M. ORBITS OF JACOBI CONSTANT C = 3.20388
ORBITS THROUGH POINTS OF THE ZERO-V CURVE

Figure 59

An interesting deviation from the regular leaf-distribution, proper to Kepler orbits, may be observed on the orbit of Figure 60. This orbit (which is very close to a periodic one) shows a denser leaf-pattern in the axial directions than in the spaces between. This orbit is initiated at (X_R = -0.74; Y_R = 0) and is not far from a collision orbit.

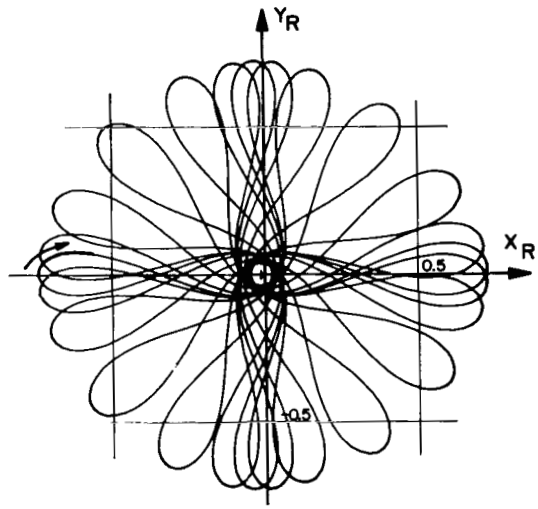

E.M. ORBIT OF JACOBI CONSTANT C=3.20388
AMBIGRADE ORBIT THROUGH (X_R=-0.74; Y_R=0)
TIME SHOWN: 38.27

Figure 60

The progression of orbits will now follow an increase of the initial point toward larger negative values on the X_R-axis: The orbits on Figures 61 and 62 are initiated at X_R = -0.760 and -0.770. The first of these is near a periodic orbit that exhibits seven leaves. The second of these is shown for continuity reasons.

If the initial point is moved a small distance, i.e., to the value of (X_R = -0.772, Y_R = 0), an orbit is generated that exhibits the fly-by effect and associated pattern changes very satisfactorily. The orbit is shown on Figures 63 to 65. The first shows the total orbit, which for practical purposes can be taken as periodic, with the time period of 44.4 units. The fly-by occurs with the apogee "A" and later again with the apogee "Q", which is symmetrically located to "A". The effect of the two

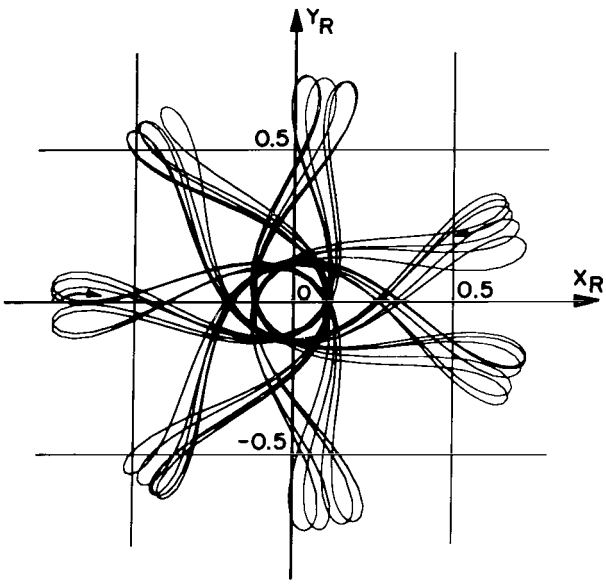

E. M. ORBIT OF JACOBI CONSTANT C = 3.20388
AMBIGRADE ORBIT THROUGH (X_R =-0.760; Y_R = 0)
TIME SHOWN : 60.0

Figure 61

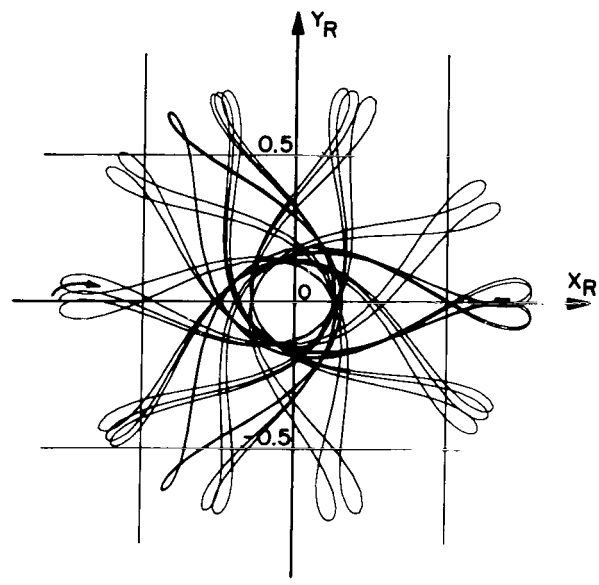

E. M. ORBIT OF JACOBI CONSTANT C = 3.20388
AMBIGRADE ORBIT THROUGH (X_R =-0.770; Y_R = 0)
TIME SHOWN : 60.0

Figure 62

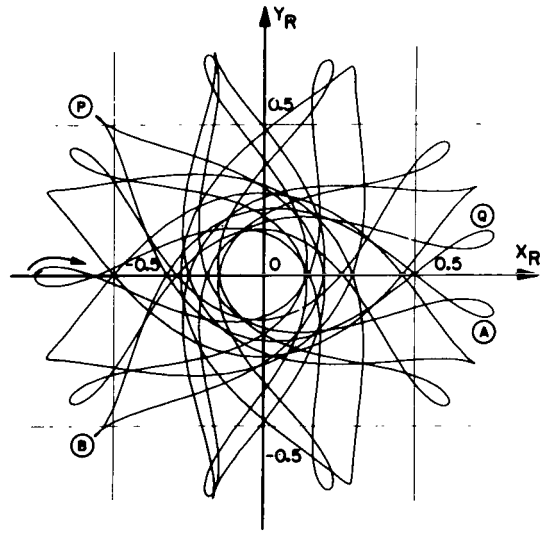

E. M. ORBIT OF JACOBI CONSTANT C = 3.20388
AMBIGRADE ORBIT THROUGH (X_R = -0.772; Y_R = 0; θ_R = 90°)
TIME SHOWN : 44.4

Figure 63

fly-bys on the orbit is brought into clearer perspective on the two following figures. On Figure 64 one follows the orbit through five apogees of nearly equal shape, till "A" is reached. Succeeding this occurrence, the apogee loop is contracted to nearly a cusp, here labeled "B". The next figure, Figure 65, resumes the orbit history at "A" and traces it till the mirror-image at "Q" is reached. All apogee-events between "A" and "Q" are, indeed, occurring in shapes that are close to a cusp.

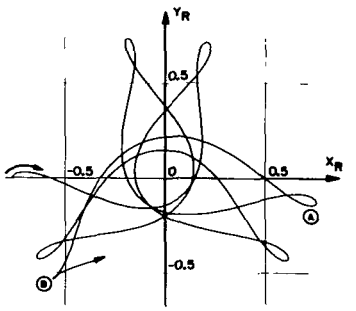

E.M. ORBIT OF JACOBI CONSTANT C = 3.20388
AMBIGRADE ORBIT THROUGH (X_R=-0.772; Y_R=0; θ_R=90°)
TIME SHOWN: 12.6

Figure 64

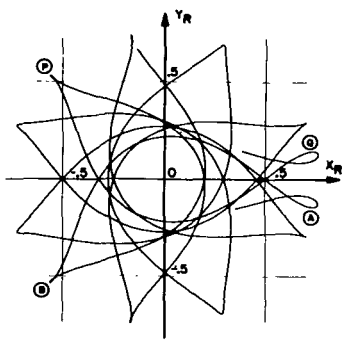

E.M. ORBIT OF JACOBI CONSTANT C = 3.20388
AMBIGRADE ORBIT THROUGH (X_R=-0.772; Y_R=0; θ=90°)
TIME SHOWN: FROM 8.82 TO 35.43

Figure 65

The decomposition of the full orbit into two well-chosen parts demonstrates also that an orbital behavior can frequently be better understood if the orbit is properly dissected.

The succeeding five orbits display a particular stability behavior, which reminds of the behavior of an undamped pendulum (Figures 66 to 70). Reference may first be taken to Figure 67. It illustrates a three-leaf periodic orbit. The four orbits on the remaining four graphs are orbits that are initiated at X_R-values quite close to that of the reference orbit. These four orbits may, in fact, be considered as perturbations to the reference orbit. The behavior of the four orbits is uniform, in that they all exhibit pendulum motions of their apogees about the apogee positions of the reference orbit. For the convenience of the reader, the apogee events are numbered in sequence of their occurences on two of the orbits.

The orbit of the last of the five graphs terminates the first sequence of ambigrade orbits, insofar as its initial condition is at the zero-velocity curve (X_R = -0.782404; Y_R = 0).

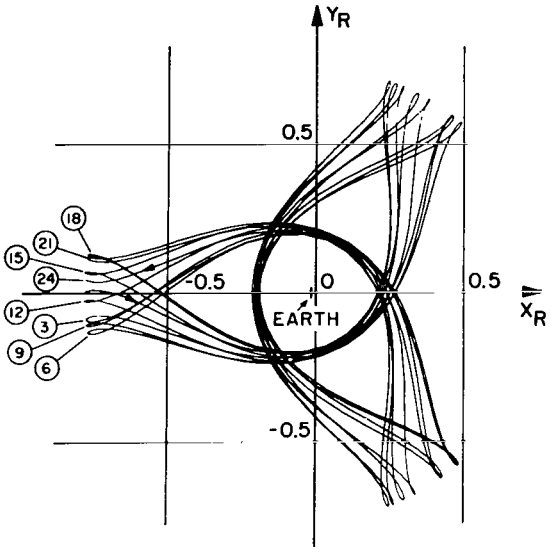

E. M. ORBIT OF JACOBI CONSTANT C = 3.20388
AMBIGRADE ORBIT THROUGH (X_R=-0.780; Y_R=0)
TIME SHOWN: 50.10

Figure 66

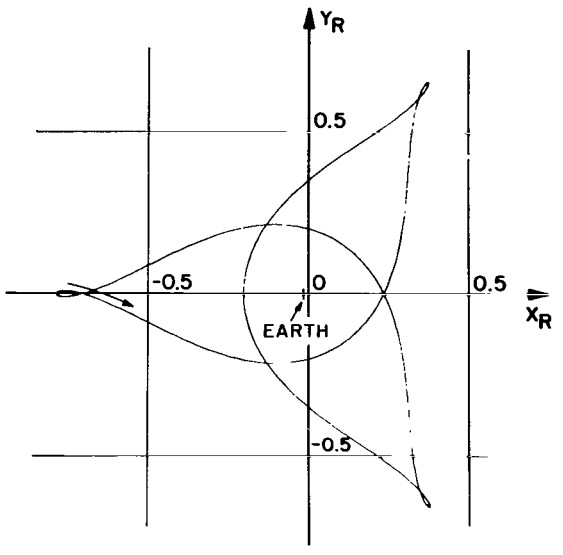

E. M. ORBIT OF JACOBI CONSTANT C = 3.20388
AMBIGRADE ORBIT THROUGH (X_R=-0.78106; Y_R=0)
PERIOD: 6.255

Figure 67

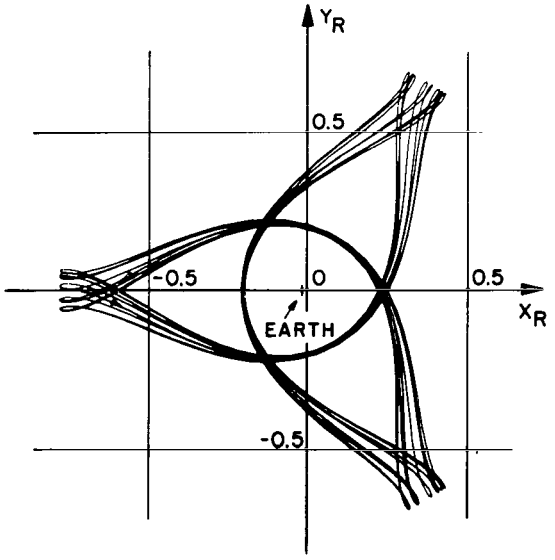

E. M. ORBIT OF JACOBI CONSTANT C = 3.20388
AMBIGRADE ORBIT THROUGH (X_R=-0.7815; Y_R=0)
TIME SHOWN: 50.08

Figure 68

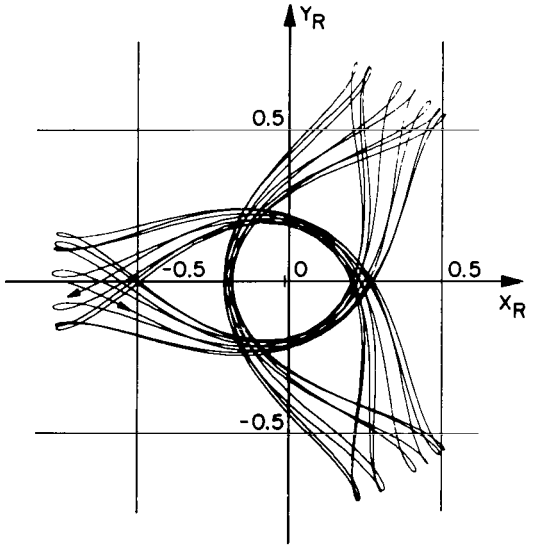

E. M. ORBIT OF JACOBI CONSTANT C = 3.20388
AMBIGRADE ORBIT THROUGH (X_R=-0.7820; Y_R=0)
TIME SHOWN: 50.05

Figure 69

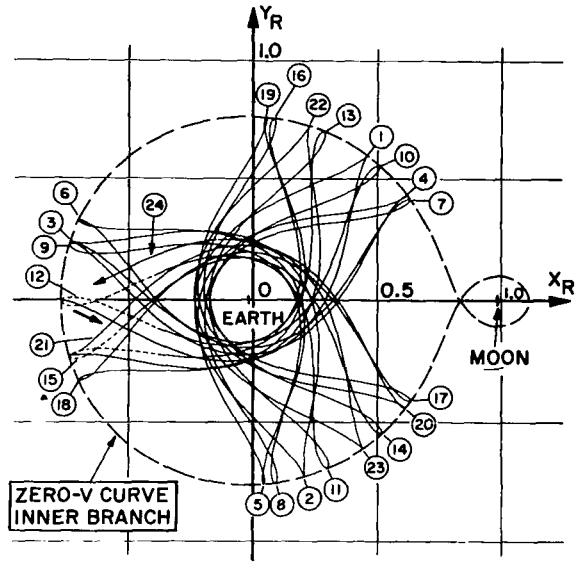

Figure 70

The points of orbit initiation are next chosen on the positive branch of the X_R-axis.

Figure 71 gives an example of a rather well-behaved orbit, in the sense of Keplerian behavior. Figures 72 and 73 depict identical orbits, shown, however, for different times. They represent another example of pattern-changes due to fly-by which occurs with the apogee labeled 19.

The orbits on the remaining four figures, Figures 74 to 77, serve well to expose a stability behavior that is strikingly different from that discussed before. The reference orbit is here again a three-leaf orbit (Figure 75). Very small variations are then made in the initial X_R-value. The effect is a brief stay of the orbit in the neighborhood of the reference orbit, followed by a rapid spreading of the apogee events into other directions.

The comparison of this group with the group of orbits shown around the orbit of Figure 67 points toward the significance of the alignment of an orbit as a criterion for its stability behavior.

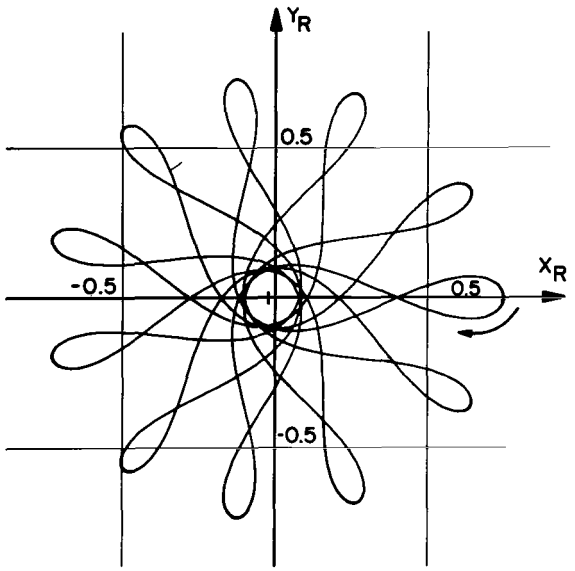

E.M. ORBIT OF JACOBI CONSTANT C = 3.20388
AMBIGRADE ORBIT THROUGH (X_R = 0.750 ; Y_R = 0) PERIOD P = 18.92

Figure 71

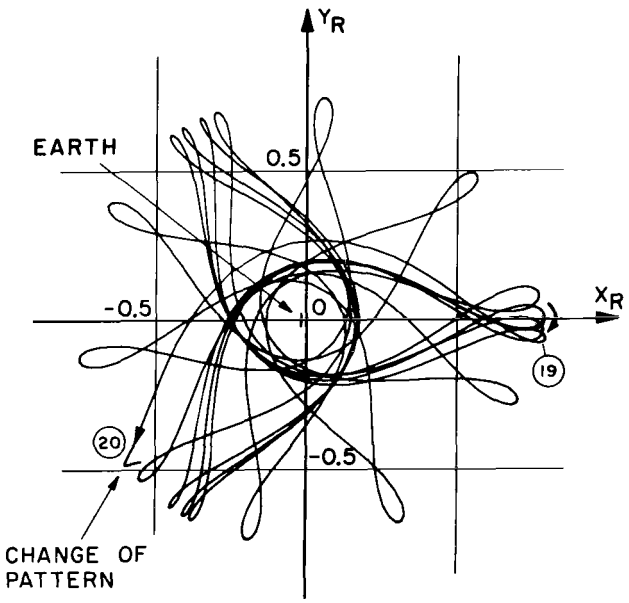

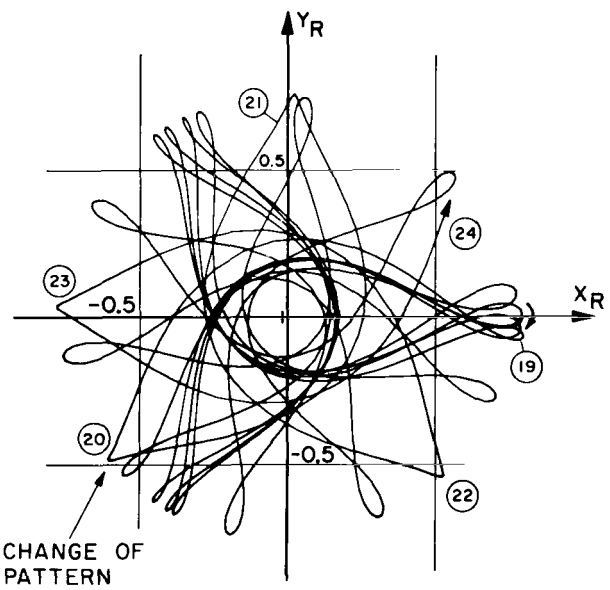

E.M. ORBIT OF JACOBI CONSTANT C = 3.20388
AMBIGRADE ORBIT THROUGH (X_R = 0.790; Y_R = 0) TIME SHOWN : 41.5

Figure 72

E.M. ORBIT OF JACOBI CONSTANT C = 3.20388
AMBIGRADE ORBIT THROUGH (X_R = 0.790; Y_R = 0) TIME SHOWN : 50.0

Figure 73

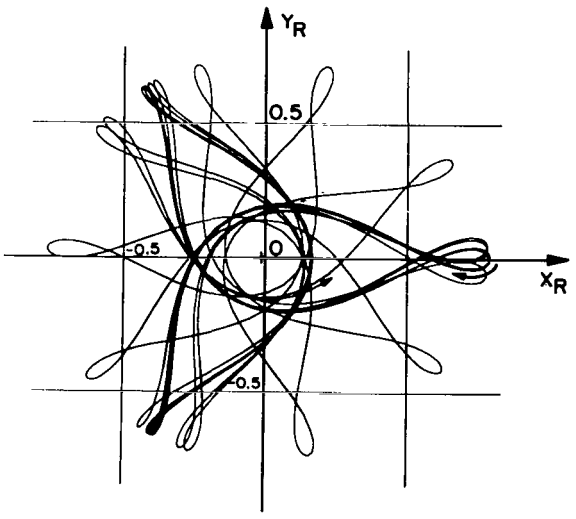

E. M. ORBIT OF JACOBI CONSTANT C = 3.20388
AMBIGRADE ORBIT THROUGH (X_R = 0.79012; Y_R = 0)
TIME SHOWN: 50.02

Figure 74

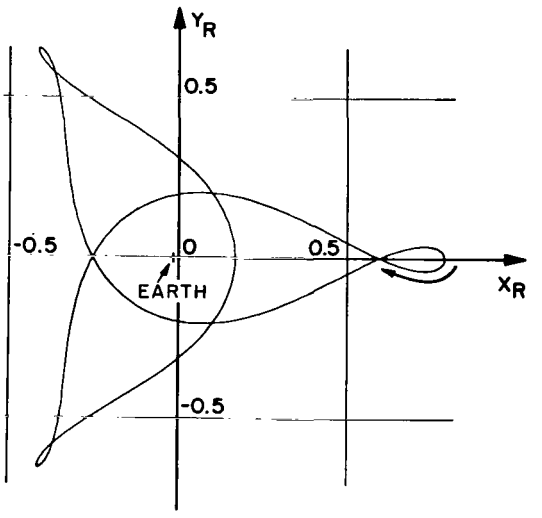

E. M. ORBIT OF JACOBI CONSTANT C = 3.20388
AMBIGRADE ORBIT THROUGH (X_R = 0.79026; Y_R = 0)
PERIOD: 6.514

Figure 75

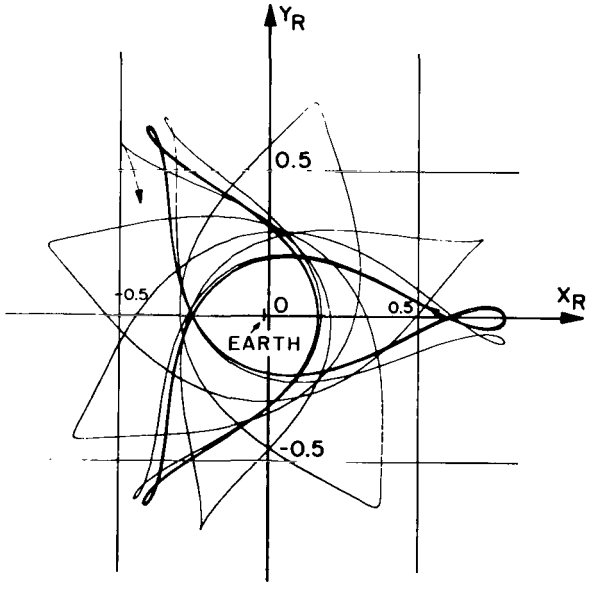

E. M. ORBIT OF JACOBI CONSTANT C = 3.20388
AMBIGRADE ORBIT THROUGH (X_R = 0.79030; Y_R = 0)
TIME SHOWN: 50.03

Figure 76

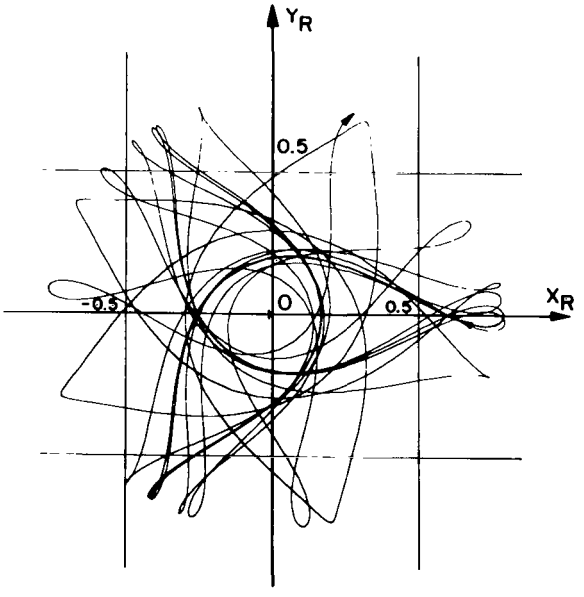

E. M. ORBIT OF JACOBI CONSTANT C = 3.20388
AMBIGRADE ORBIT THROUGH (X_R = 0.79040; Y_R = 0)
TIME SHOWN: 50.08

Figure 77

ORBITS OF THE LUNAR REGION
THE CLASSES OF RETROGRADE AND PROGRADE LUNAR ORBITS

The orbits of the lunar retrograde class show rather regular Keplerian patterns. Four examples of this are paraded on Figures 78 to 81. This series starts with the central orbit and follows with orbits of increasing belt-width. A super-position of three of these orbits is illustrated on Figure 82. The collision orbit, which terminates the sequence of retrograde orbits, will be shown and discussed later.

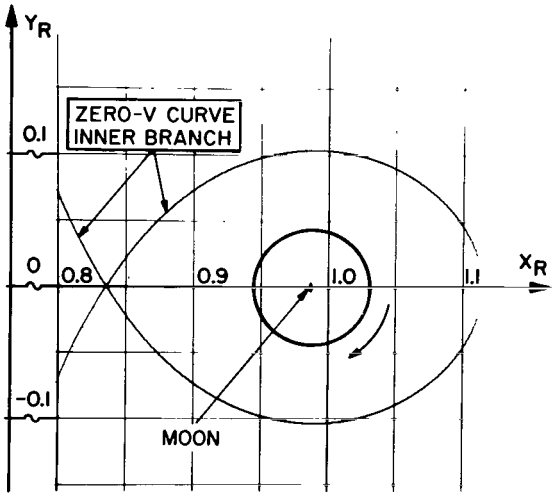

E.M. ORBIT OF JACOBI CONSTANT C=3.20388
CENTRAL ORBIT OF RETROGRADE CLASS (X_R = 1.031, Y_R = 0); PERIOD: 0.475

Figure 78

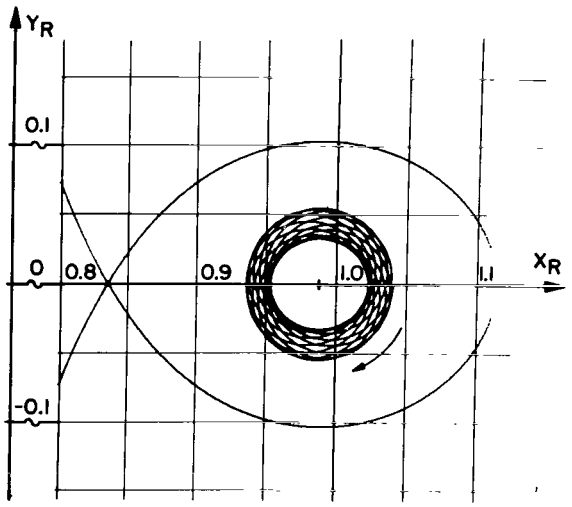

E.M. ORBIT OF JACOBI CONSTANT C=3.20388
RETROGRADE ORBIT THROUGH (X_R = 1.040; Y_R = 0) TIME SHOWN: 6.16

Figure 79

In transition to the prograde lunar class the central orbits of the retrograde and prograde class are displayed together on Figure 83. The lopsidedness of the prograde central orbit as well as its size are in marked contrast to the almost circular and symmetrically placed central orbit of retrograde direction. As to the possibility of generating an "artificial" symmetrical prograde central orbit, a suggestion is offered shortly in this chapter.

The lunar class of prograde orbits is then built up from the central orbit to the more complicated forms in a sequence of seven figures, Figures 84 to 90. As to the first figure of this

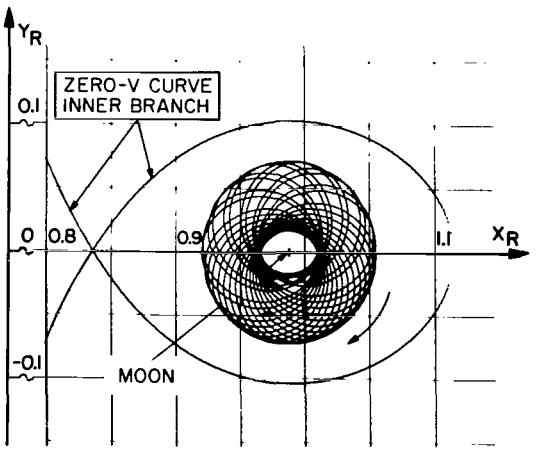

E.M. ORBIT OF JACOBI CONSTANT C=3.20388
RETROGRADE ORBIT THROUGH (X_R=1.055; Y_R=0)
TIME SHOWN: 15.0

Figure 80

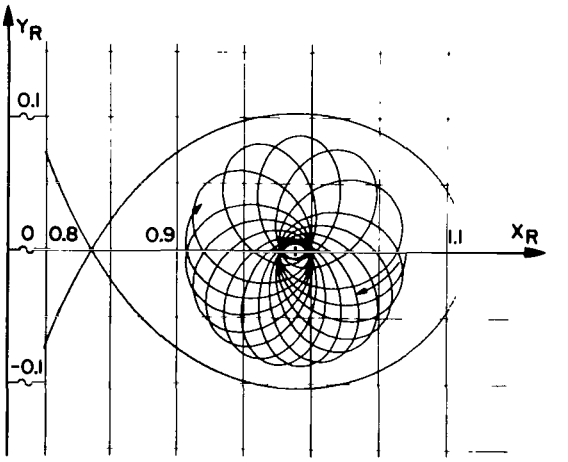

E.M. ORBIT OF JACOBI CONSTANT C=3.20388
RETROGRADE ORBIT THROUGH (X_R=1.070; Y_R=0)
TIME SHOWN: 9.25

Figure 81

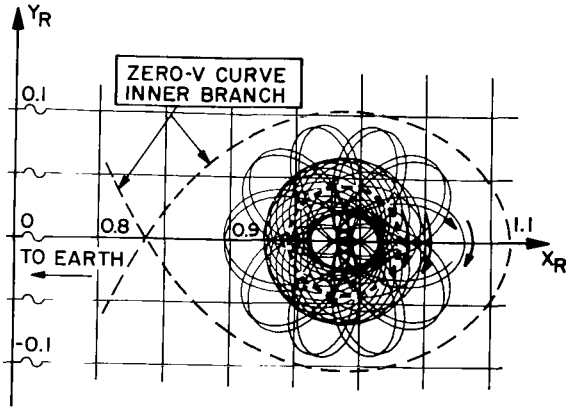

E.M. ORBIT OF JACOBI CONSTANT C=3.20388
THREE RETROGRADE ORBITS OF LUNAR REGION

Figure 82

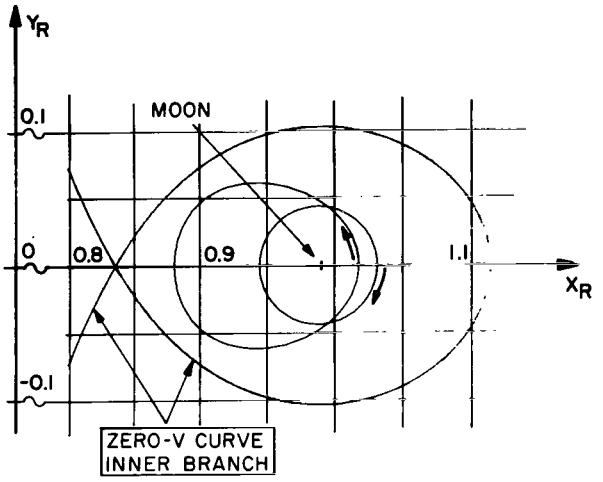

E.M. ORBIT OF JACOBI CONSTANT C=3.20388
TWO CENTRAL ORBITS IN LUNAR REGION

Figure 83

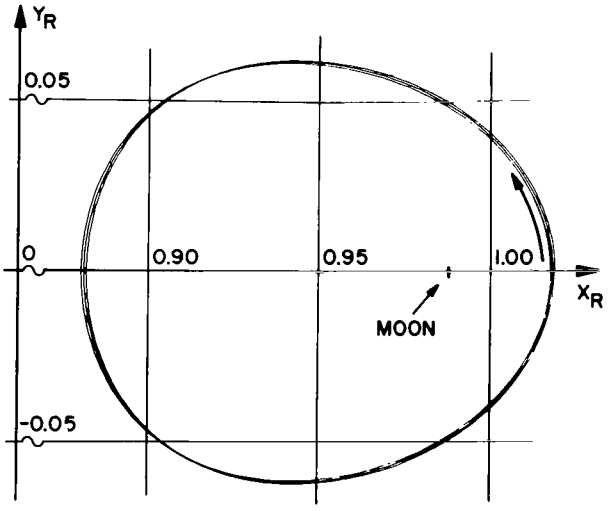

E.M. ORBIT OF JACOBI CONSTANT C=3.20388
THREE CENTRAL PROGRADE ORBITS IN LUNAR REGION X_R=1.01750 X_R=1.01814 X_R=1.01872

Figure 84

series (Figure 84), it is worthwhile to notice that this class has indeed three prograde single-loop orbits which are in close neighborhood to each other. The development of the series then follows first a horizontal expansion, while the expansion toward the vertical direction develops only gradually. Three figures of the series (Figures 87 to 89) show a central orbit superimposed to the current orbit.

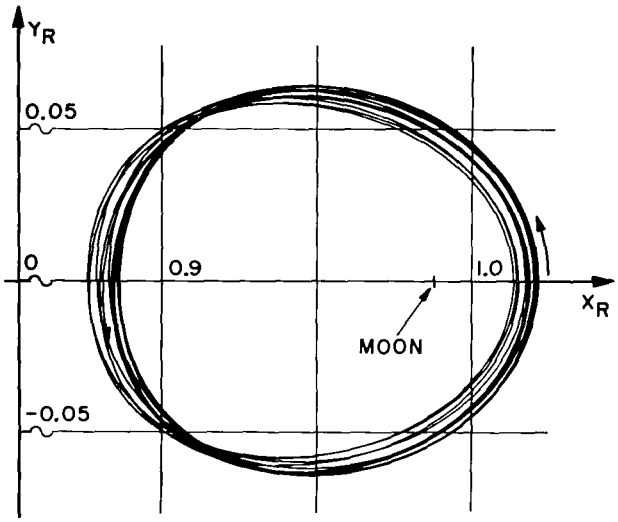

E.M. ORBIT OF JACOBI CONSTANT C= 3.20388
PROGRADE ORBIT THROUGH (X_R = 1.022; Y_R = 0)
TIME SHOWN: 15.01

Figure 85

In connection with a possible generation of a symmetrical prograde orbit, the reader's attention is drawn to the very first loop of the orbits on Figures 86 to 88. These are almost closed loops, with the "best" case occurring on the orbit of Figure 87. For clearer demonstration the first loop of this orbit is shown isolated on Figure 91. It is intelligible that by low thrust propulsion or small impulses this orbit can be changed to one that closes on itself. This orbit then would also be centered fairly well on the Moon.

THE CLASS OF AMBIGRADE LUNAR ORBITS

While the laws that govern the development of prograde lunar orbits are not fully recognized yet, those determining the patterns of ambigrade lunar orbits are easily recognizable from orbit samples, if these are properly selected and shown for a

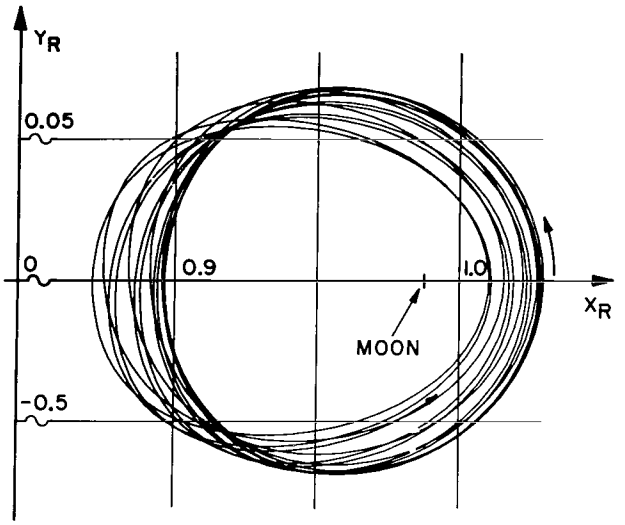

E. M. ORBIT OF JACOBI CONSTANT C = 3.20388
PROGRADE ORBIT THROUGH (X_R = 1.030; Y_R = 0) TIME SHOWN : 18.01

Figure 86

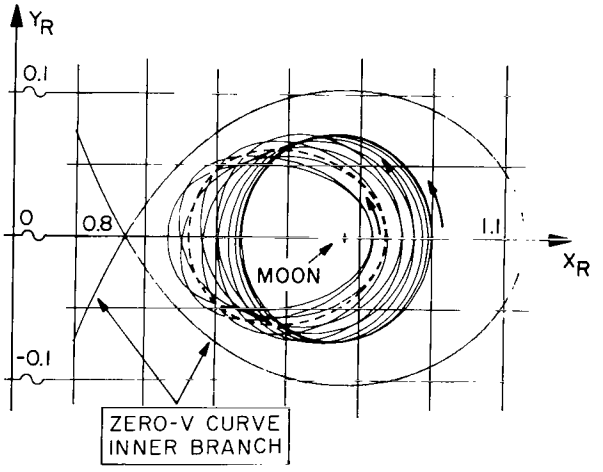

E. M. ORBIT OF JACOBI CONSTANT C = 3.20388
PROGRADE ORBIT THROUGH (X_R = 1.050 ; Y_R = 0) AND CENTRAL PROGRADE ORBIT TIME SHOWN : 15.0

Figure 87

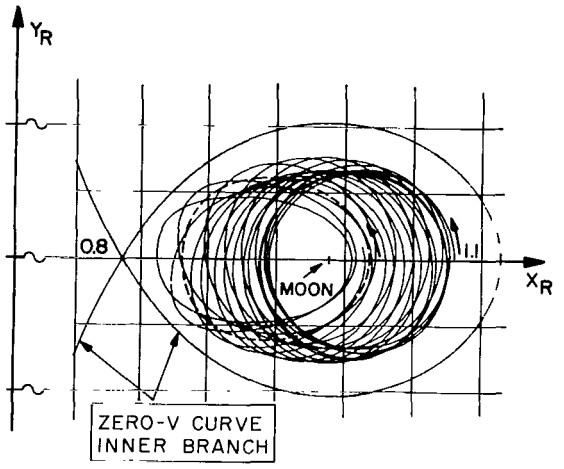

E.M. ORBIT OF JACOBI CONSTANT C=3.20388
PROGRADE ORBIT THROUGH (X_R=1.080 ; Y_R=0)
AND CENTRAL PROGRADE ORBIT
TIME SHOWN: 25.0

Figure 88

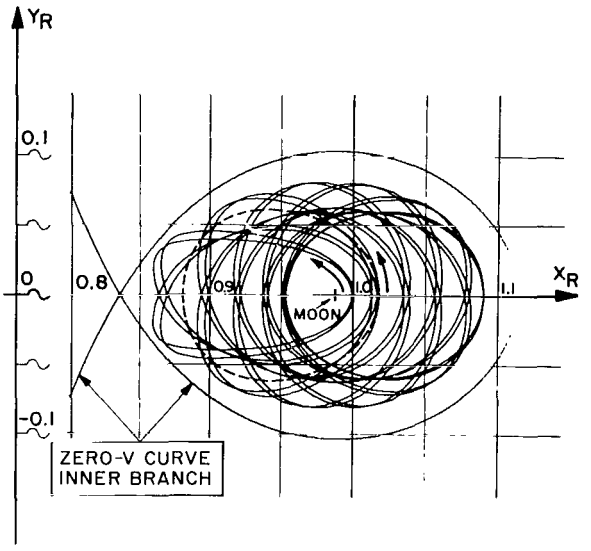

E.M. ORBITS OF JACOBI CONSTANT C=3.20388
PROGRADE ORBIT THROUGH (X_R=1.00; Y_R=0)
AND CENTRAL PROGRADE ORBIT
TIME SHOWN: 27

Figure 89

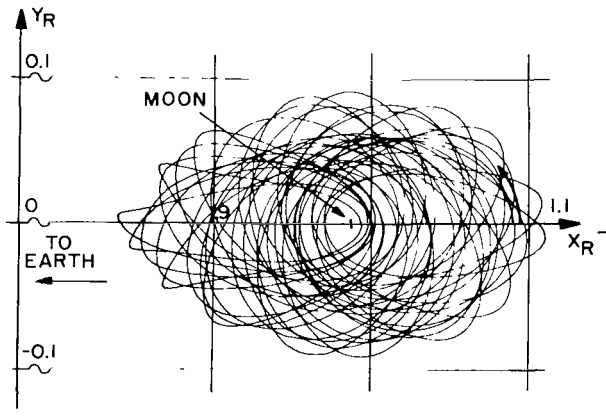

E.M. ORBIT OF JACOBI CONSTANT C=3.20388
PROGRADE ORBIT THROUGH (X_R=1.090; Y_R=0)
TIME SHOWN: 50.0

Figure 90

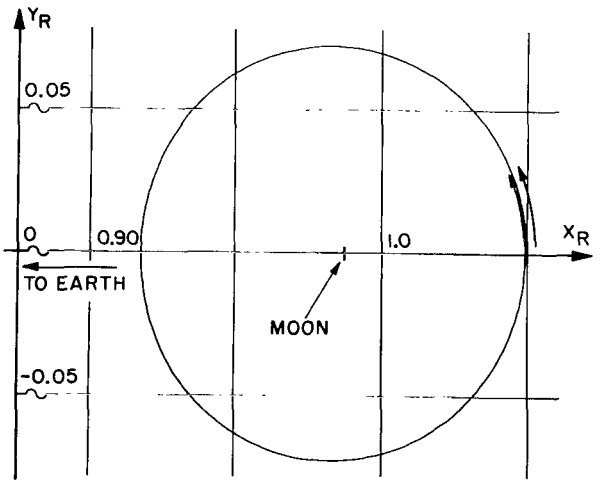

E.M. ORBIT OF JACOBI CONSTANT C= 3.20388
PROGRADE ORBIT THROUGH (X_R = 1.050; Y_R = 0)
TIME SHOWN: 1.306

Figure 91

sufficient length of orbital time. The subsequent seventeen orbits (Figures 92 to 108) serve this purpose and simultaneously constitute a survey of orbits in this class. This sequence is laid out such that all orbits are initiated at the X_R-axis with values starting at $X_R = 1.088$ and increasing for the subsequent orbits.

The first of this series (Figure 92) is a collision orbit. This orbit constitutes the limit between retrograde and ambigrade orbits. Collision is encountered between the loops that are numbered "2" and "3".

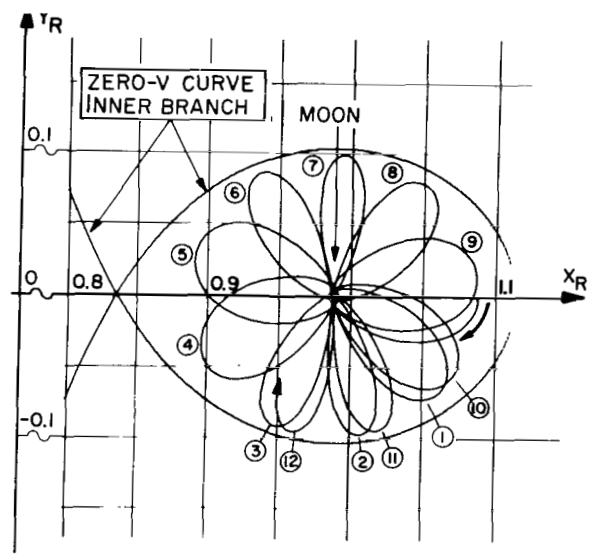

E.M. ORBIT OF JACOBI CONSTANT C = 3.20388
ORBIT COLLIDING WITH MOON
$X_R = 1.088$; $Y_R = 0$; TIME SHOWN · 8.00

Figure 92

The direction of collision is nearly minus 90° as measured from the moon relative to the positive X_R-branch.

A slight move of the initial point to the value $X_R = 1.090$ results in an orbit (Figure 93) that is prograde about the moon for motion coming from the same general direction as that resulting in the collision on the former graph, i.e., between loops "2" and "3". The same effect can be observed for the motion between loops "6" and "7", which are positioned reflective to the former two loops. The next picture (94) shows an extended history of the identical orbit.

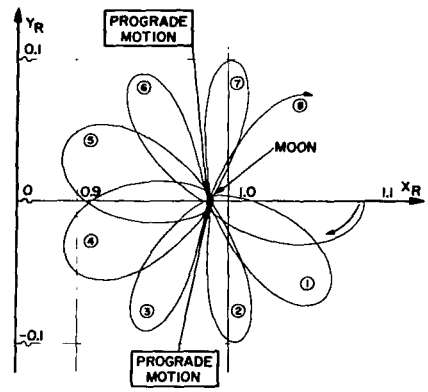

E.M. ORBIT OF JACOBI CONSTANT C=3.20388
AMBIGRADE ORBIT THROUGH (X_R=1.09; Y_R=0)
TIME SHOWN: 5.223

Figure 93

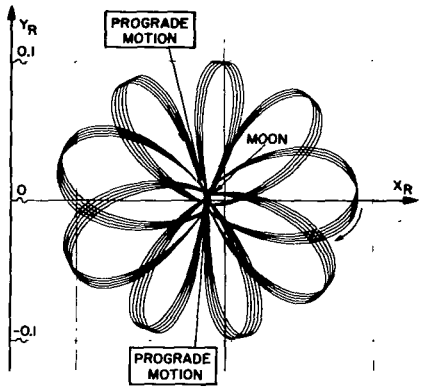

E.M. ORBIT OF JACOBI CONSTANT C=3.20388
AMBIGRADE ORBIT THROUGH (X_R=1.09; Y_R=0)
TIME SHOWN:28.21

Figure 94

Increasing the initial point to the locations X_R = 1.096, 1.100, and 1.1018 produces orbits (Figures 95 to 98) that demonstrate that the loops "2" and "6" are - to their full length - subject to gradual transformation into prograde motion. This trend is consistently followed in the remainder of the series.

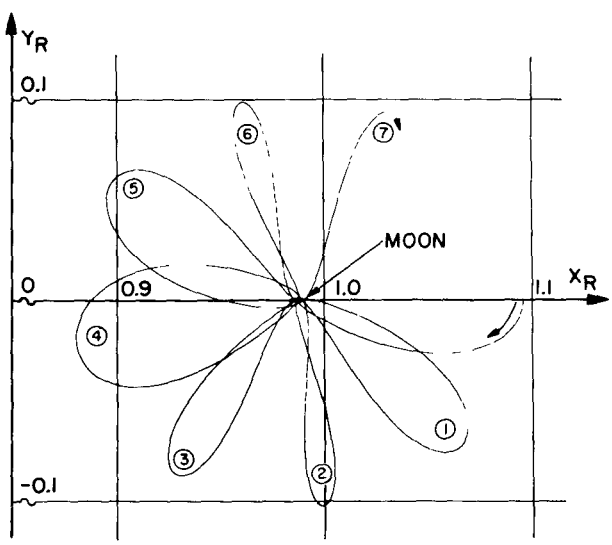

E.M. ORBIT OF JACOBI CONSTANT C=3.20388
AMBIGRADE ORBIT THROUGH (X_R=1.096; Y_R=0)
TIME SHOWN: 5.0

Figure 95

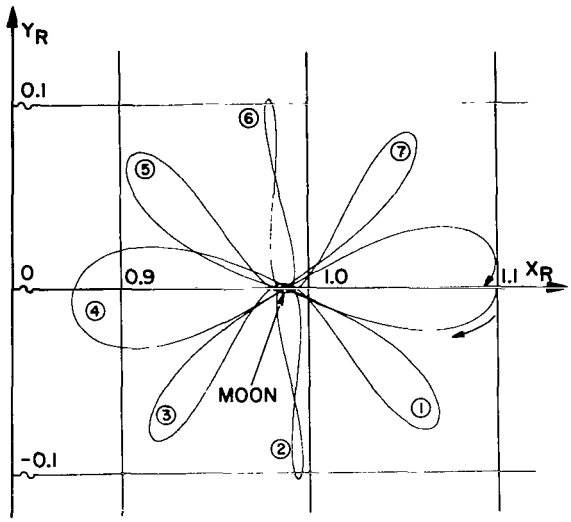

E.M. ORBIT OF JACOBI CONSTANT C=3.20388
AMBIGRADE ORBIT THROUGH (X_R=1.100; Y_R=0)
TIME SHOWN: 6.0

Figure 96

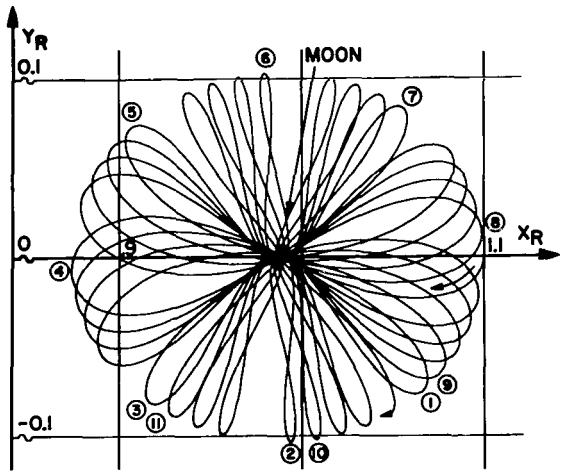

E.M. ORBIT OF JACOBI CONSTANT C=3.20388
AMBIGRADE ORBIT THROUGH (X_R=1.100; Y_R=0)
TIME SHOWN: 25.2

Figure 97

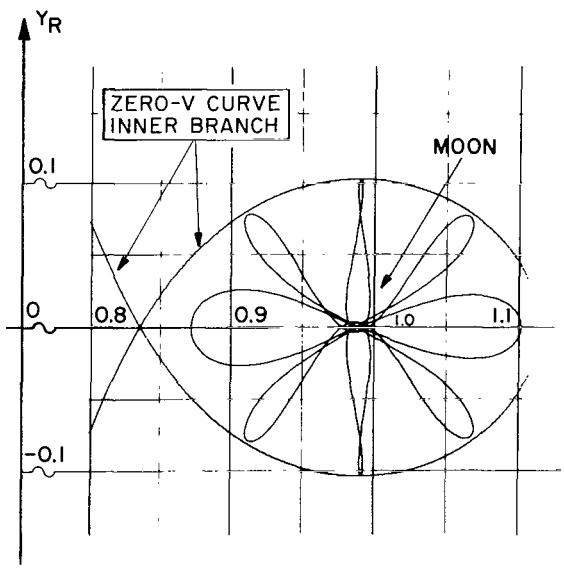

E.M. ORBIT OF JACOBI CONSTANT C=3.20388
AMBIGRADE ORBIT THROUGH (X_R=1.1018; Y_R=0)
TIME SHOWN: 6.07

Figure 98

With respect to the other loops of the orbits, the reader will observe that all loops experience the change from retrograde to prograde motion (i.e., from negative to positive $\dot{\phi}$, if ϕ is the central angle measured from the moon), but relative to each other the loops located at $\phi = +90°$ are most advanced in this development on any given orbit. This becomes evident on those figures of the remainder of the series that show orbits with a larger number of loops, as Figure 97 (which is an extension to the orbit of Figures 96), 99, 100, and 101. Once this is understood, the explanation for the particular shapes of the loops of the seven-loop-orbit on Figure 102 is also clear.

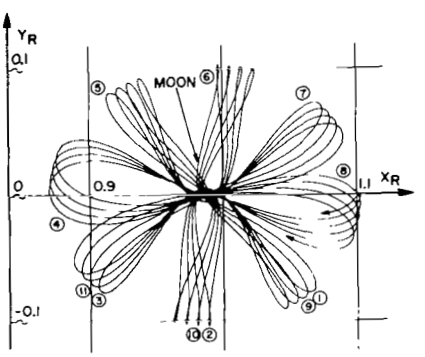

Figure 99

The remaining six figures are actually presenting only two different orbits. The first of these orbits is given in two sections of time history on Figures 103 and 104. The breakdown into two parts of orbital time serves to display the "pendulum"-type of stability, this orbit possesses. The reference orbit for which the present orbit is a perturbation, is the seven-loop periodic orbit of Figure 102. It is here worthwhile to mention that a superposition of the two parts of the orbit history on one graphs destroys the lucidity to such a degree that the governing laws of formation cannot be recognized.

The residual four graphs, Figures 105 to 108, all represent the same orbit, i.e., the orbit initiated at the very border of the lunar region. The gradual build-up of this orbit serves to show that initial unsymmetries will be complemented by the succeeding development such that finally an even distribution of loops is obtained.

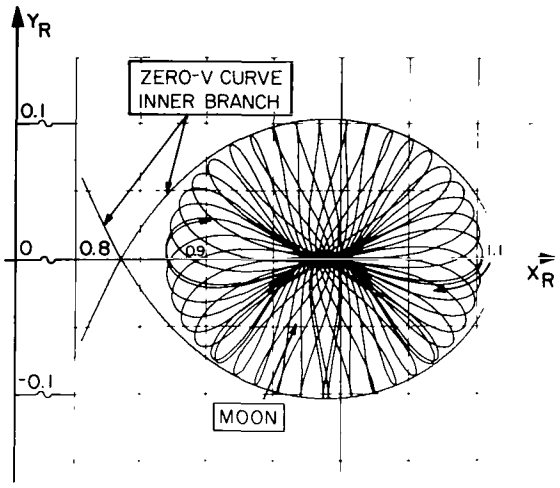

E. M. ORBIT OF JACOBI CONSTANT C = 3.20388
AMBIGRADE ORBIT THROUGH (X_R = 1.1040 ; Y_R = 0)
TIME SHOWN · 33.9

Figure 100

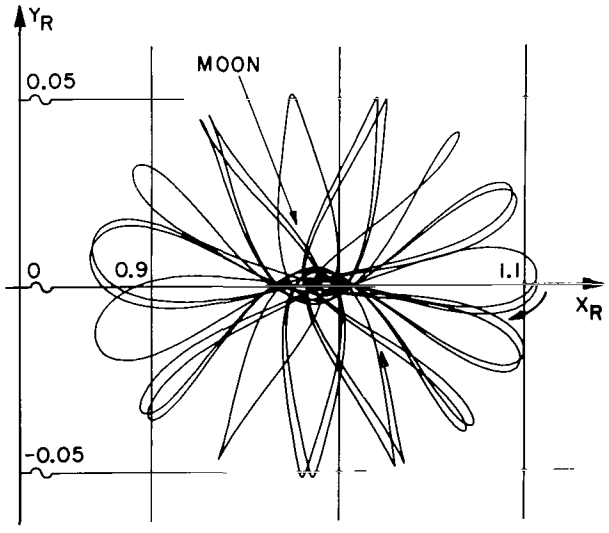

E.M. ORBIT OF JACOBI CONSTANT C = 3.20388
AMBIGRADE ORBIT THROUGH (X_R = 1.107; Y_R = 0)
TIME SHOWN: 20.01

Figure 101

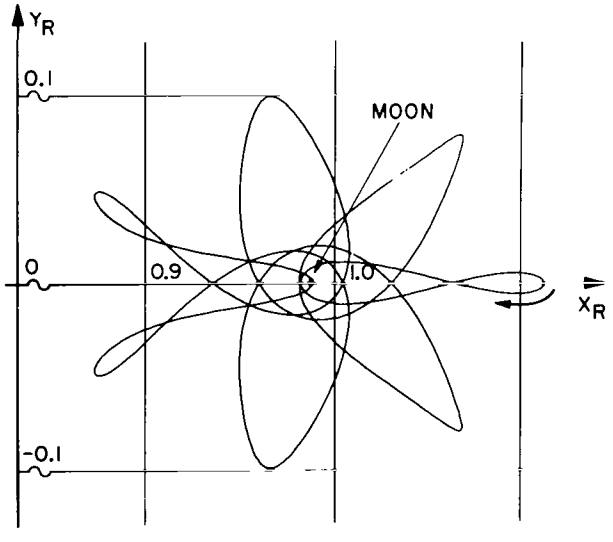

E. M. ORBIT OF JACOBI CONSTANT C = 3.20388
AMBIGRADE ORBIT THROUGH (X_R = 1.1129; Y_R = 0)
PERIOD: 6.5

Figure 102

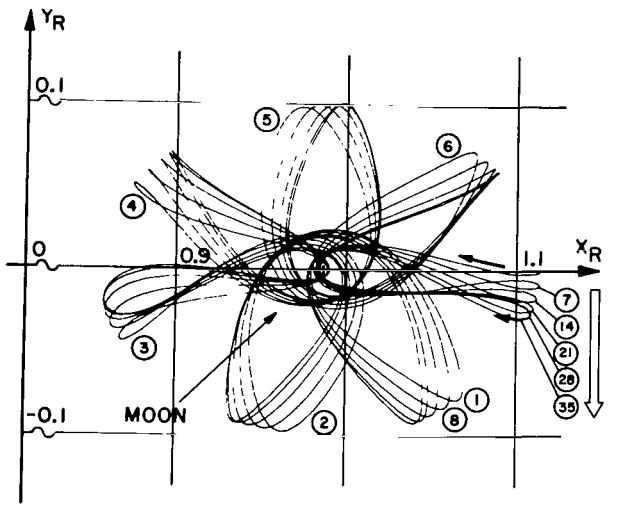

E.M. ORBIT OF JACOBI CONSTANT C = 3.20388
AMBIGRADE ORBIT THROUGH (X_R = 1.114; Y_R = 0)
TIME SHOWN: 33.56

Figure 103

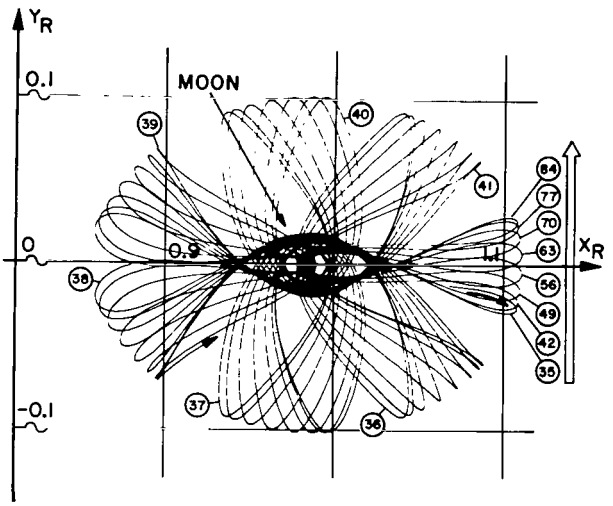

E.M. ORBIT OF JACOBI CONSTANT C = 3.20388
CONTINUATION OF
AMBIGRADE ORBIT THROUGH (X_R = 1.114; Y_R = 0)
TIME SHOWN FROM T = 32.96 TO T = 80.66

Figure 104

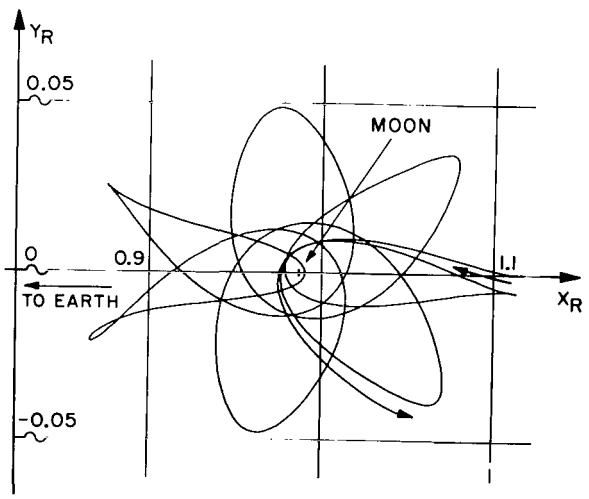

E.M. ORBIT OF JACOBI CONSTANT C = 3.20388
AMBIGRADE ORBIT THROUGH (X_R = 1.11434; Y_R = 0)
TIME SHOWN: 8.011

Figure 105

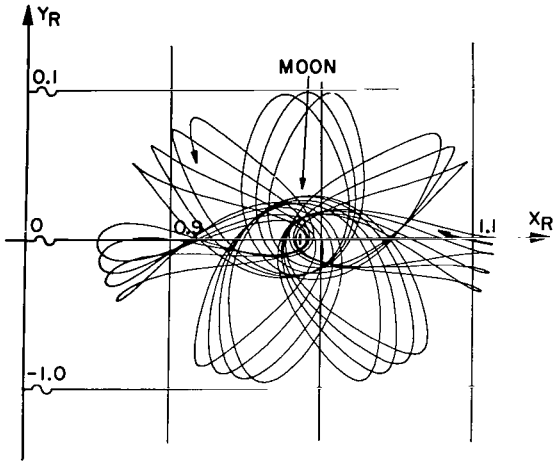

E.M. ORBIT OF JACOBI CONSTANT C = 3.20388
AMBIGRADE ORBIT THROUGH (X_R = 1.11434; Y_R = 0)
TIME SHOWN: 25.2

Figure 106

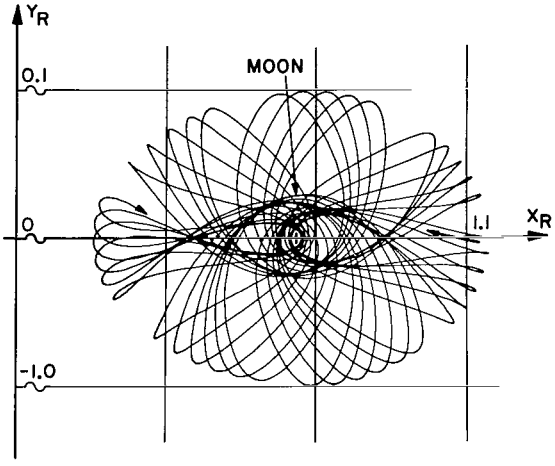

E.M. ORBIT OF JACOBI CONSTANT C = 3.20388
AMBIGRADE ORBIT THROUGH (X_R = 1.11434; Y_R = 0)
TIME SHOWN: 38.0

Figure 107

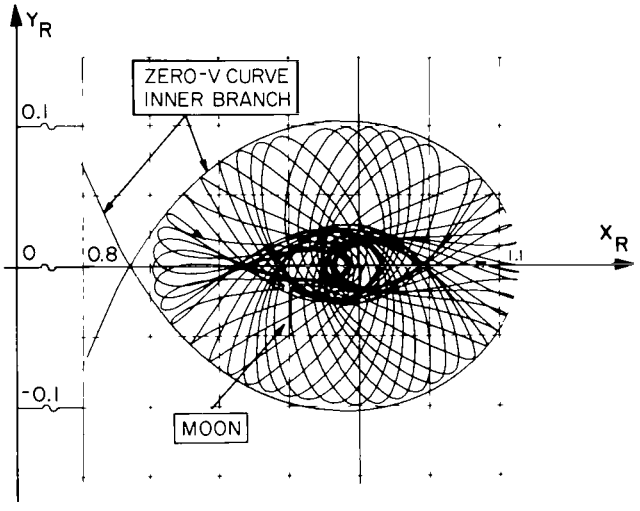

E.M. ORBIT OF JACOBI CONSTANT C = 3.20388
AMBIGRADE ORBIT THROUGH (X_R = 1.11434; Y_R = 0)
TIME SHOWN: 45.0

Figure 108

In conclusion to this series, the laws that govern the formation of the orbits of this particular series may be listed as follows:

(1) For a fixed direction ϕ from the Moon, the loops positioned at this direction undergo a consistent change toward a stronger prograde character, as the initial position of the orbit is varied to larger X_R-values.

(2) For a fixed orbit, those loops are developed furthest toward, or into, the prograde direction that are positioned closest to $\phi = \pm 90°$, and the loops that lag behind most, are positioned at $\phi = 180°$ and $\phi \pm 15°$. At $\Phi = 0°$, there is a weak local "prograde-maximum".

The information on ambigrade orbits will now turn to the orbits initiated at the X_R-axis branch that is between Moon and Earth. A sequence of five orbits is depicted on Figures 109 to 113, which series is ordered so that initial points of orbits are first closest to the Moon and succeedingly recede in direction Earth.

The first three of these figures show orbits that are periodic or very nearly so. The loops on each of these orbits show a "gradiness" pattern that follows exactly the laws formulated before.

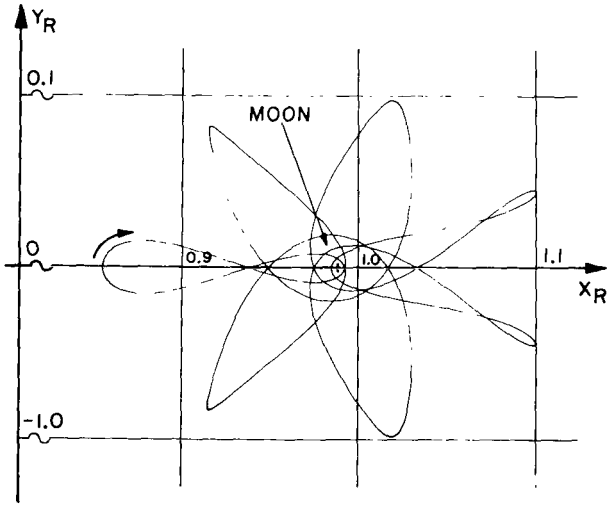

E.M. ORBIT OF JACOBI CONSTANT C = 3.20388
AMBIGRADE ORBIT THROUGH (X_R = 0.855; Y_R = 0) PERIOD : 6.47

Figure 109

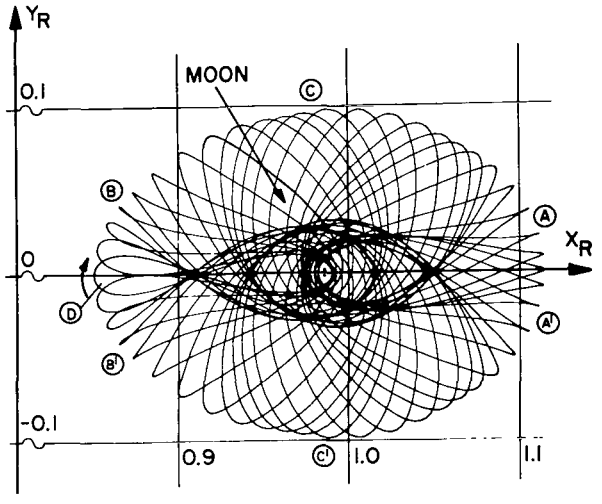

E.M. ORBIT OF JACOBI CONSTANT C=3.20388
AMBIGRADE ORBIT THROUGH (X_R=0.850; Y_R=0)

Figure 110

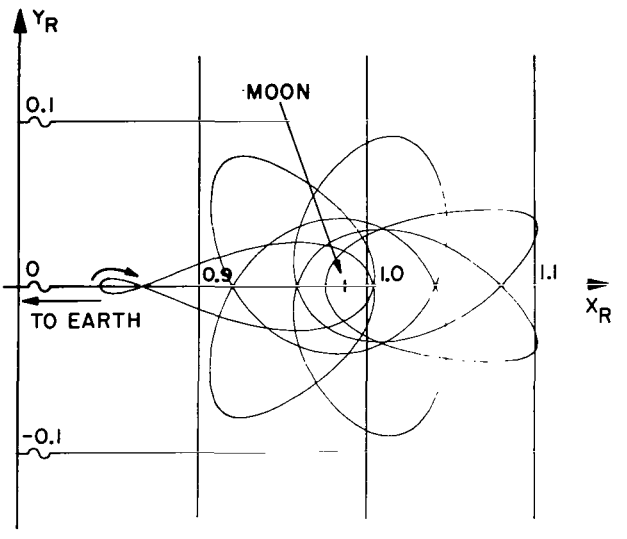

E.M. ORBIT OF JACOBI CONSTANT C=3.20388
AMBIGRADE ORBIT THROUGH (X_R=0.841; Y_R=0)
PERIOD: 8.17

Figure 111

Compliance with these laws can also be observed with the loops on the next two orbits (Figures 112 and 113) though this is not as clearly visible due to the large number of loops shown for each orbit.

The latter of these two orbits (Figure 113) is initiated at the point X_R = 0.835209, which is very close to the location of the equilibrium point L_1. This area will be subject to a special study later.

As last contribution to the description of ambigrade orbits, two figures, Figure 114 and 115, are inserted here, that indicate a method by which changes in gradiness may directly be studied. This method is similar to that discussed before for the terrestrial region; it may be called the method of successive apocenters. Two regions are singled out here:

On the first figure, departures from the zero velocity curve are between ϕ = -90° and -145°. The succeeding apocenters are between ϕ = -145° and -180° and show all retrograde motion.

On the Figure 115, departure is again from the zero-velocity curve and i.e., at points between ϕ = 0° and 30°. The second

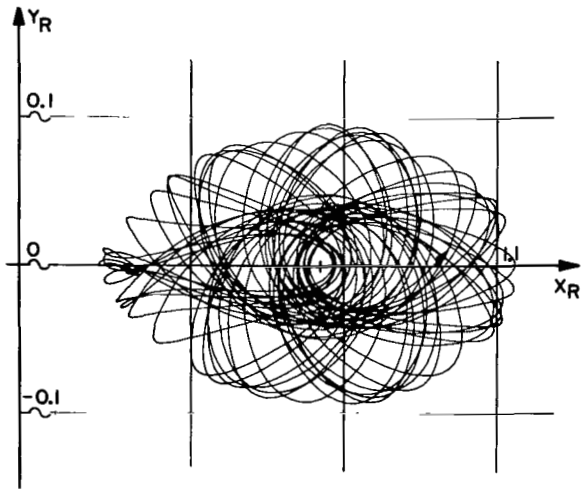

E. M. ORBIT OF JACOBI CONSTANT C = 3.20388
AMBIGRADE ORBIT THROUGH (X_R = 0.840; Y_R = 0)
TIME SHOWN: 60.0

Figure 112

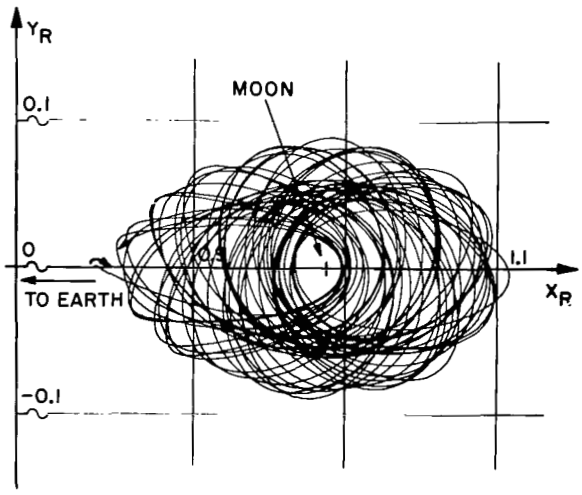

E. M. ORBIT OF JACOBI CONSTANT C = 3.20388
AMBIGRADE ORBIT THROUGH (X_R = 0.835209; Y_R = 0)
TIME SHOWN: 68.24

Figure 113

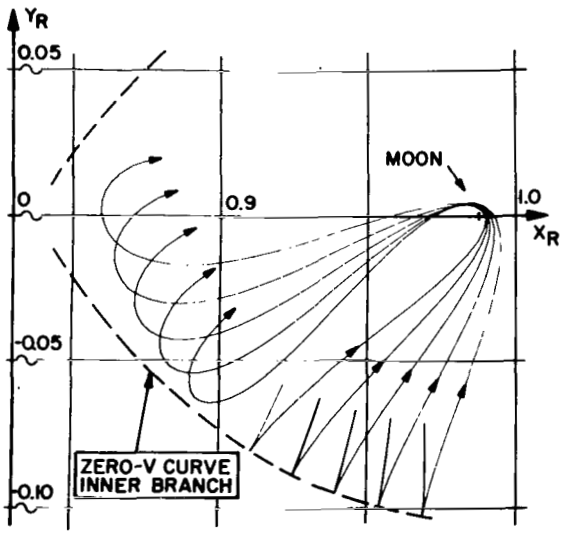

E. M. ORBIT OF JACOBI CONSTANT C=3.20388
ORBITS THROUGH POINTS OF ZERO-V CURVE

Figure 114

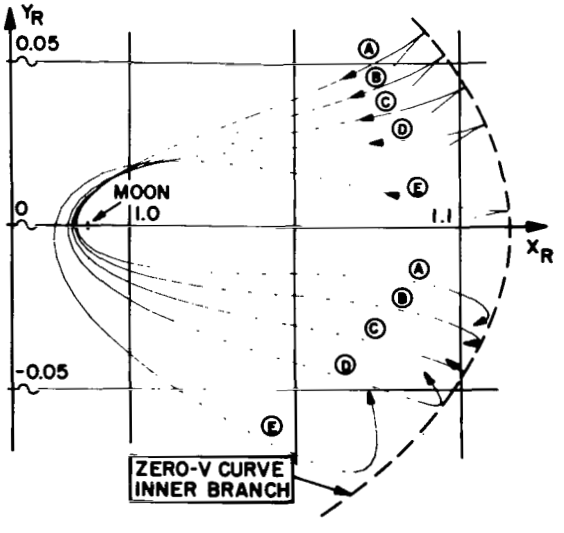

E. M. ORBIT OF JACOBI CONSTANT C=3.20388
ORBITS THROUGH POINTS OF ZERO-V CURVE

Figure 115

apocenters fall into the angular region between $\phi = 0°$ and $-30°$ and show retrograde as well as prograde motion including its transitional cusping case.

Using the method of successive apocenters, the same laws can be deducted that were derived by interpretation of phenomena observed on selected orbits.

ORBITAL BEHAVIOR IN THE NEIGHBORHOOD OF THE CISLUNAR EQUILIBRIUM POINT L_1

It is appropriate at this point to clarify the geometry of the regions in the neighborhood of the cislunar equilibrium point L_1. According to ref. 1, the separation of the terrestrial region from the lunar region for $\mu = 0.0125$ is occurring at the C-level of

$$C(L_1) = 3.2038861611$$

this value being accurate to eleven digits only. Further, if the C-level would correspond exactly to $C(L_1)$, the point L_1 would be the only common point of the two regions, located at

$$X_R(L_1) = 0.8352093934$$

accurate to 10 digits.

For the current investigation the C-level was chosen to be exactly

$$C = 3.20388.$$

Since the C-value chosen for the current investigation is smaller than the accurate value of $C(L_1)$, there exists a connecting pass between the terrestrial and lunar region at the current C-level. At the narrowest place, this pass (or "neck") has the diameter of about 0.0025 units. The shape of the pass can be seen on several of the following diagrams.

The equilibrium point L_1 is located where the pass is smallest.

There are two aspects that hold the interest of the investigator in connection with the pass. The first is concerned with the local behavior of the orbits in the neighborhood of the pass, as the formation of particular loops, etc. The second deals with the large scale behavior of orbits that pass through the pass. These aspects will be discussed sequentially.

The problem of orbital behavior "in the small" near L_1 is attacked again in two ways: Progressing along the X_R-axis and progressing along the border line.

Figures 116 to 118 serve to show the phenomena developing along the first approach. Orbits are initiated orthogonal to the X_R-axis, with positive $\dot{Y}_R$ to the left of the point L_1, and with negative $\dot{Y}_R$ to the right of L_1. Figure 116 displays one of the resulting patterns: This is a pattern that is a rather symmetrical with respect to a vertical line through L_1, which line may also be considered temporarily as dividing the lunar from the terrestrial region. From both sides, orbits that are prograde w/r to their region approach the L_1-point, while they also approach the border. (See orbits A, B, C and G, F, E on Figure 116). These orbits stay prograde till they reach the cusping orbits C and E, respectively.

A unique orbit then exists that loops about L_1 and closes on itself (orbit D). This is the libration orbit to L_1. Its time period is 2.7 units.

This pattern is supplemented by the development shown on Figure 117. Here the progression of orbits of positive $\dot{Y}_R$ is continued. It shows the cusping orbit "B" to be followed by ambigrade orbits which first belong to terrestrial orbits, later to lunar orbits. The orbit "D" on this picture is nearly cusping again. This type of orbit will be discussed shortly.

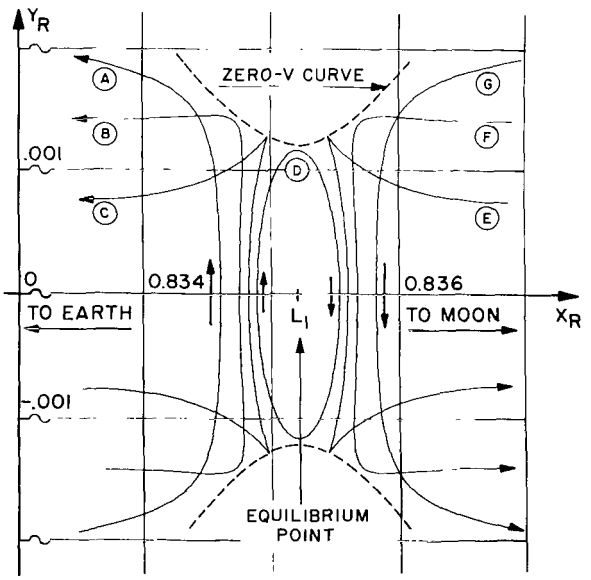

E.M. ORBITS OF JACOBI CONSTANT C = 3.20388
SEPARATED ORBITS IN THE NEIGHBORHOOD OF L_1

Figure 116

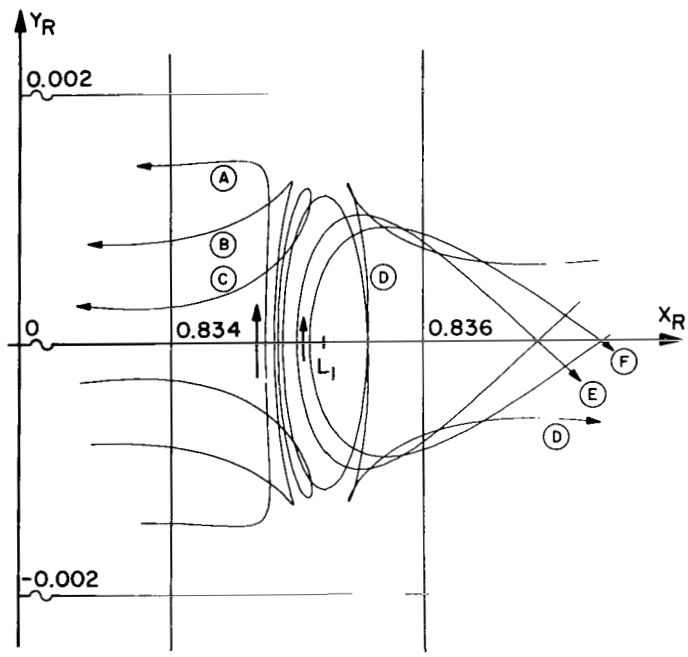

E.M. ORBITS OF JACOBI CONSTANT C=3.20388
ORBITAL BEHAVIOR IN THE NEIGHBORHOOD OF L_1

Figure 117

In agreement with the "lateral" symmetry characteristics that hold for developments "in the small", a similar progression can be shown for orbits of negative Y_R, approaching L_1 from the right.

This is corroborated by the third figure (Figure 118): Two orbits are started at the very point of L_1 in opposite directions (orbit "A" with $\Theta_R = -90°$; orbit "B" with $\Theta_R = +90°$). The orbits develop in shapes that are well symmetrical to each other. The third orbit ("C") is initiated with $\Theta_R = 100°$.

The second attack on the problem of motion near L_1 and its results are explained on hand of Figures 119 to 122.

Figure 119 shows a sequence of six orbits that all touch the lower border of the pass. As the cusps progress from the terrestrial region toward the lunar region, the orbits' second legs (downstream) swing over from the terrestrial region to the lunar region. The events connected with this transition are presented on hand of the following three figures. Figure 120 shows a sequence of orbits that all would be, progression-wise, placed between the two orbits "C" and "D" of the former graph. In this sequence (Figure 120) one notices firstly orbit "B" which is the

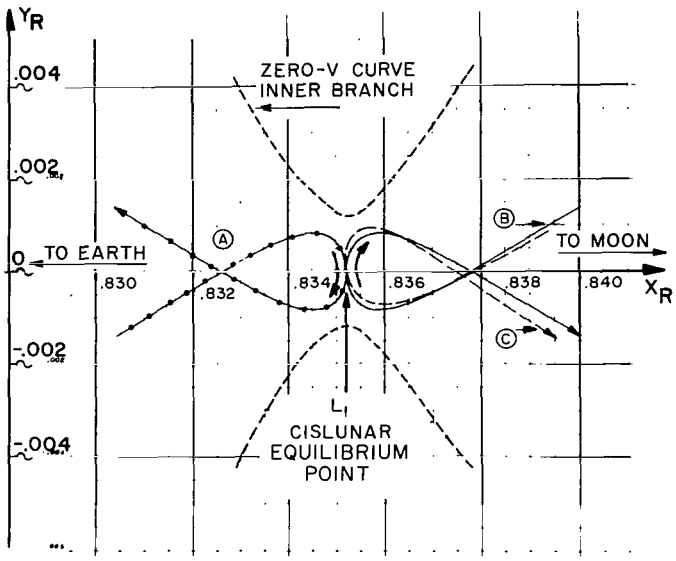

E. M. ORBITS OF JACOBI CONSTANT C = 3.20388
ORBITS THROUGH CISLUNAR EQUILIBRIUM POINT
$\theta_R(A) = -90°$; $\theta_R(B) = 90°$; $\theta_R(C) = 100°$

Figure 118

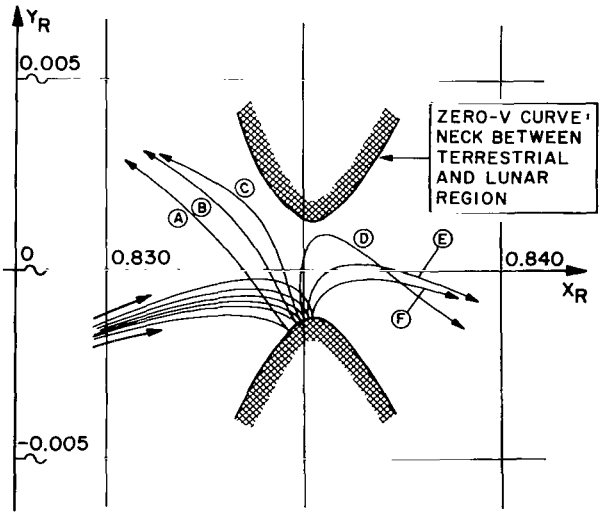

E.M. ORBITS OF JACOBI CONSTANT C = 3.20388
SIX ORBITS WITH CUSPS NEAR L_1

Figure 119

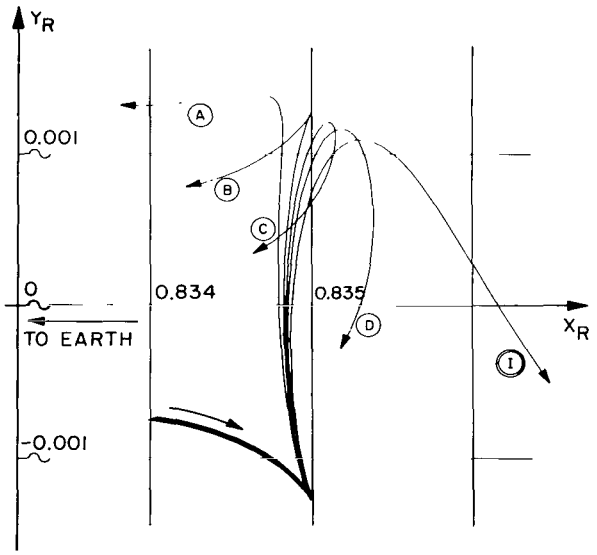

E.M. ORBITS OF JACOBI CONSTANT C = 3.20388
FIVE ORBITS WITH CUSPS NEAR L_1

Figure 120

double-cusping orbit encountered before, on Figure 116. Secondly, between orbit "D" and orbit "I", there must exist one orbit that cuts the X_R-axis orthogonally. For reflection reasons, therefore, it forms a loop about L_1 and produces a second cusp at the upper border, after which it returns into the terrestrial region. This orbit is displayed on Figure 121.

Next now, it will be attempted to make a point for the existence of a double-cusping orbit that is different from that of Figure 121 by the fact that it loops twice about L_1: Figure 122 illustrates a sequence of four orbits that all are making first a loop about L_1 (as shown by the dashed line) and after the loop are showing a pattern of motion that repeats the pattern observed on Figure 120. In particular, for continuity reasons, the conclusion is permissible that there exists an orbit between orbits "G" and "H" that crosses the X_R-axis orthogonally. This then is the double-looping, double-cusping orbit.

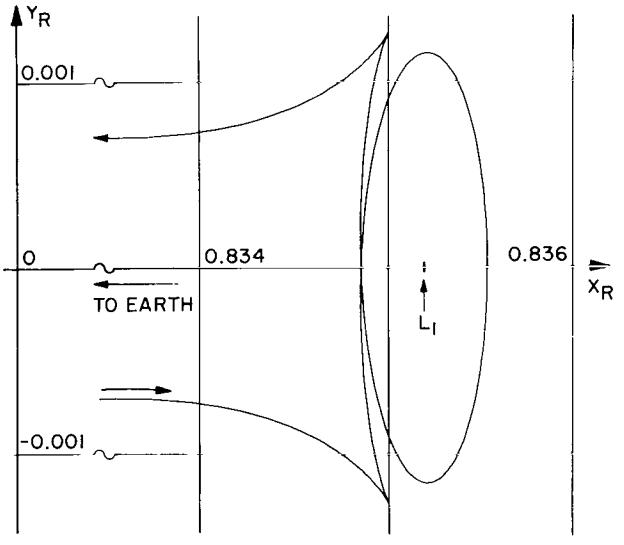

E.M. ORBIT OF JACOBI CONSTANT C = 3.20388
SYMMETRIC ORBIT WITH LOOP AROUND L_1

Figure 121

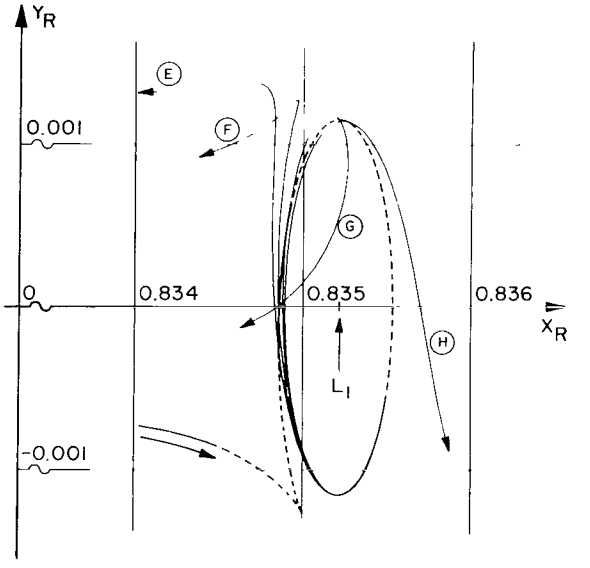

E.M. ORBITS OF JACOBI CONSTANT C = 3.20388
FOUR CUSPING ORBITS WITH LOOPS AROUND L_1

Figure 122

The same type of argument can be used to show the existence of double-cusping orbits with more loops.

BI-REGIONAL ORBITS

In reference to the problem of "large scale behavior" of orbits that visit the neighborhood of L_1, it may be pointed out that those orbits, which, after visit, return to their original region, were discussed to some extent within the classes to which they belong. What remains to be studied, however, is the important class of orbits that - in the course of passing through the neighborhood of L_1 - cross from the lunar territory over into the terrestrial, or reverse.

This investigation is particularly important for the current C-level, because the orbits passing through the gap may, for practical purposes, be considered orbits of the lowest possible C-level that are able to cross over.

For any substantial width of the pass between regions, a good survey of all possible bi-regional orbits would be organized along a procedure as schematically presented on Figure 123. At appropriately spaced points along the separatrix (or any other suitably chosen line that connects the two branches of the C-curve across the gap) orbits are initiated that e.g., have directions toward the terrestrial region, ranging in path-angles from 90° to minus 90°, the steps being chosen to fit a reasonable grid-size. The orbits are computed for positive time as well as negative (backward) time.

Due to the laws of reflection on the X_R-axis, there is an option of this method or the alternate of choosing points on half of the separatrix only and initiating orbits through these points into directions that are representative for the full circle. Again both directions on the time scale are to be computed, except for the orbits originating at the point on the X_R-axis. There are two more options from lateral symmetry.

In terms of the symbolic labeling of Figure 118, two of the four options are A, B, C, D, E, F and A, B, C, D, E', F'.

On the present C-level the gap is so narrow that the selection of two points on the separatrix is sufficient for representation of "all" points on the separatrix. The points chosen are the upper border point and the point on the X_R-axis, i.e., the point L_1. For the upper point, where the velocity magnitude is zero, a directional variation is without meaning.

Figure 124 traces the course of three orbits through the gap, i.e., the cusping orbit and two orbits through L_1, these with directions of 180 and 140 degrees.

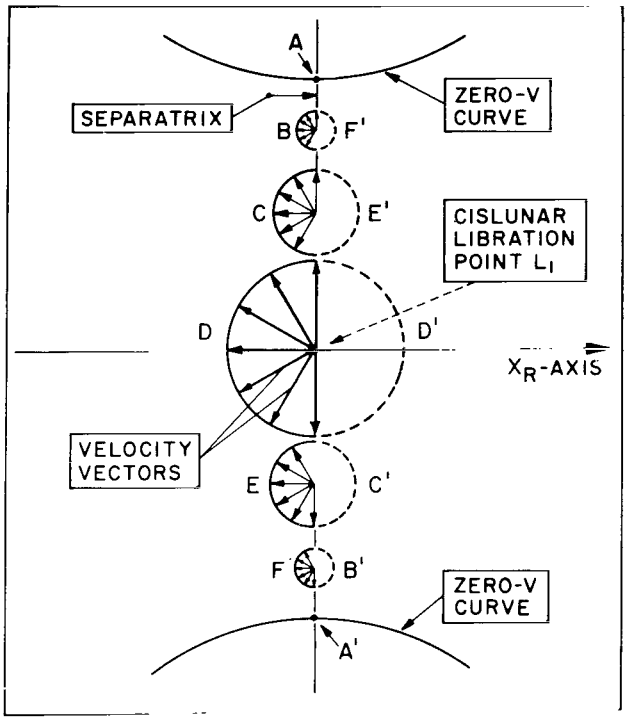

APPLICATION OF REFLEXION LAWS
IN THE COMPUTATION OF BIREGIONAL ORBITS

Figure 123

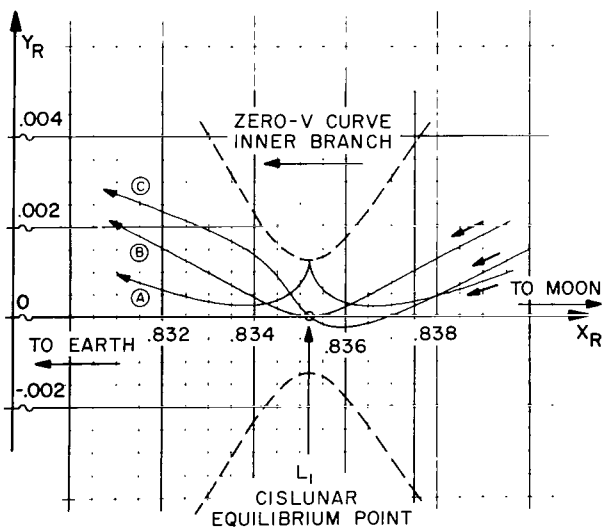

E.M. ORBITS OF JACOBI CONSTANT C=3.20388

CROSS-OVER PORTIONS OF BI-REGIONAL ORBITS
$\theta_R(B)=180°$ $\theta_R(C)=140°$

Figure 124

These same three orbits are illustrated for a longer time period on the next graph, Figure 125. The traces of the three orbits are seen to coincide practically for all time shown. This is true for all directions for which the orbits are bi-regional.

The time periods here, if counted from the event of crossing the separatrix, are forward about ten units and backwards four units. On the former figure, Figure 124, the times run to about one unit in both directions.

A study of the behavior of some bi-regional orbits on still longer time-histories is documented in the remaining four figures of this section (Figures 126-129). The first one shows the orbit "B" of Figure 124 now traced to 102 units of time (i.e., about 14 calendar months), while the backward tracing of this orbit is done on Figure 127 to about four calendar months. (However, the application of reflection reverses the time direction and shows the mirror image of the lunar region orbit.)

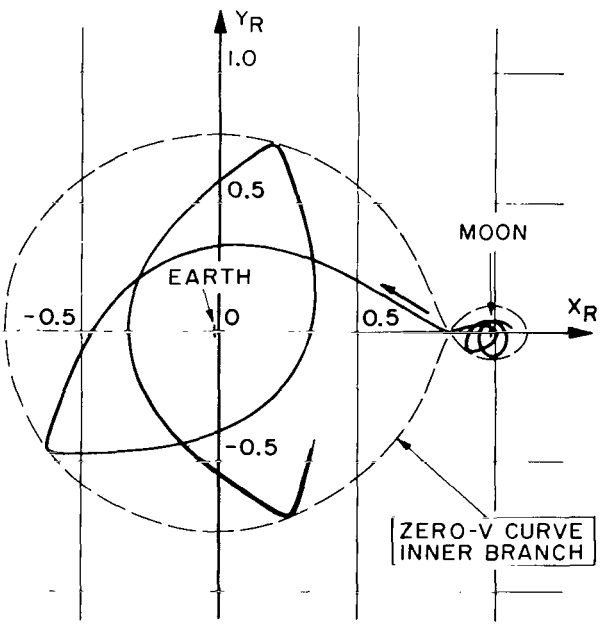

E.M. ORBITS OF JACOBI CONSTANT C=3.20388
BIREGIONAL ORBITS CROSSING
FROM LUNAR INTO TERRESTRIAL REGION

Figure 125

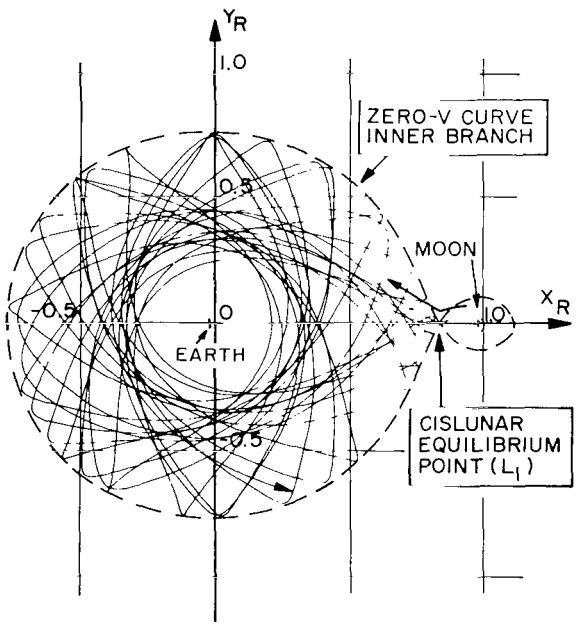

E.M. ORBIT OF JACOBI CONSTANT C=3.20388:
BI-REGIONAL ORBIT THROUGH (X_R=.835209;
Y_R=0; θ=180°) TIME SHOWN: 102.0

Figure 126

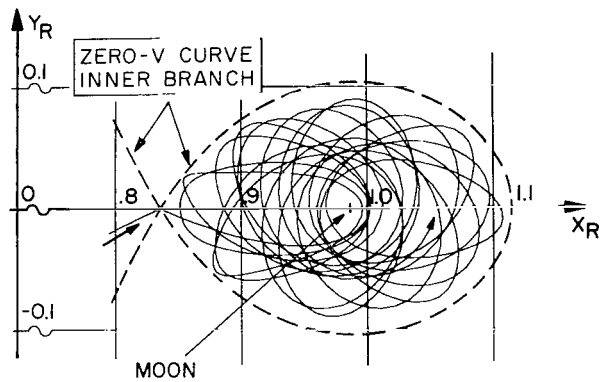

E.M. ORBIT OF JACOBI CONSTANT C=3.20388

BI-REGIONAL ORBIT THROUGH (X_R=.835209; Y_R=0)
LUNAR REGION PART; TIME SHOWN : 26.6

Figure 127

The last two figures of this chapter then trace the history of the terrestrial part of the orbit "A" of Figure 124. The history is shown first for 52 time units, and next for 102 time units. For better visibility, the apogees of the orbit on Figure 128 are numbered sequentially.

Several interesting and important conclusions can be made from the orbital behavior observable here with the bi-regional orbits:

(1) All orbits that connect lunar and terrestrial regions on the lowest energy level, maintain a rather large distance from both, Earth and Moon. To obtain trajectories that commute between the neighborhoods of the two masses, additional energy would be needed either for making directly connecting flights or for orbit-transfer maneuvers.

(2) Placing a satellite at the cislunar equilibrium point L_1 from either Earth or Moon requires an energy level higher than the "lowest", the additional energy needed either for transfer maneuvers, or for a braking impulse at L_1, or a combination of both.

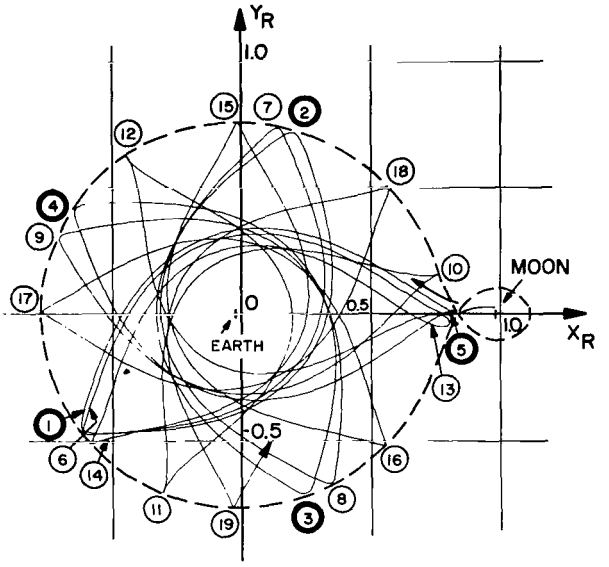

E.M. ORBIT OF JACOBI CONSTANT C= 3.20388 :
BI-REGIONAL ORBIT THROUGH (X_R= .835209 ; Y_R= .001217) TIME SHOWN : 52

Figure 128

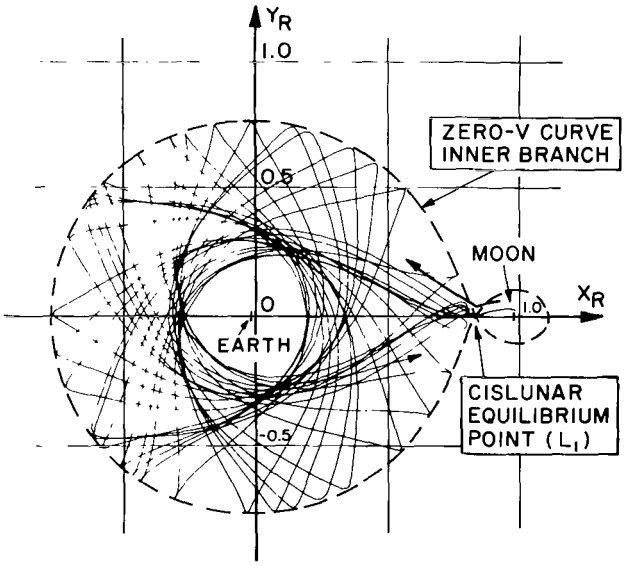

E. M. ORBIT OF JACOBI CONSTANT C = 3.20388
BIREGIONAL ORBIT THROUGH (X_R=.835209; Y_R=.001217)
TIME SHOWN: 102

Figure 129

OUTER REGION ORBITS

The investigation of the patterns formed by the orbits that exist outside the empty area for C = 3.20388 will be carried through in three steps. First retrograde orbits will be studied that are initiated at the positive X_R-axis at directions orthogonal to the axis. Secondly, orbits will be initiated at various points along two isotachs, with velocities parallel to the isotach. The last part will be concerned with orbits initiated with prograde velocity directions, resulting in ambigrade orbits.

The retrograde series is started with the orbit that cusps at the point of intersection of the positive X_R-axis with the outer zero-velocity curve (X_R = 1.2092). The orbit history (Figure 130) is traced forward and backwards of the cusping event for 73.4 time units. This orbit reaches a maximum distance from the origin of about 8 units, after which it returns to the vicinity of the zero-velocity curve.

For the subsequent orbit (Figure 131) the point of orbit initiation is shifted to the location (X_R = 1.215; Y_R = 0). The effect of this shift is a contraction of the dimension of the orbit against the former orbit to a maximum radius of about 6

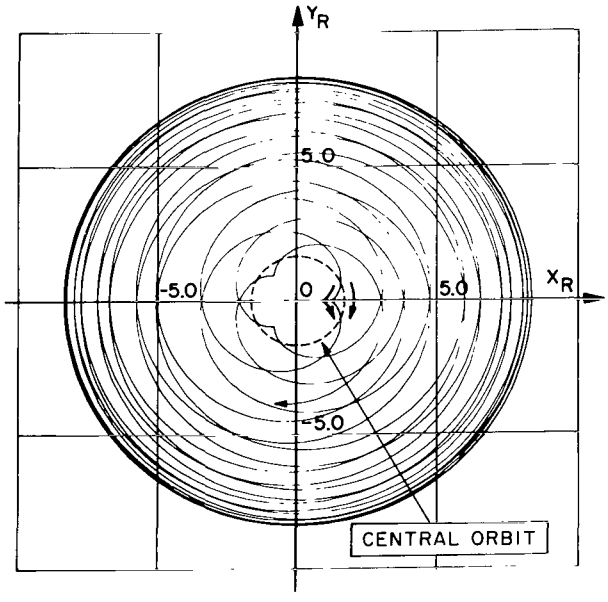

E. M. ORBITS OF JACOBI CONSTANT C=3.20388
CUSPING ORBIT THROUGH (X_R=1.20921; Y_R=0)
AND CENTRAL ORBIT OF OUTER REGION
TIME SHOWN ON CUSPING ORBIT: ±73.4

Figure 130

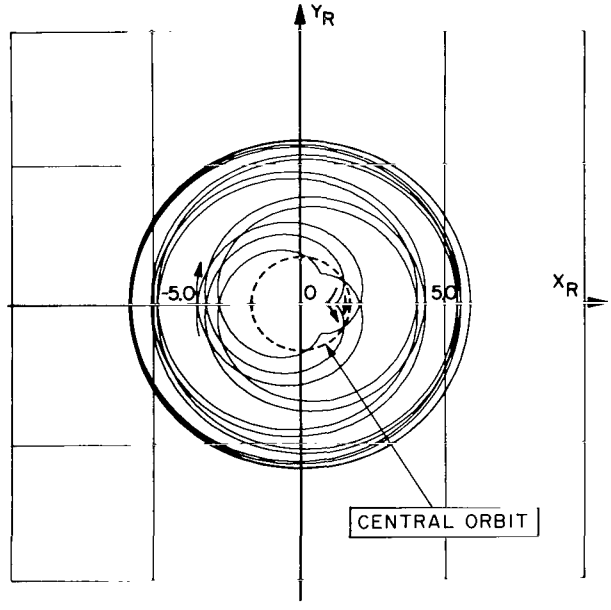

E. M. ORBIT OF JACOBI CONSTANT C=3.20388
RETROGRADE ORBIT THROUGH (X_R=1.215; Y_R=0)
AND CENTRAL ORBIT OF OUTER REGION
TIME SHOWN: ±50.2

Figure 131

units. This orbit is also traced beyond its second minimum, for positive and negative time. The central orbit, to which the present series of retrograde orbits will finally contract, is already shown with the graphs of the last two orbits (see dashed curve).

The development of this series toward the central orbit is illustrated by the sequence of the next five figures, Figures 132 to 136. The central orbit itself is passing through the point (X_R = 1.713; Y_R = 0) and shows a period of 11.64 units (Figure 136).

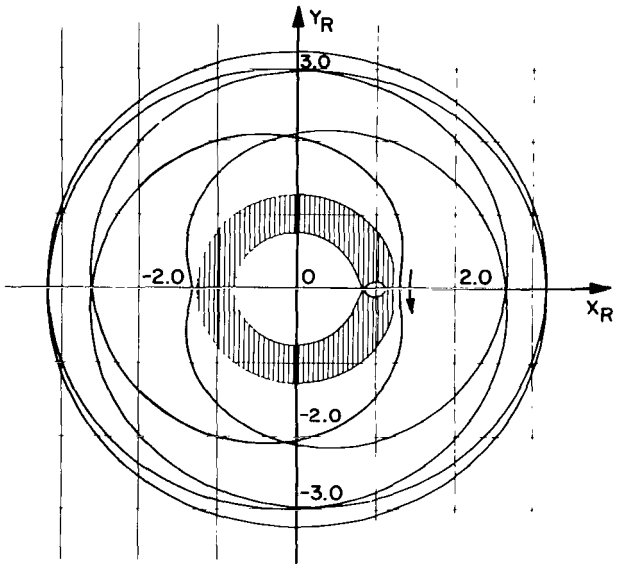

E. M. ORBIT OF JACOBI CONSTANT C = 3.20388
RETROGRADE ORBIT THROUGH (X_R = 1.30032; Y_R = 0)
PERIOD: 44.9

Figure 132

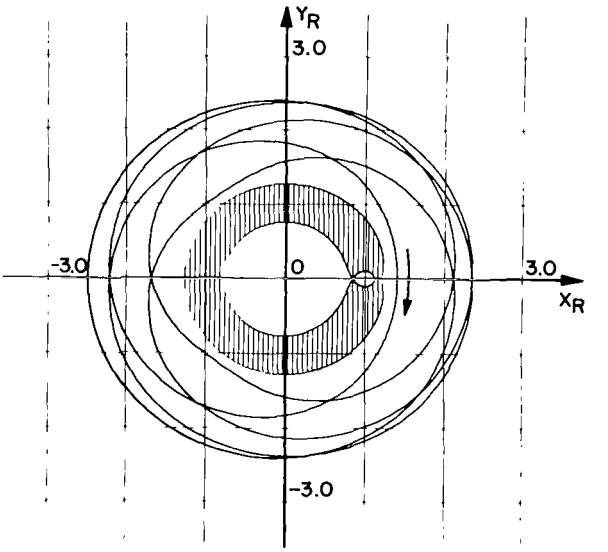

E. M. ORBIT OF JACOBI CONSTANT C = 3.20388
RETROGRADE ORBIT THROUGH (X_R = 1.40; Y_R = 0)
PERIOD: 51.0

Figure 133

It is worth noting that the central orbit, at its crossing point with the positive X_R-axis, shows a velocity maximum, in contrast to the existence of a velocity minimum at the positive X_R-axis for the first orbits of this series (zero-velocity for the very first one). There is an interesting gradual travel of the first minimum-velocity-point from the positive X_R-axis toward the negative X_R-axis as the series progresses beyond the orbit of Figure 133. At the moment the right hand axis point loses the position of a minimum-velocity point, it acquires the position of a maximum-velocity point. Both extrema are understood, in general, as local extrema, only.

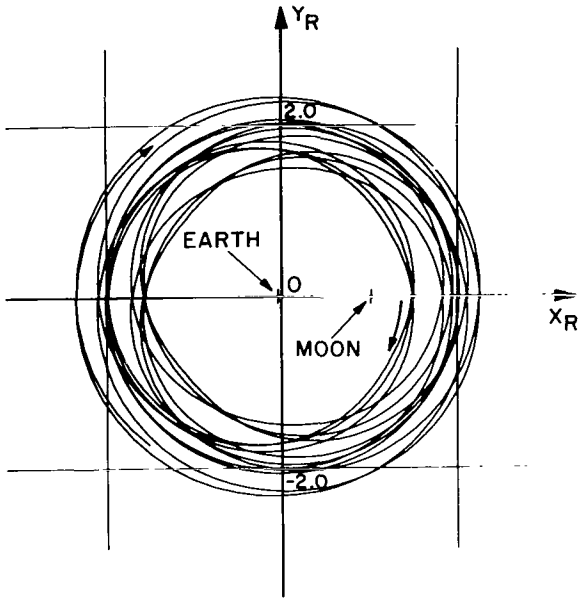

E.M. ORBIT OF JACOBI CONSTANT C = 3.20388
RETROGRADE ORBIT THROUGH (X_R = 1.480; Y_R = 0)
TIME SHOWN: ± 71.04

Figure 134

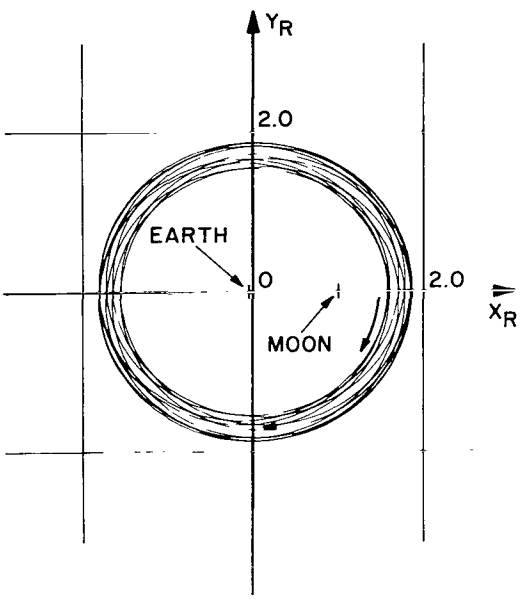

E.M. ORBIT OF JACOBI CONSTANT C = 3.20388
RETROGRADE ORBIT THROUGH (X_R = 1.580; Y_R = 0)
TIME SHOWN: ± 60.1

Figure 135

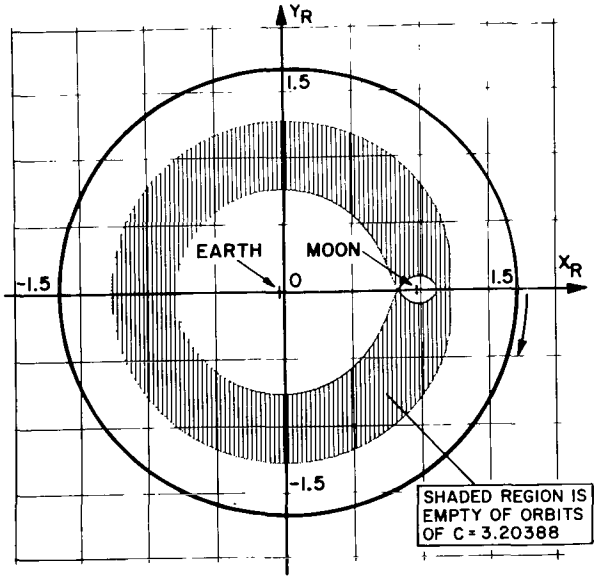

E.M. ORBIT OF JACOBI CONSTANT C = 3.20388
CENTRAL ORBIT OF RETROGRADE CLASS OF
OUTER REGION (X_R = 1.713; Y_R = 0; PERIOD: 11.64)

Figure 136

Contrasted to the last series will now be a series of those retrograde orbits that start orthogonally to the negative X_R-axis. This series finds itself illustrated on the four figures, Figures 137 to 140. The progression is reverse to that of the former series in that the series starts with an orbit close to the central one. By pulling the initial point of the orbits stepwise closer to the zero-velocity curve, the overall size of the orbits increases. In this progression the maximum point of the orbits goes beyond all limits before that orbit is reached that touches the zero-velocity curve. This last orbit is depicted on Figure 140.

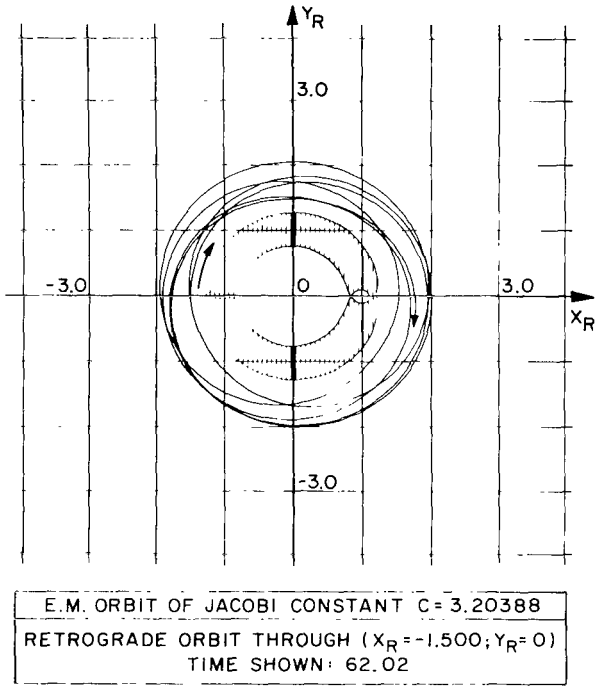

Figure 137

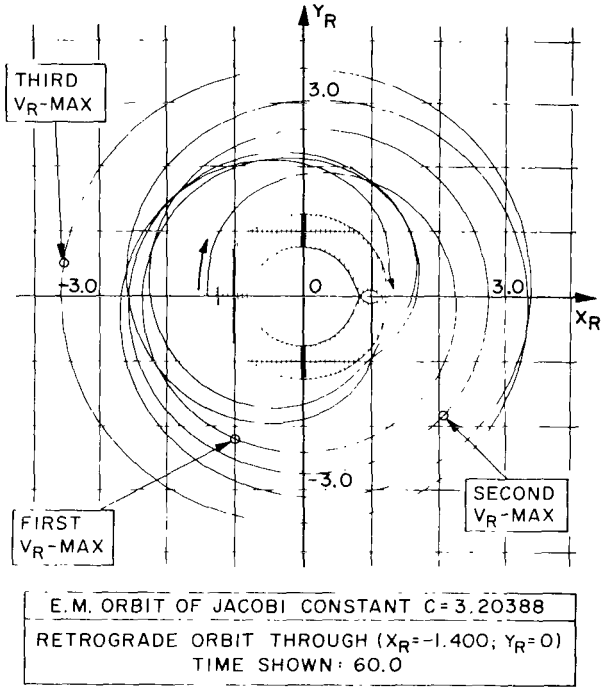

Figure 138

The contrast in orbital behavior between the last orbit and the orbit that was initiated with zero-velocity at the positive X_R-axis (Figure 130) before, gives rise to the question, what the behavior will be for those orbits that are started at other points of the same zero-velocity curve. This question will be considered next.

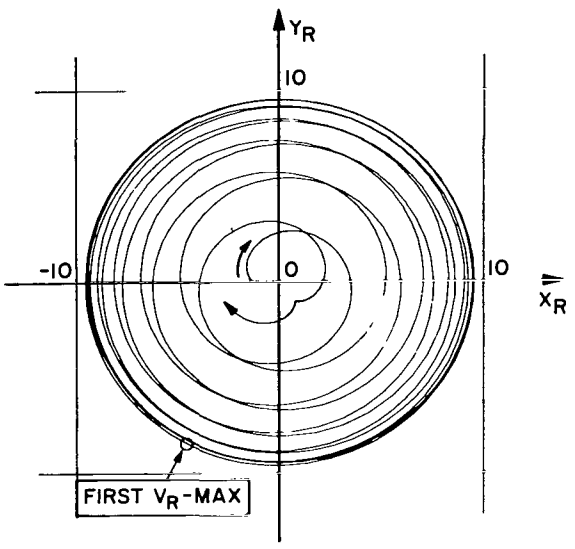

E.M. ORBIT OF JACOBI CONSTANT C = 3.20388
RETROGRADE ORBIT THROUGH (X_R = -1.275; Y_R = 0)
TIME SHOWN: 83.1

Figure 139

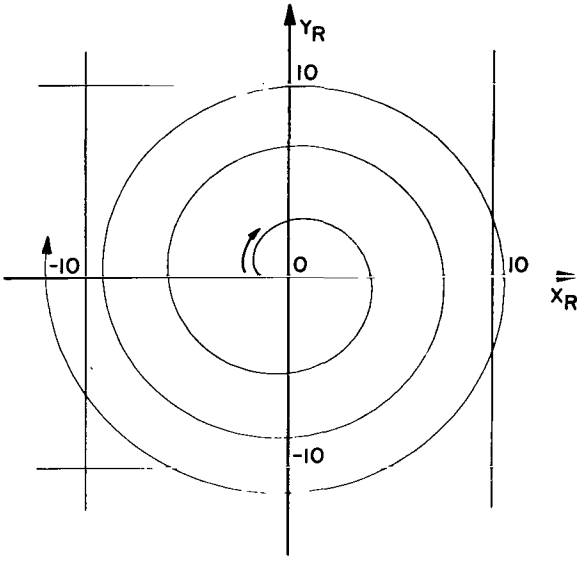

E.M. ORBIT OF JACOBI CONSTANT C = 3.20388
RETROGRADE ORBIT THROUGH (X_R = -1.26765; Y_R = 0)
TIME SHOWN: 21.4

Figure 140

FLY-BY EFFECT ON OUTER REGION ORBITS

The fly-by effect discussed here is different from that discussed before for orbits of the terrestrial region. Concern is here given to the question of relative magnitude of radial distances an orbit assumes before and after a close approach to the EM-system. Obviously this effect does not exist for cases where close approach is exactly on the (positive or negative) X_R-axis, since reflection laws provide here the answer. The dependence of the effect on the central angle ϕ, under which close approach is measured, will conveniently be established by varying the close approach point along an isotach, to start with e.g., the zero-velocity curve. The procedure is indicated on Figure 141 where five short time-orbits are shown, each of which cusping on the border curve. Note is taken that again the reflection laws allow to restrict the study to either the upper or the lower half of the isotach, if orbit histories are computed forward as well as backward.

The effect on these orbits is shown by the succeeding seven graphs, Figures 142 to 148. The first of these is the symmetrical case again, providing a comparison basis for the next cases. Figures 143 and 144 show the orbit history before and after a close approach through the border point: (X_R = 1.21246; Y_R = 0.057889).

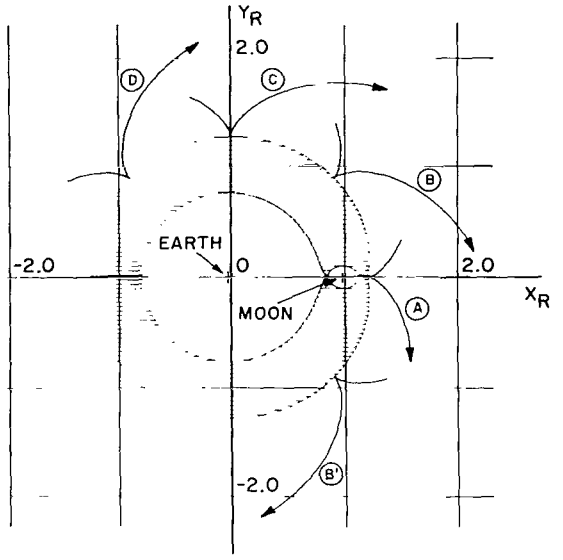

E.M. ORBIT OF JACOBI CONSTANT C = 3.20388
FIVE CUSPING ORBITS OF OUTER REGION

Figure 141

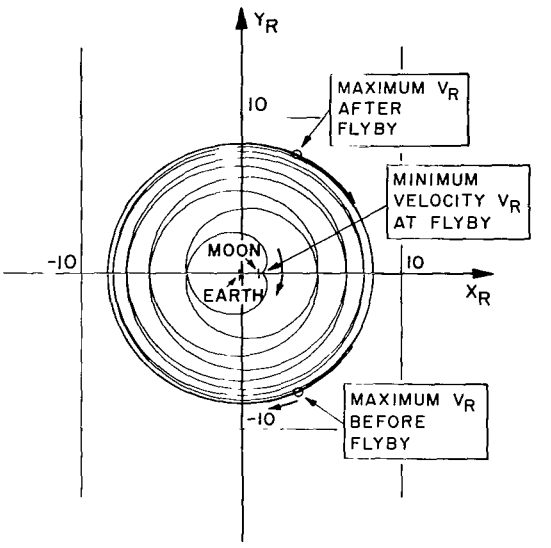

E.M. ORBIT OF JACOBI CONSTANT C = 3.20388
CUSPING ORBIT THROUGH (X_R = 1.20921; Y_R = 0)
TIME OF V_R-MAXIMA = ±33.82

Figure 142

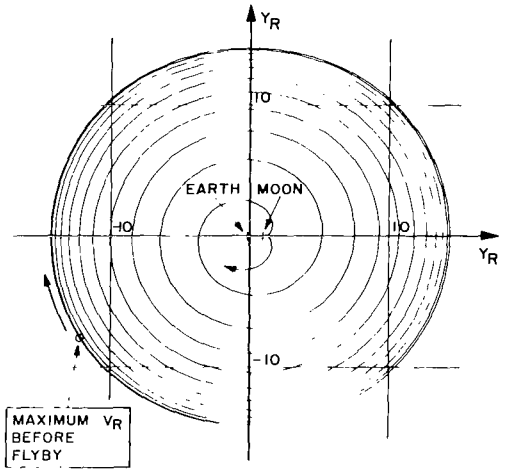

E.M. ORBIT OF JACOBI CONSTANT C = 3.20388
CUSPING ORBIT THROUGH (X_R = 1.21246; Y_R = 0.057889)
TIME OF V_R-MAXIMUM = -69.95

Figure 143

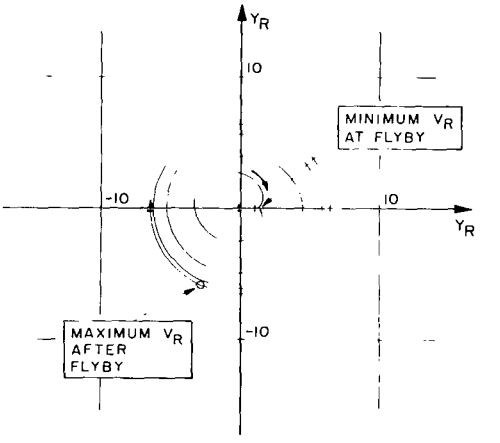

E.M. ORBIT OF JACOBI CONSTANT C = 3.20388
CUSPING ORBIT THROUGH (X_R = 1.21246, Y_R = 0.057889)
TIME OF V_R-MAXIMUM = 24.48

Figure 144

For the two branches the maximum-velocity points are marked on the figures, from which can be recognized that there is a reduction-through fly-by — from a maximum distance of about 14 units to a maximum distance of about 6 units.

If the point of close approach is raised further along the zero-velocity curve, as to the point: (X_R = 1.2022; Y_R = 0.35194), both upstream and downstream maxima of the orbit history are at larger distances than on the former orbit (Figure 145 and 146), but the upstream maximum lies at infinity, while the maximum after fly-by is at a distance of about 13 units.

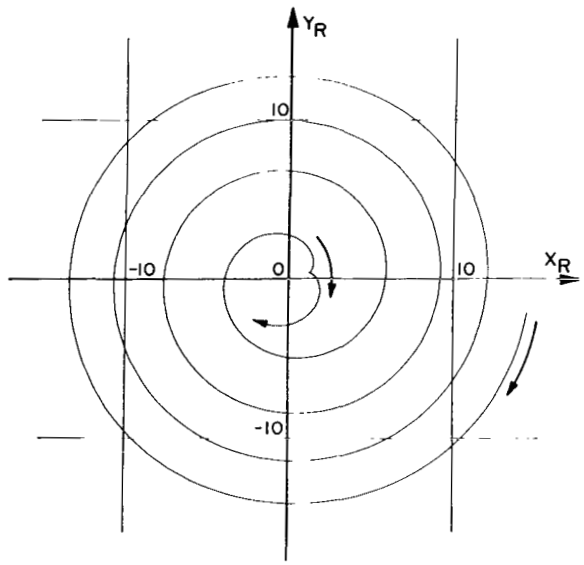

E.M. ORBIT OF JACOBI CONSTANT C = 3.20388
CUSPING ORBIT THROUGH (X_R=1.2022; Y_R=0.35194)
TIME SHOWN: -27.2 TO +4.4

Figure 145

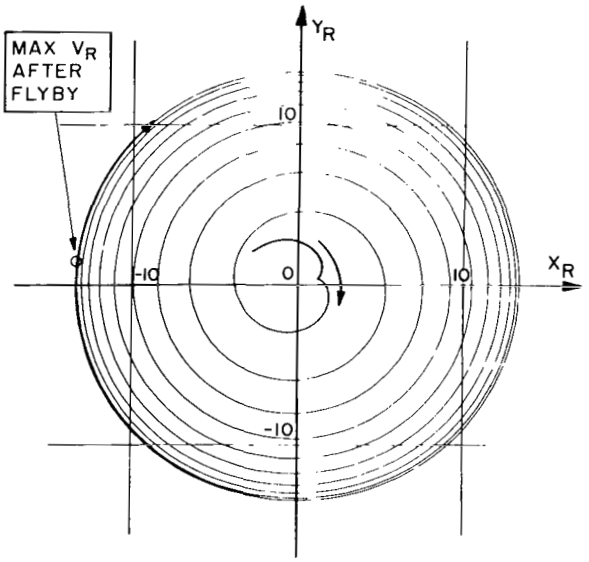

E.M. ORBIT OF JACOBI CONSTANT C = 3.20388
CUSPING ORBIT THROUGH (X_R=1.2022; Y_R=0.35194)
TIME SHOWN: -4.0 TO + 64

Figure 146

While the effect of fly-by within the former orbit is a reduction in maximum distance, the fly-by effect for the latter orbit can be called a "capture" (at least a temporary one).

For orbits whose close approach points are reflective to those of the former two cases, one would speak of an increase in maximum distance and of an escape-maneuver, respectively.

The magnitude of the fly-by effect will now briefly be studied for orbits that have their close approach-point on the isotach of C = 3.25. The position of this curve in relation to the zero-velocity curve can be seen on Figure 147. There also are shown four short-time orbits that are tangential to the isotach 3.25.

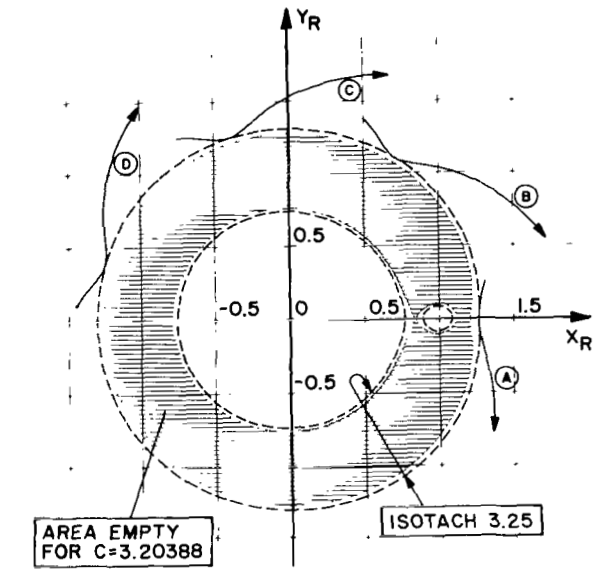

E.M. ORBITS OF JACOBI CONSTANT C=3.20388
FOUR ORBITS TANGENTIAL TO ISOTACH 3.25

Figure 147

Of the orbits computed here, only two will be demonstrated. Figure 148 shows the orbit that is orthogonal to the positive X_R-axis, and Figure 149 displays the forward and backward history of the orbit through the point: (X_R = 1.2318; Y_R = 0.3894). This is nearly that point on the isotach where the ratio between the maximum distances before and after fly-by is largest. As this figure demonstrates, the fly-by effect for orbits starting on the isotach 3.25 is considerably smaller than that for orbits through points on the zero-velocity curve.

A summary of the fly-by effect connected with the outer-region orbits of the C-level of 3.20388 is then presented in diagrammatic form on Figures 150 and 151. The pictures show radial distances of apocenters for two successive apocenters plotted over the angular location of the pericenter that occurs between the two apocenters, the angle being measured from the origin in mathematically positive direction. The first figure is concerned with orbits that are cusping on the zero-velocity curve. The second figure is for orbits that are tangential to the isotach of 3.25. Notice that the second of the figures carries the abscissa through +180° while the first one shows an abscissa range of only 10 degrees.

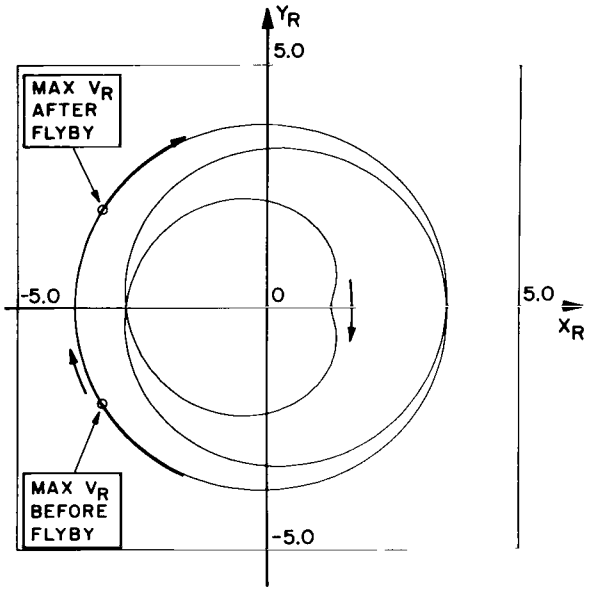

E.M. ORBIT OF JACOBI CONSTANT C = 3.20388
RETROGRADE ORBIT THROUGH (X_R = 1.2664 ; Y_R = 0)
TIME SHOWN : ±14.2
ORBIT TANGENTIAL TO ISOTACH 3.250

Figure 148

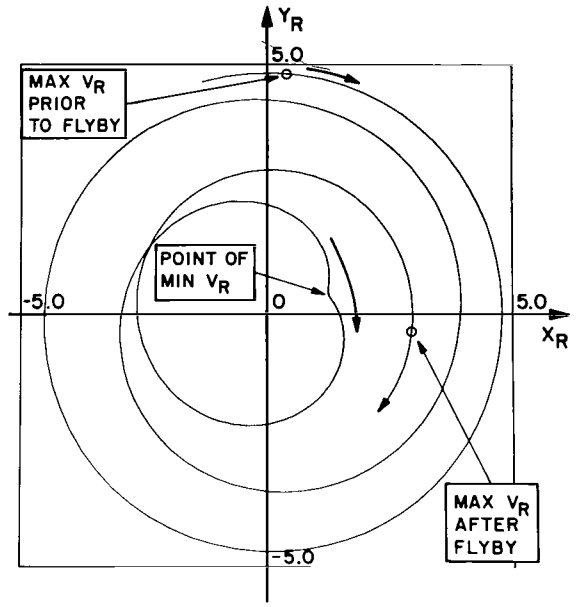

E.M. ORBIT OF JACOBI CONSTANT C = 3.20388
RETROGRADE ORBIT THROUGH (X_R = 1.2318; Y_R = 0.3894)
TIME SHOWN : -17.3 TO +10.7
ORBIT TANGENTIAL TO ISOTACH 3.250

Figure 149

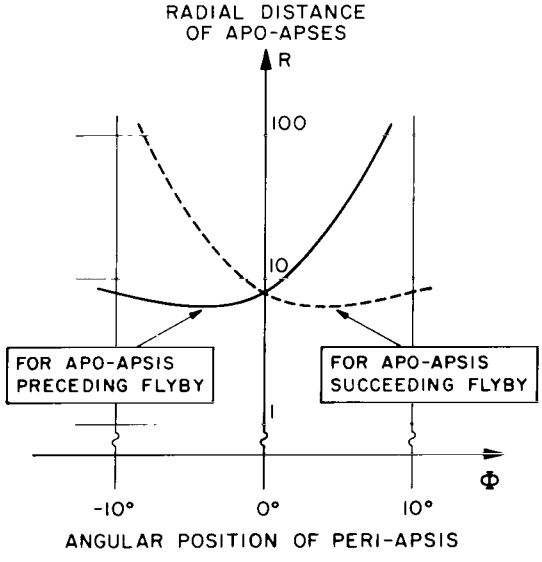

E.M. ORBITS OF JACOBI CONSTANT C = 3.20388
RADIAL DISTANCES OF APO-APSES
BEFORE AND AFTER FLYBY
VS. ANGULAR POSITION OF FLYBY POINTS
FLYBY-POINTS ARE ON ZERO-V-CURVE

Figure 150

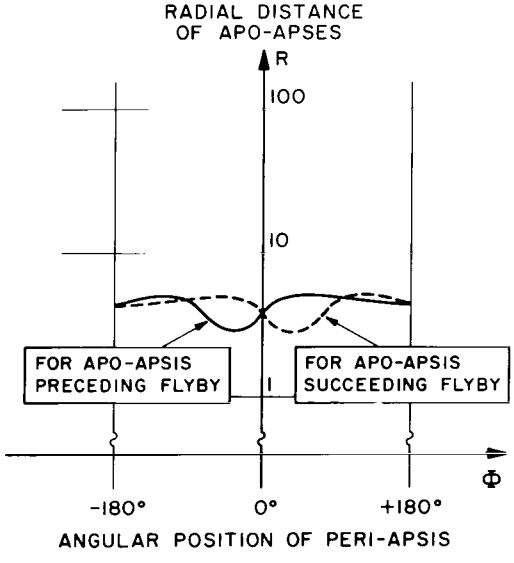

E.M. ORBITS OF JACOBI CONSTANT C = 3.20388
RADIAL DISTANCES OF APO-APSES
BEFORE AND AFTER FLYBY
VS. ANGULAR POSITION OF FLYBY POINTS
FLYBY-POINTS ARE ON THE ISOTACH : C = 3.25

Figure 151

AMBIGRADE ORBITS OF THE OUTER REGION

Since the orbit that cusps at the intersection of the positive X_R-axis with the zero-velocity curve, has a first apocenter of finite distance, continuity considerations demand that there is also a group of orbits (though it may be small, comparatively) that start in prograde direction on the positive X_R-axis and have an apocenter of finite distance. The orbits are, in fact, ambigrade since the motion reverses very soon.

Of this group, two examples will be shown on the following four figures, Figures 152 to 155. The first two pictures show two different time histories of the orbit through the point: (X_R = 1.210; Y_R = 0). The second couple of figures accommodate two corresponding views for the orbit through (X_R = 1.212; Y_R = 0).

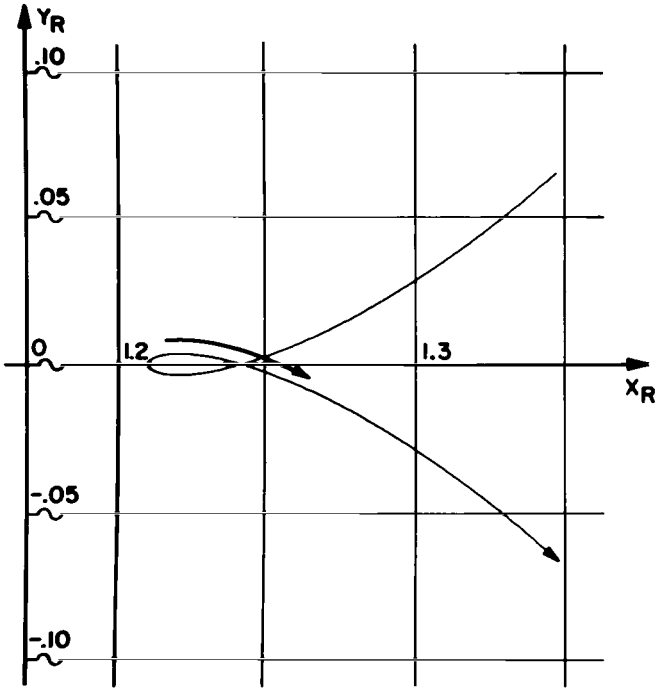

E.M. ORBIT OF JACOBI CONSTANT C = 3.20388
AMBIGRADE ORBIT THROUGH (X_R = 1.210; Y_R = 0; θ_R = 90°)
TIME SHOWN : ±0.9

Figure 152

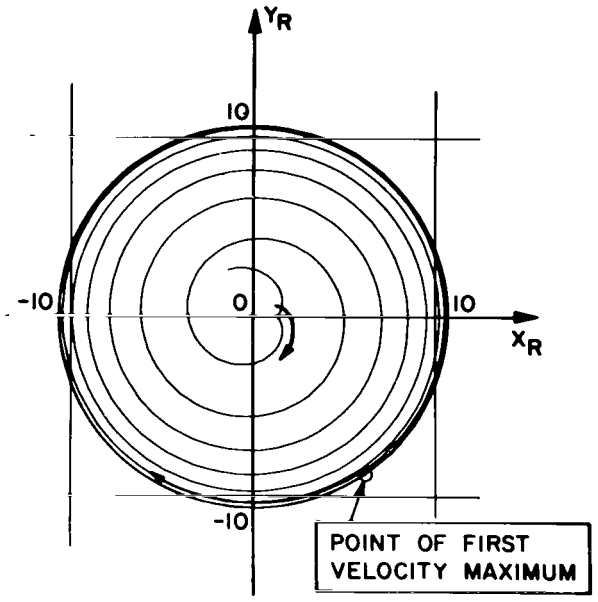

E.M. ORBIT OF JACOBI CONSTANT C = 3.20388
AMBIGRADE ORBIT THROUGH (X_R = 1.210; Y_R = 0; θ_R = 90°)
TIME SHOWN : -4.2 TO +56.01

Figure 153

It is recalled that the cusping orbit which intersects the X_R-axis with zero-velocity at the value of X_R = 1.2092, reaches a first maximum of about 8 units.

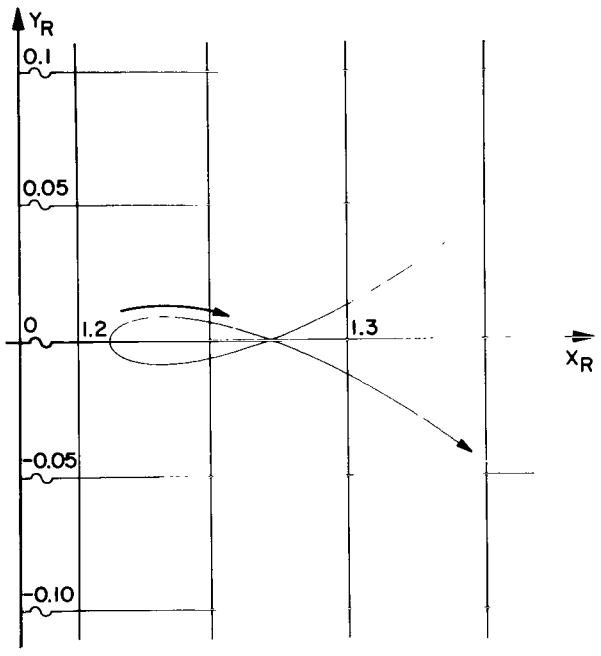

E.M. ORBIT OF JACOBI CONSTANT C = 3.20388
AMBIGRADE ORBIT THROUGH (X_R = 1.212; Y_R = 0; θ = 90°)
TIME SHOWN: ±0.84

Figure 154

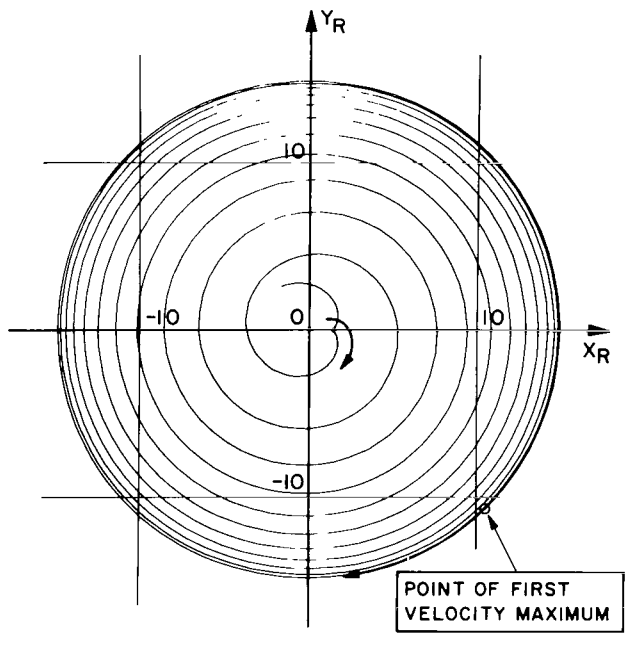

E.M. ORBIT OF JACOBI CONSTANT C = 3.20388
AMBIGRADE ORBIT THROUGH (X_R = 1.212; Y_R = 0; θ_R = 90°)
TIME SHOWN: -4.2 TO +73.98

Figure 155

The two ambigrade orbits reach a first maximum of 10 units and of 15 units, respectively.

With the increase of initial X_R, the apocenter distances from the origin grow rapidly. The ambigrade orbits are becoming escape orbits, before their pericenters have reached the X_R-value of 1.30.

REFERENCES

1. Szebehely, V.: Theory of Orbits. Academic Press, New York, 1967.
2. Arenstorf, R. F.: New Regularization of the Restricted Problem of Three Bodies. Astronomical Journal, Vol. 68, No. 8, October 1963.
3. Hoelker, R. F.; and Winston, B. P.: A Comparison of a Class of Earth-Moon Orbits with a Class of Rotating Kepler Orbits. NASA TN D -4903, November 1968.
4. McGann, J. C., Jr.: Implementation of C-Curve Value Problem. Report No. 226 of Service Technology Corporation, Cambridge, Mass., June 1969.
5. Masucci, P. F.: Unpublished Notes and Communications through the period of 1968 to 1970, Boston University, Boston, Massachusetts.
6. Broucke, R. A.: Periodic Orbits in the Restricted Three-body Problem with Earth-Moon Masses. JPL TR 32-1168, February 1968.

NASA-Langley, 1970 —— 30 C-130

"The aeronautical and space activities of the United States shall be conducted so as to contribute . . . to the expansion of human knowledge of phenomena in the atmosphere and space. The Administration shall provide for the widest practicable and appropriate dissemination of information concerning its activities and the results thereof."

—NATIONAL AERONAUTICS AND SPACE ACT OF 1958

NASA SCIENTIFIC AND TECHNICAL PUBLICATIONS

TECHNICAL REPORTS: Scientific and technical information considered important, complete, and a lasting contribution to existing knowledge.

TECHNICAL NOTES: Information less broad in scope but nevertheless of importance as a contribution to existing knowledge.

TECHNICAL MEMORANDUMS: Information receiving limited distribution because of preliminary data, security classification, or other reasons.

CONTRACTOR REPORTS: Scientific and technical information generated under a NASA contract or grant and considered an important contribution to existing knowledge.

TECHNICAL TRANSLATIONS: Information published in a foreign language considered to merit NASA distribution in English.

SPECIAL PUBLICATIONS: Information derived from or of value to NASA activities. Publications include conference proceedings, monographs, data compilations, handbooks, sourcebooks, and special bibliographies.

TECHNOLOGY UTILIZATION PUBLICATIONS: Information on technology used by NASA that may be of particular interest in commercial and other non-aerospace applications. Publications include Tech Briefs, Technology Utilization Reports and Notes, and Technology Surveys.

Details on the availability of these publications may be obtained from:

SCIENTIFIC AND TECHNICAL INFORMATION DIVISION

NATIONAL AERONAUTICS AND SPACE ADMINISTRATION

Washington, D.C. 20546